NCAT Report 11-03

EVALUATION OF MIXTURE PERFORMANCE AND STRUCTURAL CAPACITY OF PAVEMENTS UTILIZING SHELL THIOPAVE®

Phase II: Construction, Laboratory Evaluation and Full-Scale Testing of Thiopave® Test Sections – One Year Report

By
Dr. David H. Timm
Mary M. Robbins
Dr. J. Richard Willis
Dr. Nam Tran
Adam J. Taylor

July 29, 2011

National Center for Asphalt Technology
NCAT
at AUBURN UNIVERSITY

277 Technology Parkway ■ Auburn, AL 36830

NCAT Report 11-03

EVALUATION OF MIXTURE PERFORMANCE AND STRUCTURAL CAPACITY OF PAVEMENTS UTILIZING SHELL THIOPAVE®

Phase II:
Construction, Laboratory Evaluation and Full-Scale Testing
of Thiopave® Test Sections – One Year Report

By
Dr. David H. Timm
Mary M. Robbins
Dr. J. Richard Willis
Dr. Nam Tran
Adam J. Taylor

National Center for Asphalt Technology
Auburn University

Sponsored by
Shell Oil Products, USA

July 29, 2011

ACKNOWLEDGEMENTS

This project was sponsored by Shell Oil Products, USA. The project team appreciates and thanks Shell Oil Products, USA for their sponsorship of this project. Richard May of Shell Sulfur Solutions deserves special recognition for providing detailed technical and editorial review of this document.

DISCLAIMER

The contents of this report reflect the views of the authors who are responsible for the facts and accuracy of the data presented herein. The contents do not necessarily reflect the official views or policies of Shell Oil Products, USA or the National Center for Asphalt Technology, or Auburn University. This report does not constitute a standard, specification, or regulation. Comments contained in this paper related to specific testing equipment and materials should not be considered an endorsement of any commercial product or service; no such endorsement is intended or implied.

TABLE OF CONTENTS

LIST OF TABLES

LIST OF FIGURES

1. INTRODUCTION

1.1 Background

Asphalt cement prices and the need for more environmentally-friendly asphalt pavements have renewed interest in utilizing sulfur as a binder replacement option. Replacing virgin binder with sulfur has the potential to improve pavement performance by increasing the modulus of the asphalt concrete (AC); thereby, reducing pavement strain and improving performance. Furthermore, replacing the costly binder with another waste product from petroleum refining is economically sound. However, early attempts at utilizing sulfur in the 1970's was done in molten liquid form added directly to the asphalt binder, which caused unacceptable levels of hydrogen sulfide (H_2S) to be emitted during production and construction of the pavement (Strickland et al., 2008). This posed a rather large obstacle to widespread use of sulfur-extended asphalt mix (SEAM) as the environment for plant and paving crews could be considered hazardous.

To overcome the hydrogen sulfide environmental hazard, Shell Sulfur Solutions recently developed a new pelletized sulfur formulation called Thiopave© (Figure 1). The Thiopave system features sulfur pellets combined with a warm mix additive (WMA) that allows for production at temperatures around 275°F (135°C). At this temperature, hydrogen sulfide emissions are reduced to an acceptably low level. When fabricating laboratory mixes, the compaction aid is preblended with the virgin binder while sulfur pellets are added to the mixture immediately after the binder/compaction aid and aggregate have been combined. When plant-producing Thiopave mixes, the compaction aid is added to the asphalt stream before it reaches the aggregate. The pellets are added through the reclaimed asphalt pavement (RAP) collar.

Figure 1.1 Thiopave Pellets and Compaction Aid (Timm et al., 2009)

To evaluate the new formulation, the National Center for Asphalt Technology (NCAT) conducted extensive laboratory testing on a variety of Thiopave mix designs in preparation for constructing two full-scale experimental test sections at the NCAT Test Track. The goal of the laboratory testing was to provide sufficient information regarding the mechanistic and performance characteristics to guide decisions regarding the construction of particular pavement cross-sections. Part of the investigation utilized the mechanistic-empirical pavement design guide (MEPDG) and PerRoad to make performance (i.e., rutting, cracking) and pavement response (i.e., stress, strain) predictions.

The initial laboratory investigation considered five mixtures consisting of a control (no Thiopave) and four Thiopave options. The control mix was designed to the standard 4 percent

air void content. The Thiopave mixtures consisted of replacing 30 and 40 percent of the virgin binder with Thiopave at 2 and 3.5 percent design air void content, respectively (Timm et al., 2009). The lower design air void contents were intended to improve the mix flexibility and fatigue performance by increasing overall binder content which would help offset some of the stiffening created in the mixture by adding Thiopave. The mixtures designed at 2 percent air were considered a "rich bottom" material that would have much improved fatigue and moisture resistance characteristics. The 3.5 percent air mixtures were considered more typical of intermediate layers in the AC cross section.

After the preliminary mix designs had been completed, an array of laboratory tests was conducted on each mixture. Full discussion of these test results is beyond the scope of this report; however, these results have been fully documented in NCAT Report 09-05 (Timm et al., 2009). Only a few key observations from this testing related to mechanistic characterization are discussed in the following paragraphs.

An important observation from the lab testing was a measurable increase in dynamic modulus (E^*) over a two week aging cycle. Figure 1.2 summarizes the aging effect for each mixture at 10 Hz and 21°C. The Thiopave mixtures (also known as "SEAM" in the earlier study) increased modulus by approximately 300 to 400 ksi over the two week period with nearly no discernable increase in the control mixture. A key question raised by these data was whether a measurable modulus increase over time would also be measured in full-scale test sections under falling weight deflectometer testing.

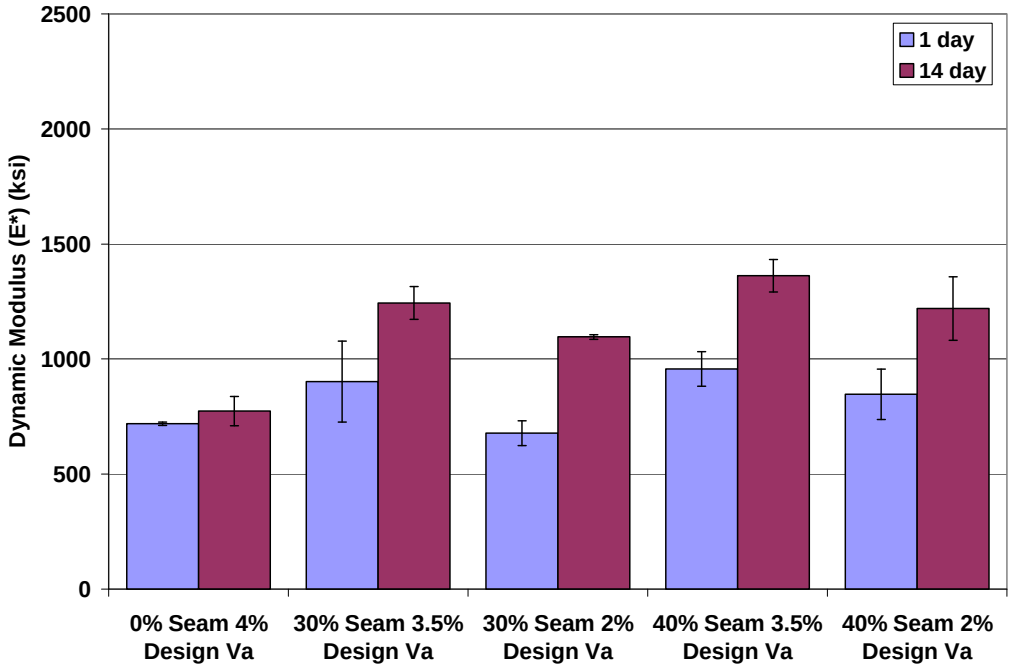

Figure 1.2 E* Results at 10 Hz and 21°C for All Mixtures After 1 and 14 Days of Curing (Timm et al., 2009)

E* testing conducted over three temperatures and six frequencies enabled master-curves to be created for each mixture. The master-curves served to quantify the modulus magnitude in

addition to serving as primary inputs to the MEPDG and PerRoad. Figure 1.3 summarizes the five master-curves. Significant increases in stiffness of the Thiopave materials were noted relative to the control mixture. The stiffest among these was the 40% Thiopave at 3.5% air void mixture. Since increased stiffness results in lower strain levels, this mixture was recommended for intermediate layers in the full-scale test section. However, it was not recommended for use at the top of the pavement because several other comparative test sections and a control section of equal thickness were being constructed with the same surface wearing course mixture. The 30% Thiopave at 2% air void mixture was selected for the bottom lift to provide a less stiff, more flexible rich bottom layer with better fatigue resistance, as discussed previously.

A further question raised by the E^* data was whether similar observations of increased modulus would be made in the field for pavements comprised of combinations of these materials under falling weight deflectometer (FWD) testing.

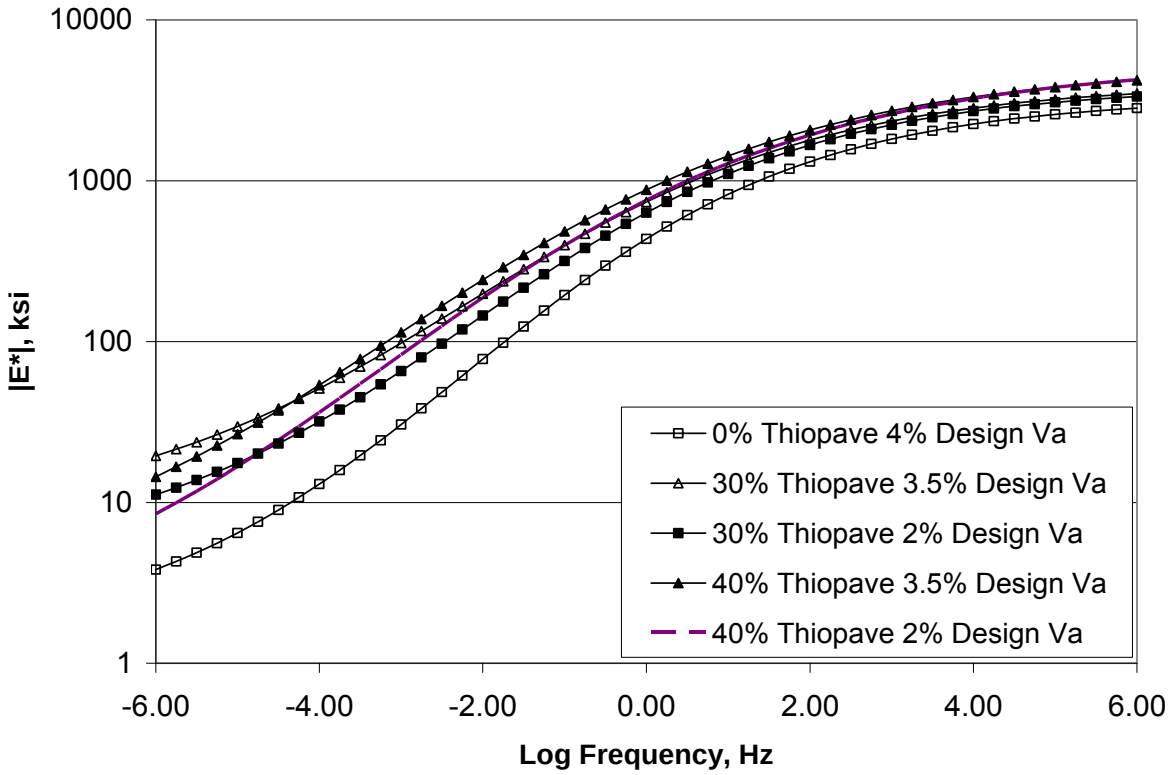

Figure 1.3 Dynamic Modulus Master Curves (Timm et al., 2009)

Beam fatigue testing conducted at 600, 400 and 200 με indicated a general loss in fatigue life as the amount of Thiopave was increased over the control mixture (Figure 1.4). This was especially true at the two higher strain levels. It was interesting to note the 30% Thiopave material at 2% air voids approached the same number of cycles to failure as the control mixture at 200 με. At higher strain levels, it performed better than the other Thiopave materials. Although the higher moduli of the Thiopave mixtures should lead to lower strain levels, these fatigue curve observations naturally led to specifying this mixture in the bottom of the full-scale sections to minimize the potential for decreased overall fatigue performance of the Thiopave sections relative to the control.

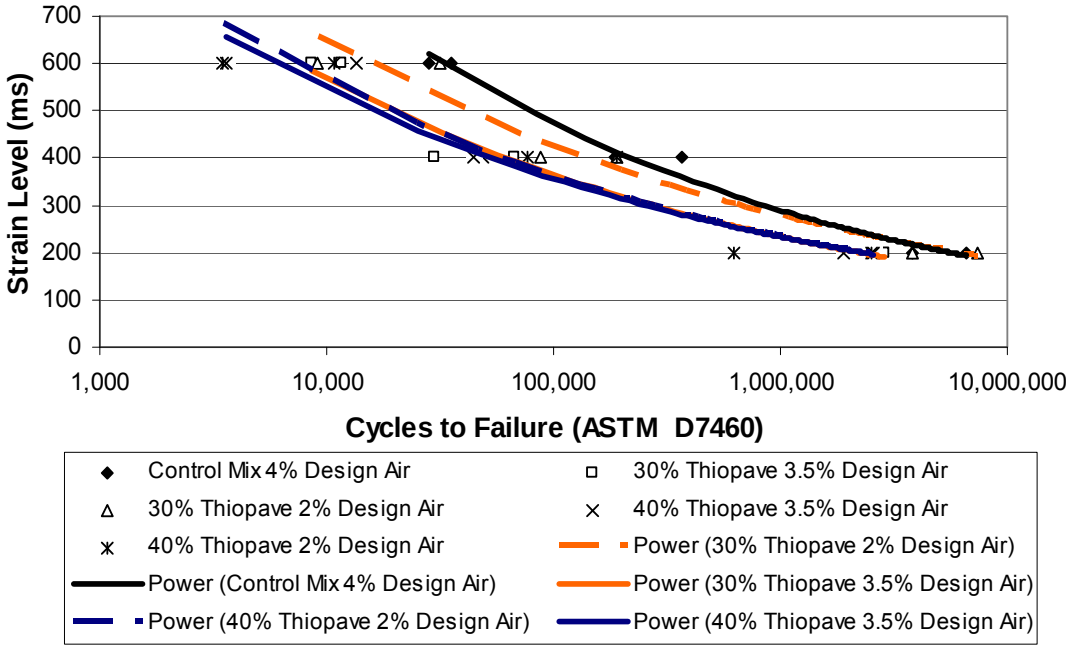

Figure 1.4 Beam Fatigue Test Results (Timm et al., 2009)

While the laboratory testing was being conducted, evaluations using the MEPDG and PerRoad were made of potential full-scale sections. The MEPDG simulations examined eight potential cross-sections as illustrated in Figure 1.5. Though details regarding the simulations are documented elsewhere (Timm et al., 2009), the results of the simulations are shown in Figures 1.6 and 1.7 for rutting and fatigue, respectively. In general, better performance was predicted as the amount of Thiopave increased and/or when the design air voids were decreased because of the relatively higher modulus. The reductions in predicted distress for both fatigue and rutting, between the control and any of the Thiopave sections, were judged significant in the previous study (Timm et al., 2009). Whether these trends would translate to actual performance was a motivating question in building the two full-scale test sections.

The PerRoad investigation was intended to evaluate the same eight potential Thiopave sections, in addition to the control, in the context of strain distributions. Corresponding to the MEPDG simulations, the PerRoad investigation focused on tensile strain at the bottom of the AC (fatigue cracking) and vertical strain at the top of the subgrade (rutting). Again, the details have been documented elsewhere (Timm et al., 2009) with the results summarized in Figures 1.8 and 1.9. As found in the MEPDG simulations, there was a general reduction in strain response with an increase in Thiopave. Also, higher air voids at each Thiopave content resulted in lower predicted strain levels. How these results would translate to the field was also an issue of high priority.

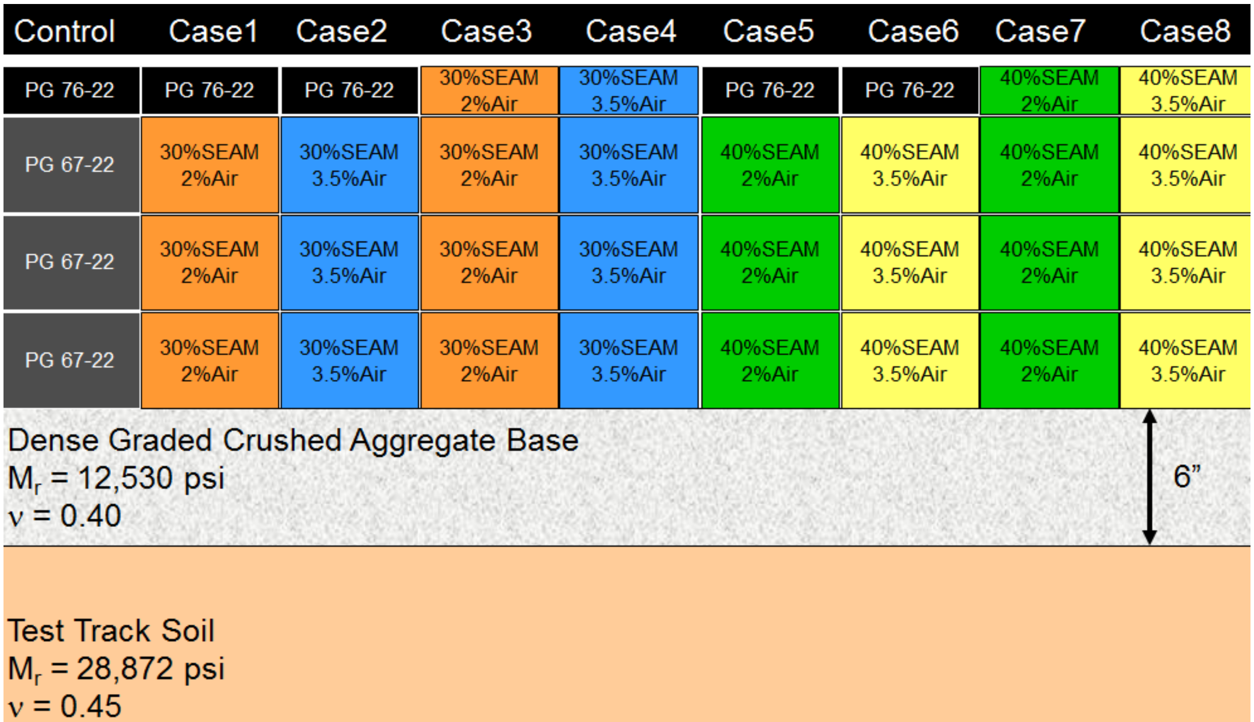

Figure 1.5 MEPDG Thiopave Test Sections (Timm et al., 2009)

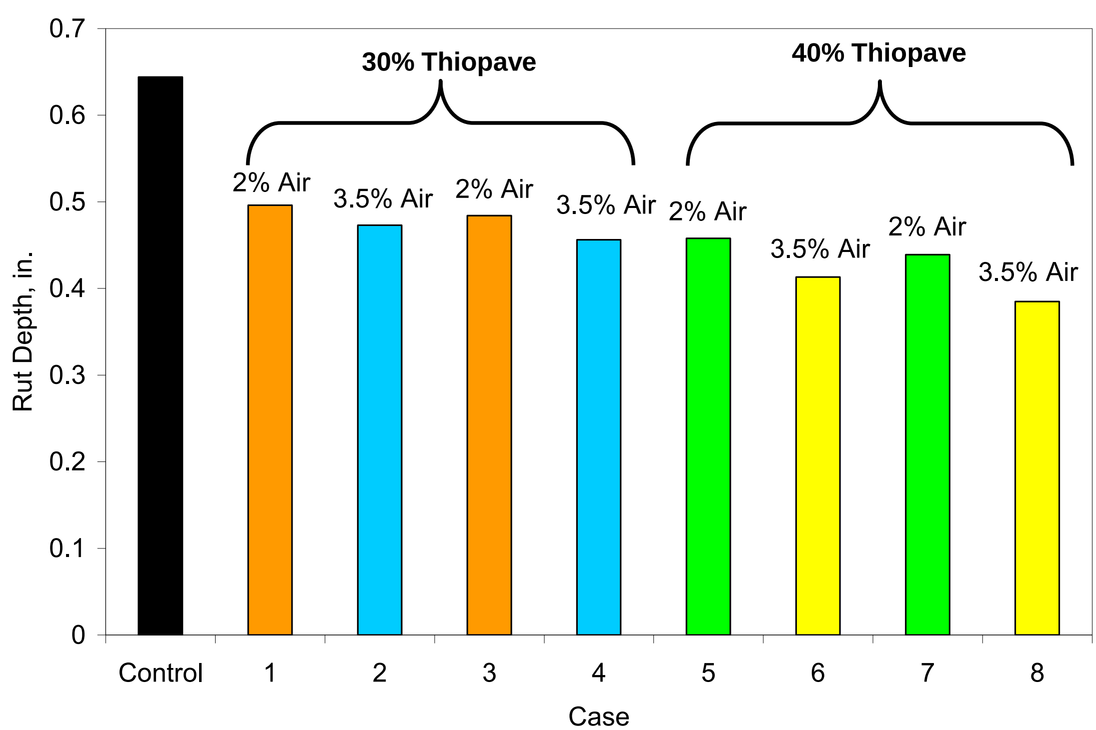

Figure 1.6 MEPDG Rutting Comparison (Timm et al., 2009)

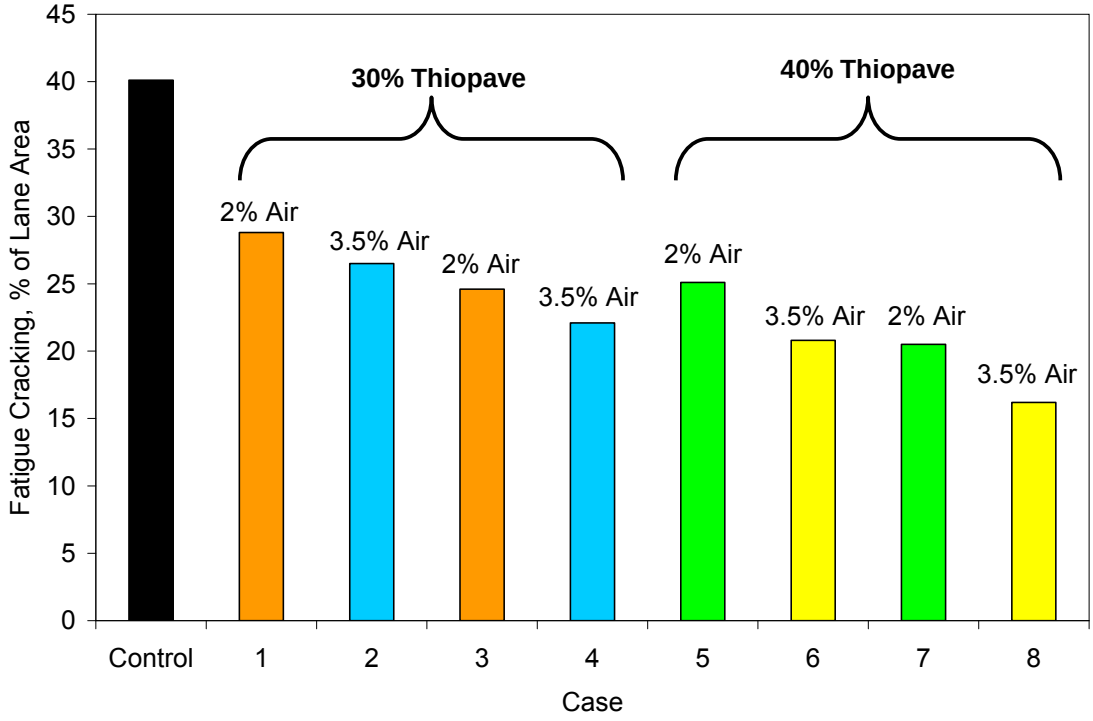

Figure 1.7 MEPDG Fatigue Cracking Comparison (Timm et al., 2009)

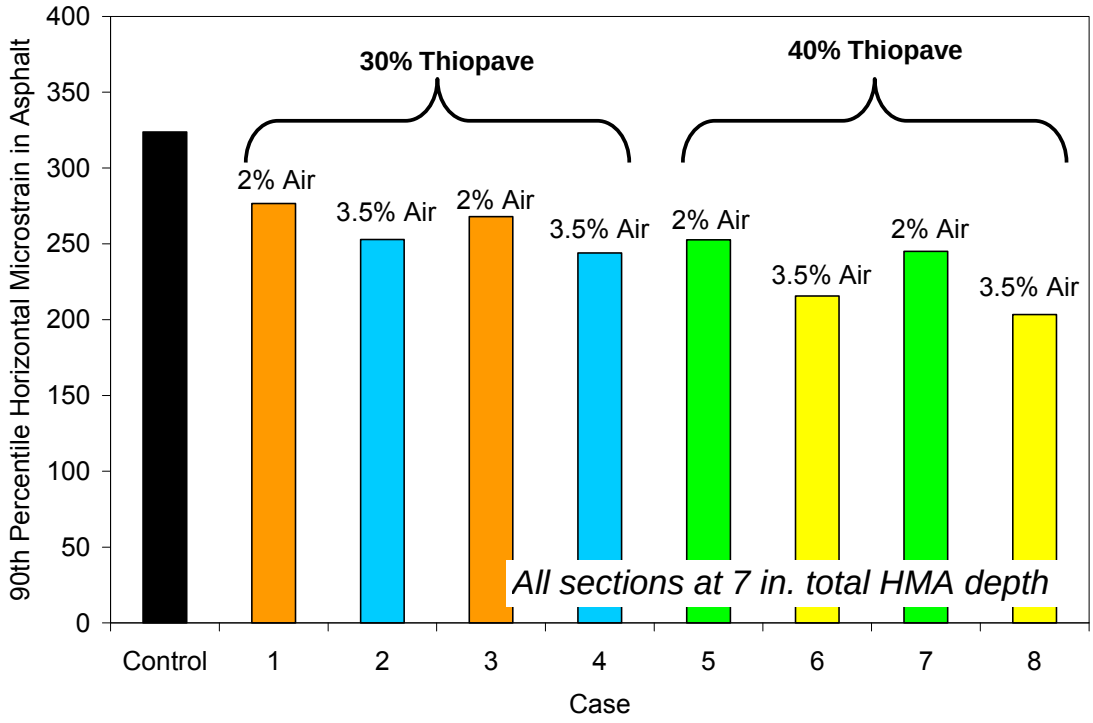

Figure 1.8 90th Percentile HMA Strain (Timm et al., 2009)

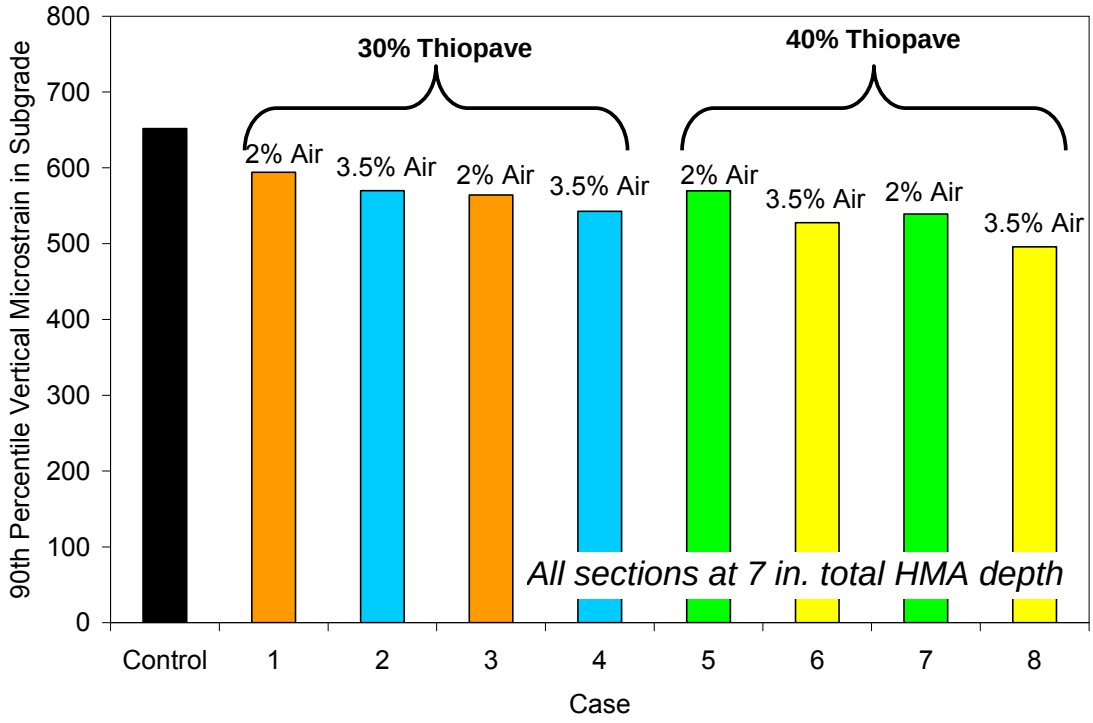

Figure 1.9 90th Percentile Subgrade Strain (Timm et al., 2009)

Based on the preliminary lab data and design simulations, it was decided to construct two sections at the Test Track. One section was 7 inches thick to compare directly against a number of other sections, including the control, having the same thickness in the 2009 research cycle. The other section was 9 inches thick to examine perpetual pavement concepts and compare against existing sections of similar thickness.

At the writing of this report in September 2010, approximately one year of traffic (5 million ESAL) had been applied to the sections. Though many of the questions regarding longer-term performance will require further traffic to fully answer, some of the issues mentioned above can now be directly addressed using data generated during construction, in the laboratory and under dynamic vehicle and falling weight deflectometer (FWD) loading.

1.2 Objectives and Scope of Work

The objective of this report was to document the findings from the Shell Thiopave and control sections at the Test Track after one year of testing. The findings include data obtained during construction, laboratory-determined mechanistic properties, deflection testing, dynamic strain and pressure measurements in addition to preliminary performance results. This report will also serve as a reference document for subsequent documentation of these sections.

2. INSTRUMENTATION

Central to this investigation were the embedded earth pressure cells, asphalt strain gauges and temperature probes installed at different points in the construction process. The installation of the gauges will be discussed in the following section on construction while the gauges themselves are discussed in this section.

Figure 2.1 illustrates the gauge array used in this investigation. The instruments and arrangement were consistent with previous experiments at the Test Track (Timm et al., 2004; Timm, 2009) to provide continuity and consistency between research cycles. Within each section, an array of twelve asphalt strain gauges was used to capture strain at the bottom of the asphalt concrete. The gauges, manufactured by CTL, were installed such that longitudinal (parallel to traffic) and transverse (perpendicular to traffic) strains could be measured. Two earth pressure cells, manufactured by Geokon, were installed to measure vertical stress at the asphalt concrete/aggregate base interface. Temperature probes, manufactured by Campbell Scientific, were installed just outside the edge stripe to measure temperature at the top, middle and bottom of the asphalt concrete, in addition to 3 inches deep within the aggregate base. Full explanation regarding the sensors and arrangement has been previously documented (Timm, 2009).

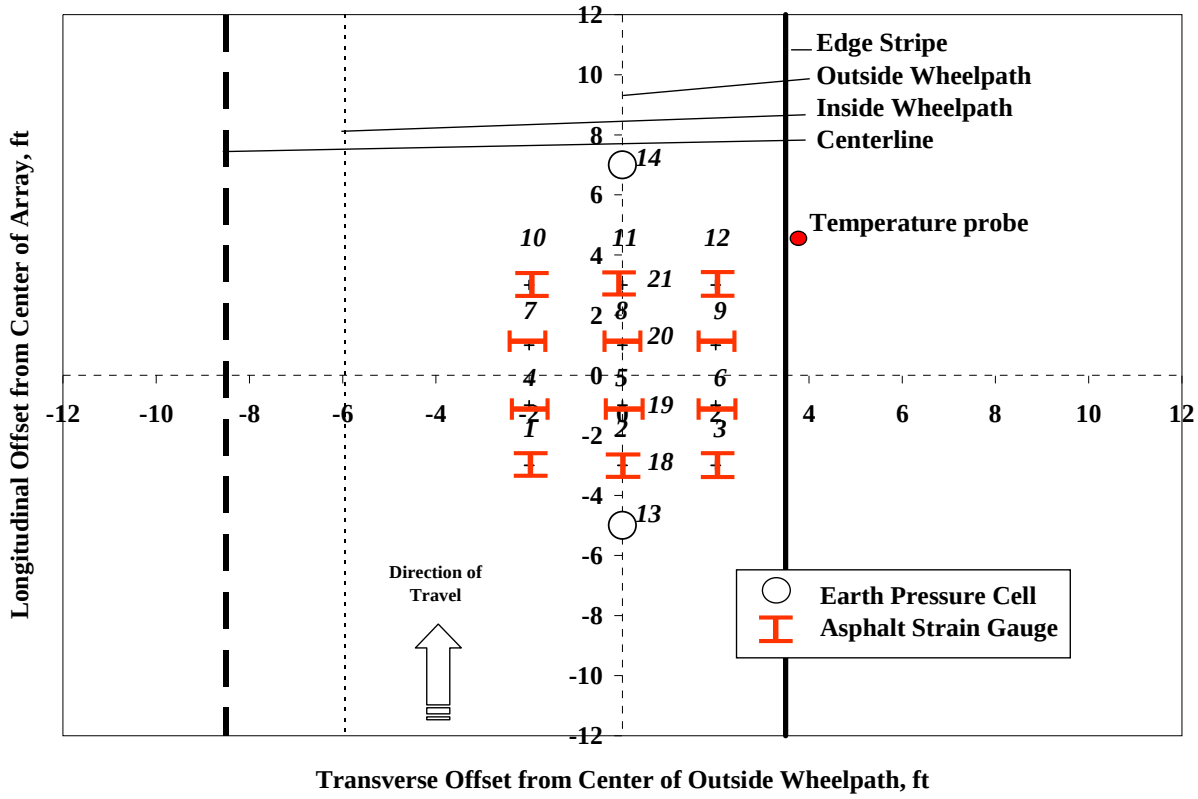

Figure 2.1 Gauge Array

3. MIX DESIGN, CONSTRUCTION AND INSTRUMENTATION INSTALLATION

This section documents the mix design, production and construction of the Thiopave sections, in addition to the control section, at the Test Track. Where appropriate, gauge installation procedures are also discussed. Figure 3.1 illustrates the as-designed pavement sections. The mix types and lift thicknesses are indicated in Figure 3.1 where the lifts are numbered top-to-bottoom (e.g., 1 = surface mix). Although previous simulations had considered using Thiopave material in the surface, discussions with the sponsor concluded in using non-Thiopave materials for the surface lifts in this specific experiment. It should be noted that Thiopave has been used in surface mixtures at the Test Track for other experiments (sections E9, W2 and W7). Also of note was that the actual plant-produced mixes contained less Thiopave than evaluated in the earlier laboratory study and intended for this investigation. This is important since the preliminary analyses and findings discussed above were based on 30 to 40 percent Thiopave. During construction of the test sections, the mixtures were produced with 22 to 39 percent Thiopave. Some differences that will be noted later in this report between predictions and measurements may be attributed to the lower-than-designed amount of Thiopave.

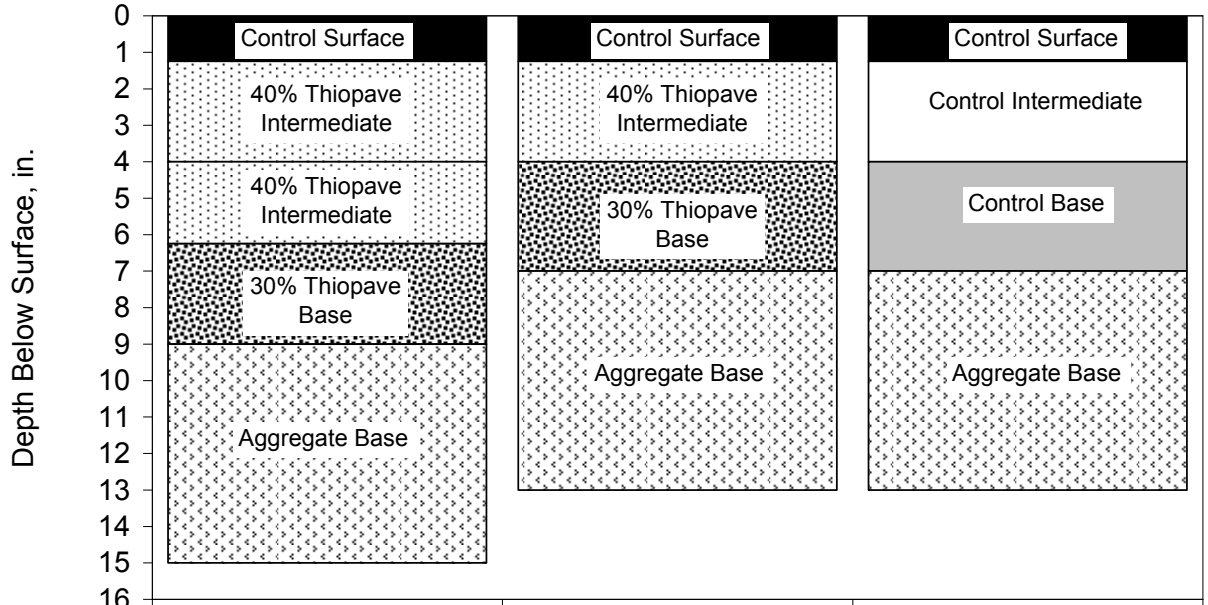

	Thiopave 9"	Thiopave 7"	Control 7"
Agg Base	6	6	6
Lift4	2.75		
Lift3	2.25	3	3
Lift2	2.75	2.75	2.75
Lift1	1.25	1.25	1.25

Figure 3.1 Cross-Section Design: Materials and Lift Thicknesses.

3.1 Mix Design

A summary of mix-design results are provided here with more details available in Appendix A. In subsequent sections, details regarding the as-built properties of the mixtures are provided.

There are five mixtures in this study that can be subdivided into "Thiopave-modified" and "Control" mixtures. The control mixtures included surface, intermediate and base courses while the Thiopave mixtures were intermediate and base courses. The aggregate gradations were a blend of granite, limestone and sand using locally-available materials. Distinct gradations were developed for each control mixture (surface, intermediate and base) to achieve the necessary volumetric targets as the binder grade and nominal maximum aggregate size (NMAS) changed between layers. The Thiopave mixture gradations matched the intermediate control mixture gradation. Table 3.1 lists the gradations by mixture type. The Thiopave asphalt mixture design executed for this experiment is available in another report (Timm et al., 2009).
The mixtures were designed using the Superpave gyratory compactor (SGC) with 80 design gyrations. This level of compaction was determined through discussion and consensus with the representative sponsor groups. Table 3.1 lists the pertinent mix design parameters and resulting volumetric properties for each of the five mixtures. Note the relatively-higher binder percentages obtained for the Thiopave mixtures resulting from lower design air voids. Specifically, the intermediate mix was design at 3.5% air voids and the base mix was designed for 2% air voids. This was done, in part, to somewhat mitigate the stiffening effect the Thiopave-modification would have on these mixtures and provide better durability.

Table 3.1 Mix Design Gradations and Properties

Mixture Type	Control			Thiopave	
Lift	Surface	Intermediate	Base	Intermediate	Base
Sieve Size, mm	**Aggregate Gradation, Percent Passing Sieve Size**				
25	100	100	100	100	100
19	100	93	93	93	93
12.5	100	82	84	82	82
9.5	100	71	73	71	71
4.75	78	52	55	52	52
2.36	60	45	47	45	45
1.18	46	35	36	35	35
0.6	31	24	25	24	24
0.3	16	12	14	12	12
0.15	10	7	8	7	7
0.075	5.8	3.9	4.6	3.9	3.9
Property	**Mix Design Parameters**				
Virgin Asphalt PG Grade	76-22	76-22	67-22	67-22	67-22
Target Thiopave, % of combined binder wt	0	0	0	40	30
Design Air Voids (VTM), %	4	4	4	3.5	2
Virgin Binder, % wt of mix	5.8	4.7	4.6	3.7	4.4
Thiopave and Compaction Aid, % wt of mix	0	0	0	2.5	1.9
Total Combined Binder (P_b), % wt of mix	5.8	4.7	4.6	6.2	6.3
Effective Binder (P_{be}), % wt of mix	5.1	4.1	4.1	5.6	5.8
Total Combined Binder (V_b), % vol of mix	13.4	11.3	11.1	12.2	13.2
Effective Binder (V_{be}), % vol of mix	11.8	10.0	9.9	11.1	12.1
Dust Proportion (DP)	1.1	0.9	1.1	0.7	0.7
Maximum Specific Gravity (G_{mm})	2.483	2.575	2.574	2.581	2.558
Voids in Mineral Aggregate (VMA), %	15.8	13.9	13.9	14.6	14.1
Voids Filled with Asphalt (VFA), %	75	71	71	76	86

3.2 Construction and Instrumentation Installation

At the Test Track, sections are designated according to their respective tangents (North = N; South = S) and section numbers (1 through 13 on each tangent). The Thiopave sections were placed in N5 and N6 while the control section was placed in S9, as shown in Table 3.2. Section placement was based on availability of sections and for ease of construction.

Table 3.2 Random Locations

	Distance From Start of Section, ft		
Random Location	N5 (Thiopave 9”)	N6 (Thiopave 7”)	S9 (Control 7”)
1	53	47	32
2	92	84	114
3	177	116	139
4 (center of gauges)	127	101	76

Within each test section, prior to any construction activities, four random longitudinal stations (RL’s) were established with three transverse offsets (outside wheelpath (OWP), inside wheelpath (IWP) and between wheelpath (BWP)) at each RL. These locations were numbered sequentially from 1 through 12 with each location corresponding to a particular RL and offset. Figure 3.2 shows these locations schematically. RL 1, 2 and 3 were randomly selected from 50-ft subsections within the center 150 ft of each section. Transition areas of 25 ft at either end of each section allow for mixture and elevation changes as needed. RL 4 was placed at the center of the instrumentation array within each section. Table 3.2 lists the random location stations for each section. These locations were important during construction in that they were the locations of nuclear density testing, and survey points for thickness. Once traffic began, they served as locations for frequent FWD testing and determination of transverse profiles.

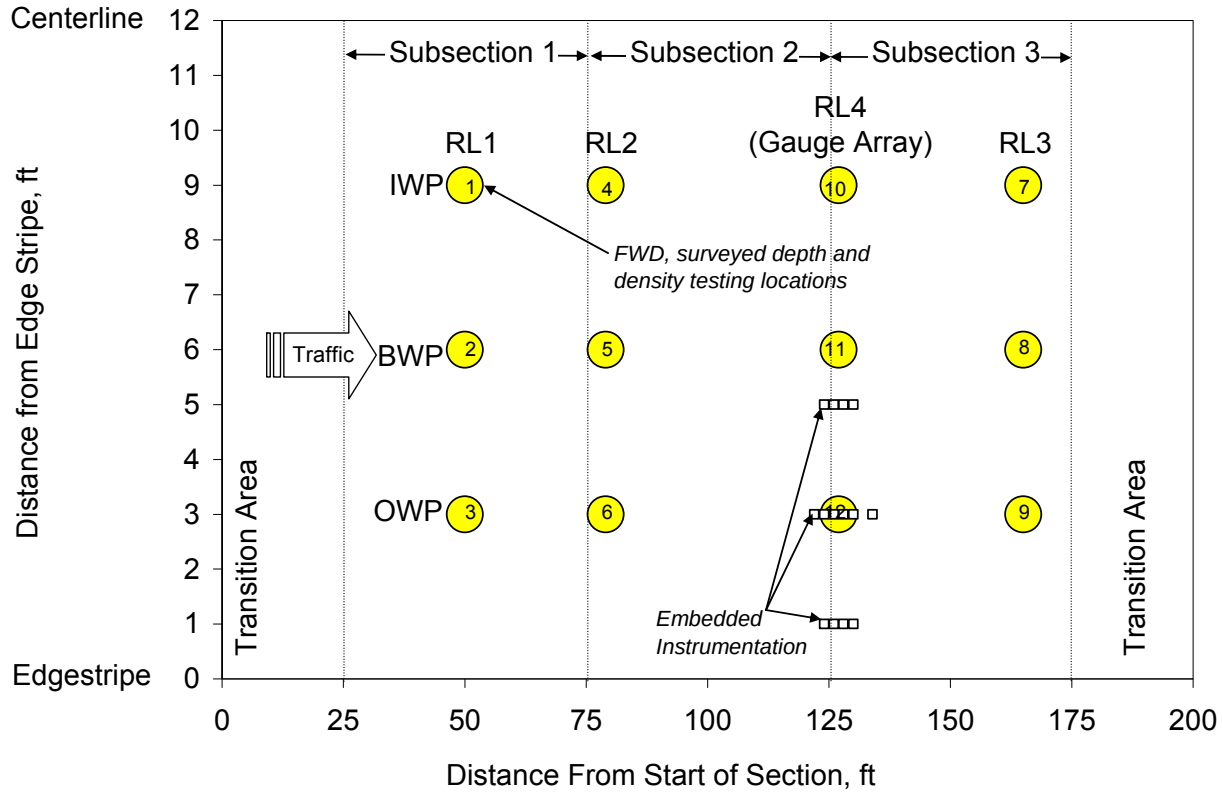

Figure 3.2 Random Location and Instrumentation Schematic

In each section, the subgrade was compacted to target density and moisture contents. Since this experiment was designed to build upon previous findings, it was imperative to build a similar foundation, in terms of moisture contents and unit weights, that had been built previously. Using as-built information from the 2003 experiment as the standard, the minimum subgrade unit weight was set at 119.9 lb/ft^3 with a target moisture content of 9%. The subgrade was consistent with the materials used in previous research cycles and has been well-documented (Taylor and Timm, 2009). The subgrade was classified as an AASHTO A-4(0) metamorphic quartzite soil obtained on-site. Table 3.3 lists the average dry unit weight and moisture content achieved in each section.

Table 3.3 Subgrade Dry Unit Weight and Moisture Contents

Test Section	N5 (Thiopave 9")	N6 (Thiopave 7")	S9 (Control 7")
Average Dry Unit Weight, lb/ft^3	122.3	123.4	123.4
Average Moisture Content, %	9.52	8.9	9.2

After the subgrade had been brought to proper elevation, density and moisture content, the subgrade earth pressure cells were installed following previously-established procedures (Timm et al., 2004; Timm, 2009). Each gauge was installed such that it was nearly flush with the top of the subgrade, with sieved subgrade material below and on top of the gauge to prevent stress concentrations or damage from stone contact on the plate surface. Figure 3.3 shows an installed plate without the covering material, while Figure 3.4 shows the final surveyed elevation being determined with only the plate face uncovered. After the final survey, cover material was hand-placed on the gauge followed by construction of the aggregate base.

Figure 3.3 Subgrade Earth Pressure Cell Installation Prior to Final Covering

Figure 3.4 Final Survey of Subgrade Earth Pressure Cell

Following earth pressure cell installation, placement of the dense-graded aggregate base commenced. The aggregate base was consistent with that used in previous research cycles and has been well-documented (Taylor and Timm, 2009). The aggregate base was a crushed granite material often used in Alabama by the state department of transportation (ALDOT). Figure 3.5 illustrates the prepared subgrade with a portion of the aggregate base in place. A small amount of aggregate base was hand placed on the earth pressure cell to protect it from construction traffic until all the material was placed and compacted.

Figure 3.5 Subgrade and Aggregate Base

The design called for approximately 6 inches of aggregate base to be placed in each section. Surveyed depths were determined at each of the 12 random locations in each section. Figure 3.6 summarizes the surveyed thicknesses at each location (values are tabulated in Appendix B). The random locations and offsets are noted in the figure and correspond to the numbering scheme in Figure 3.2. Overall, slightly less than 6 inches was placed in each section with slightly thicker aggregate base toward the outside of the lane compared to the inside of the lane. The N6 Thiopave section had significantly less aggregate base, especially at the inside wheelpath (IWP). The fact that 6 inches was not achieved uniformly is less important than knowing exactly what the thicknesses were for the purposes of mechanistic evaluation and backcalculation of FWD data. Each section was compacted to target density and moisture contents following the same guidelines for consistency as explained above for subgrade construction. The minimum unit weight was 139.5 lb/ft^3 at 4% moisture.. Table 3.4 summarizes these data for each section.

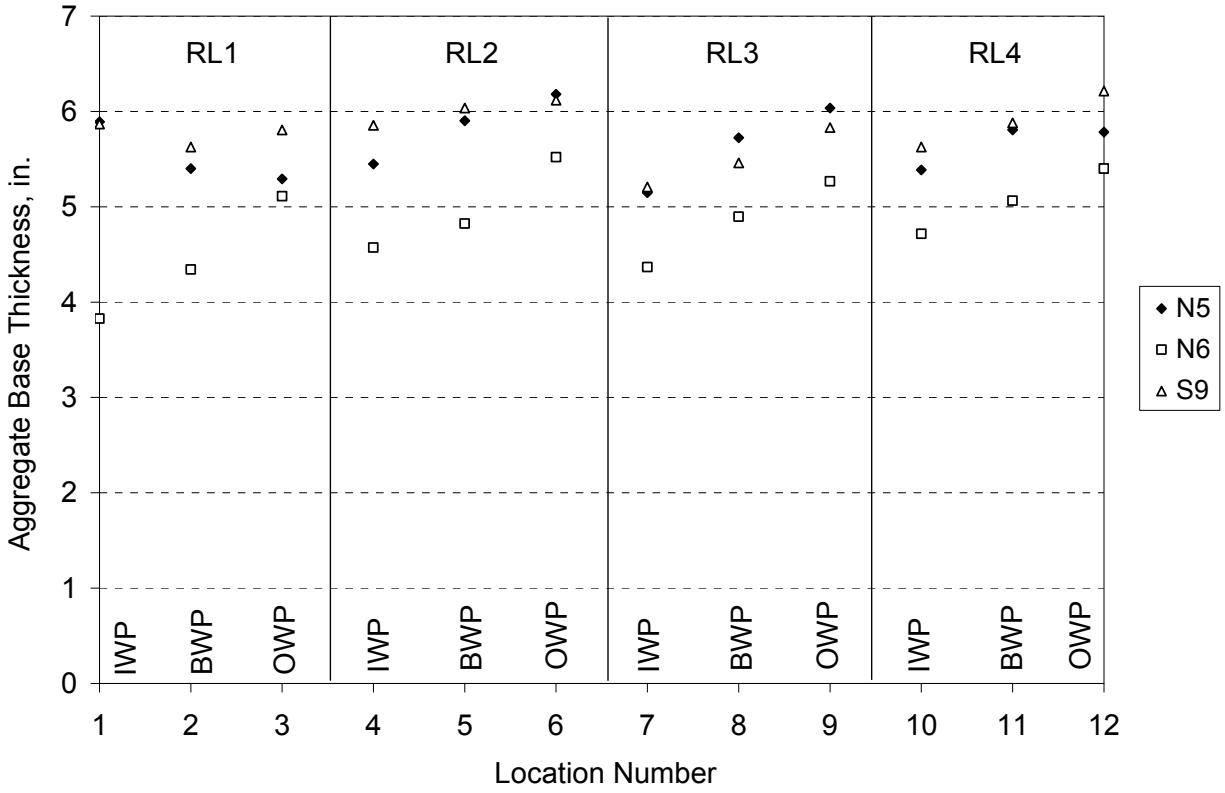

Figure 3.6 Surveyed Aggregate Base Thickness

Table 3.4 Aggregate Base Dry Unit Weight and Moisture Contents

Test Section	N5 (Thiopave 9")	N6 (Thiopave 7")	S9 (Control 7")
Average Dry Unit Weight, lb/ft^3	140.1	140.3	140.2
Average Moisture Content, %	4.2	4.1	5.0

Once the aggregate base was complete, work began on installing the asphalt strain gauges and aggregate base earth pressure cell. Again, previously-established procedures (Timm et al., 2004; Timm, 2009) were followed in laying out and installing the gauges. The sequence of photos in Figure 3.7 highlights the installation procedure and more detail can be found elsewhere (Timm et al., 2004; Timm, 2009).

(a) (b)

(c) (d)

(e)

Figure 3.7 Gauge Installation: (a) Preparing grid and laying out gauges; (b) Trench preparation; (c) Gauges placed for paving; (d) Placing protective cover material over each gauge; (e) Paving over gauges

Table 3.5 lists the dates on which each pavement lift was constructed. The lifts are numbered from top to bottom of the pavement cross section. As indicated by merged columns in the table, maximum paving lengths were achieved in N5 and N6 while paving the upper three lifts in each section. This helped maintain continuity between the sections so that the main experimental variable (thickness) could be better evaluated between these sections.

Table 3.5 Date of Paving

	Test Section		
Asphalt Layer	N5	N6	S9
Lift 1 (surface)	August 3, 2009		July 16, 2009
Lift 2	July 24, 2009		July 14, 2009
Lift 3	July 23, 2009		July 3, 2009
Lift 4 (bottom)	July 23, 2009	NA	NA

Though the primary purpose of this experiment was to validate and understand the field performance of new paving technologies, a secondary objective was to characterize asphalt mixtures using these new technologies in the laboratory. To provide materials for testing in the laboratory, each unique binder mixture was sampled in the field during the paving operation. One 5-gallon bucket of each liquid binder was sampled from the appropriate binder tank at the plant during the mixture production run. At the end of each day, the binder was taken back to the NCAT laboratory for testing purposes.

Before construction, a testing plan was developed to determine the amount of material needed per mix design to complete its laboratory characterization. This testing plan was used to determine the number of 5-gallon buckets to be filled. The testing plan varied depending on the type of mix (base, intermediate or surface mix) and the sponsor's requests for particular tests. Table 3.6 provides the tally of buckets sampled for each mix associated with this project. Upon completion of material sampling, the mix was transferred to an off-site storage facility where it was stored on pallets. Also included in Table 3.6 are the sections and lifts that the bucket samples represented.

Table 3.6 Material Inventory for Laboratory Testing

Mixture Description	Thiopave Base	Thiopave Intermediate	Control Surface	Control Base	Control Intermediate
Mixture Sampled	N5-4	N5-2	N5-1	S8-3	S8-2
Number of 5-Gallon Buckets	34	23	42	30	12
Section and Lifts Using Mix	N5-4 N6-3	N5-3 N5-2 N6-2	N5-1 N6-1 S9-1	S9-3	S9-2

Under ideal circumstances, mixture samples would have been taken from a sampling tower from the back of a truck. However, the amount of material needed to completely characterize each mixture made this sampling methodology impossible to achieve. Therefore, another sampling methodology was developed to ensure mixture quality and quantity was maintained throughout

the sampling process. When the mixtures arrived at the Test Track for paving, each truck transferred its material to the material transfer vehicle (MTV). After a sufficient amount of the mixture had been transferred into the paver, the MTV placed additional mix into the back of a flatbed truck. The mixtures were then taken back to the parking lot behind the Test Track's on-site laboratory for sampling, loading into buckets and long-term storage on pallets (Figure 3.8).

a) Unloading Mix from Truck b) Sampling Mix

c) Loading Mix into Buckets d) Mix Storage

Figure 3.8 Mixture Sampling for Lab Testing

Table 3.7 contains pertinent as-built information for each lift in each section. Lift 1 in each section was comprised of the control mixture with identical asphalt contents and similar in place density. Lifts 2 and 3 in N5 and lift 2 in N6 were designed to have 40% Thiopave, but due to production issues at the asphalt plant, lower-than-expected Thiopave contents were obtained. Similarly, the bottom lifts in N5 and N6 were intended to have 30% Thiopave but were produced at 22%. Discussions between the NCAT researchers and Shell Sulfur Solutions engineers concluded in proceeding with the experiment with these Thiopave contents. The higher total asphalt contents in the lower lifts of N5 and N6 relative to the control resulted from designing the Thiopave mixtures at 2% air voids while the control mixtures were designed at 4%. The lower design air voids were meant to yield higher asphalt contents with the expectation of better fatigue performance. It should also be noted that a PG 67-22 binder served as the base asphalt for the Thiopave mixes. The PG 76-22 mixtures (lift 1 in all sections and lift 2 in the control) were modified with SBS polymer. All sections and lifts met or exceeded 92.5% of maximum theoretical density (less than 7.5% air voids). Full details regarding each as-built lift are contained in Appendix A. It should be noted when looking at the QC versus mix design

volumetric data in Appendix A that differences in volumetric properties likely stemmed from not reaching the target Thiopave percentages during production.

Table 3.7 As-Built Properties of Asphalt Concrete

Section	N5 (Thiopave 9")				N6 (Thiopave 7")			S9 (Control 7")		
Lift	1	2	3	4	1	2	3	1	2	3
NMAS, mm[a]	9.5	19	19	19	9.5	19	19	9.5	19	19
PG Grade (Virgin Binder)[b]	76-22	67-22	67-22	67-22	76-22	67-22	67-22	76-22	76-22	67-22
Delivery Temperature, F[c]	288	243	229	225	282	238	249	275	316	254
% Total Binder[d]	6.1	5.7	5.6	6.2	6.1	5.7	6.1	6.1	4.4	4.7
% Thiopave[e]	0	39	33	22	0	35	22	0	0	0
$\%G_{mm}$[f]	94.1	93.0	92.9	93.6	93.8	92.9	93.7	93.1	92.8	92.6

[a]NMAS: nominal maximum aggregate size
[b]PG Grade (Virgin Binder): asphalt grade without Thiopave modification
[c]Delivery Temperature: surface temperature of mix measured directly behind paver with infrared device
[d]% Total Binder: total gravimetric asphalt content (includes Thiopave material where indicated). Determined by ignition oven.
[e]%Thiopave: percent of total binder percentage that is Thiopave
[f]$\%G_{mm}$: percent of maximum theoretical density

Of particular interest in Table 3.7 were the measured temperatures behind the paver. The Thiopave system includes a warm mix additive that allows for lower production temperatures as demonstrated by the reduced temperatures in the lower lifts of N5 and N6 relative to the lower lifts in S9. Additionally, during construction, temperatures were monitored over time for each lift. The purpose was to evaluate whether the Thiopave system behaved in a fundamentally-different manner in terms of cooling rates relative to HMA.

The evaluation of temperature was made by measuring surface temperature approximately every three minutes after the mat was placed until final compaction was achieved. Simulations of mat cooling were then conducted using relevant input data such as time of day, paving date and ambient conditions. The simulations were conducted using the MultiCool software which was originally developed in Minnesota (Chadbourn et al., 1998) for cold weather conditions and adapted for multilayer conditions in California (Timm et al., 2001). Since MultiCool uses fundamental heat transfer equations coupled with assumed material properties, significant differences between the measured and predicted cooling rates would signify a material behaving in a fundamentally-different manner or having different heat-transfer properties.

Further details regarding the temperature investigation are documented elsewhere (Vargas and Timm, 2011), while the measured and simulated cooling curves are presented in Figures 3.9, 3.10 and 3.11 for N5, N6 and S9, respectively. Based on these data, it was concluded that MultiCool provided satisfactory predicted cooling curves for each material tested. In fact, the MultiCool predictions were somewhat better for the Thiopave materials than the control mixtures. This indicates that the materials are cooling in a similar manner and can be simulated with confidence using the MultiCool software.

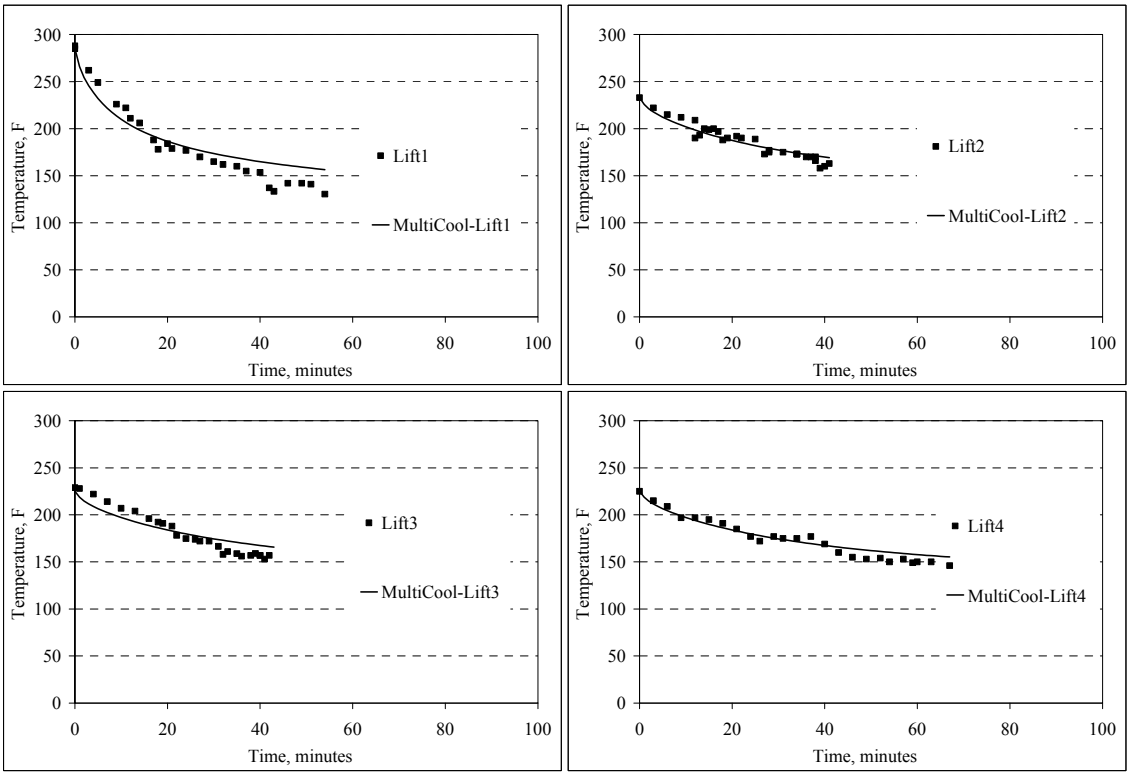

Figure 3.9 N5 Measured and Predicted Cooling Curves (Lifts 1, 2, 3 and 4)

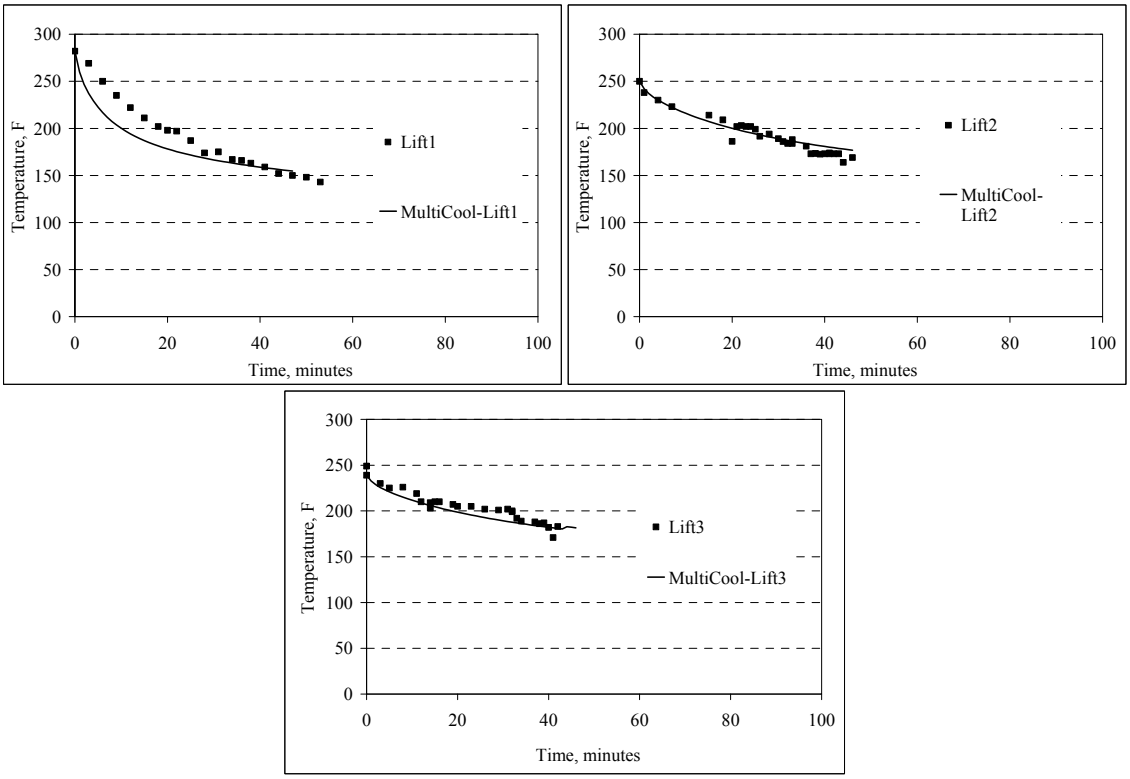

Figure 3.10 N6 Measured and Predicted Cooling Curves (Lifts 1, 2 and 3)

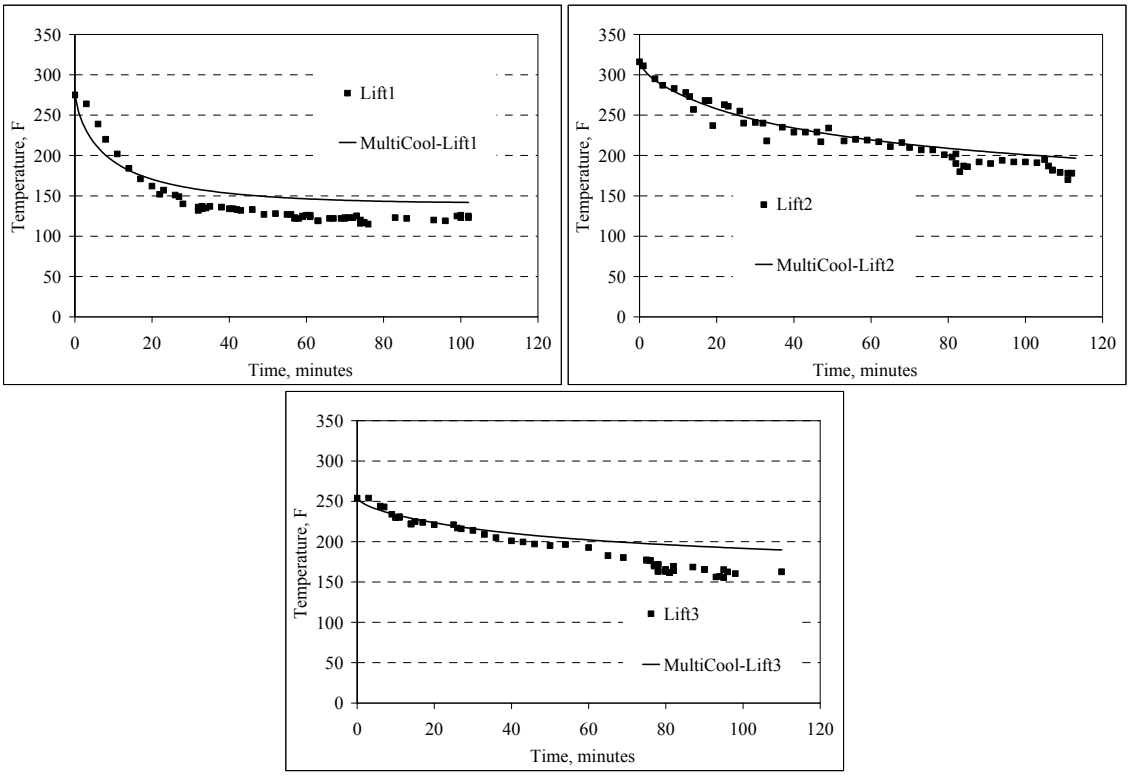

Figure 3.11 S9 Measured and Predicted Cooling Curves (Lifts 1, 2 and 3)

After paving each lift of AC, depths at the 12 locations (Figure 3.2) within each section were surveyed. This provided very specific lift thickness information in addition to overall pavement depth. Figure 3.12 summarizes these data by providing average depths for each lift of each section. More detailed information is contained in Appendix B. Overall, the sections were constructed very close to their target AC thicknesses (9 inches for N5; 7 inches for N6 and S9).

Soon after paving was complete, temperature probes were installed in each section. The probes were installed as an array of four thermistors to provide temperature at the pavement surface, mid-AC, bottom-AC and 3 inches below AC. Figure 3.13 illustrates two parts of the probe installation. After the vertical hole had been drilled, the probes were coated in roofing asphalt and inserted into the hole. The cable was tacked to the bottom of the slot running to the edge of the pavement, then run through conduit into the data acquisition box.

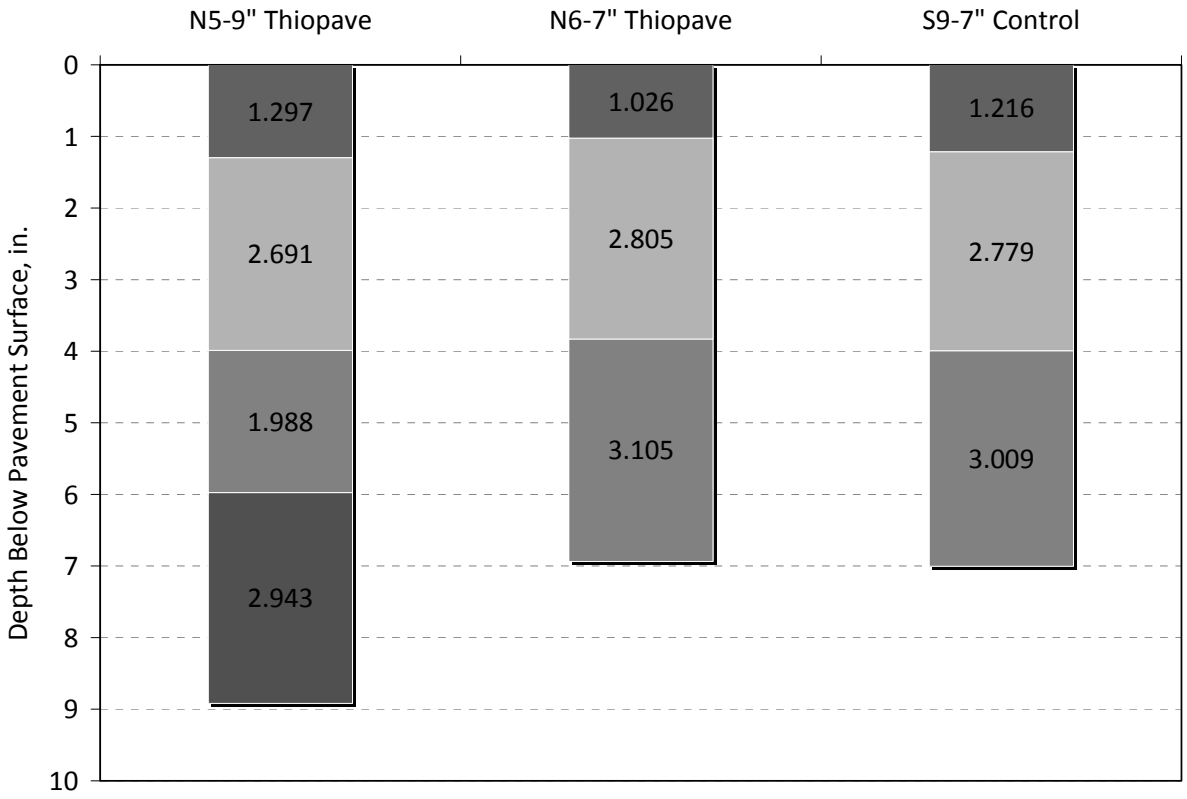

Figure 3.12 Average Lift Thicknesses

Figure 3.13 Temperature Probe Installation

At the conclusion of construction, all gauges were checked for functionality. Figure 3.14 shows the survival rate for the strain gauges in each of the three sections. The figure indicates that all strain gauges survived construction in N5 and N6 while 83.3% (10 of 12) gauges survived in the control section (S9). However, when redundancy was considered, S9 had one gauge survive in each of the three offsets (center-, right-, left-of-wheelpath) and directions (longitudinal and transverse). All the pressure plates survived the construction process.

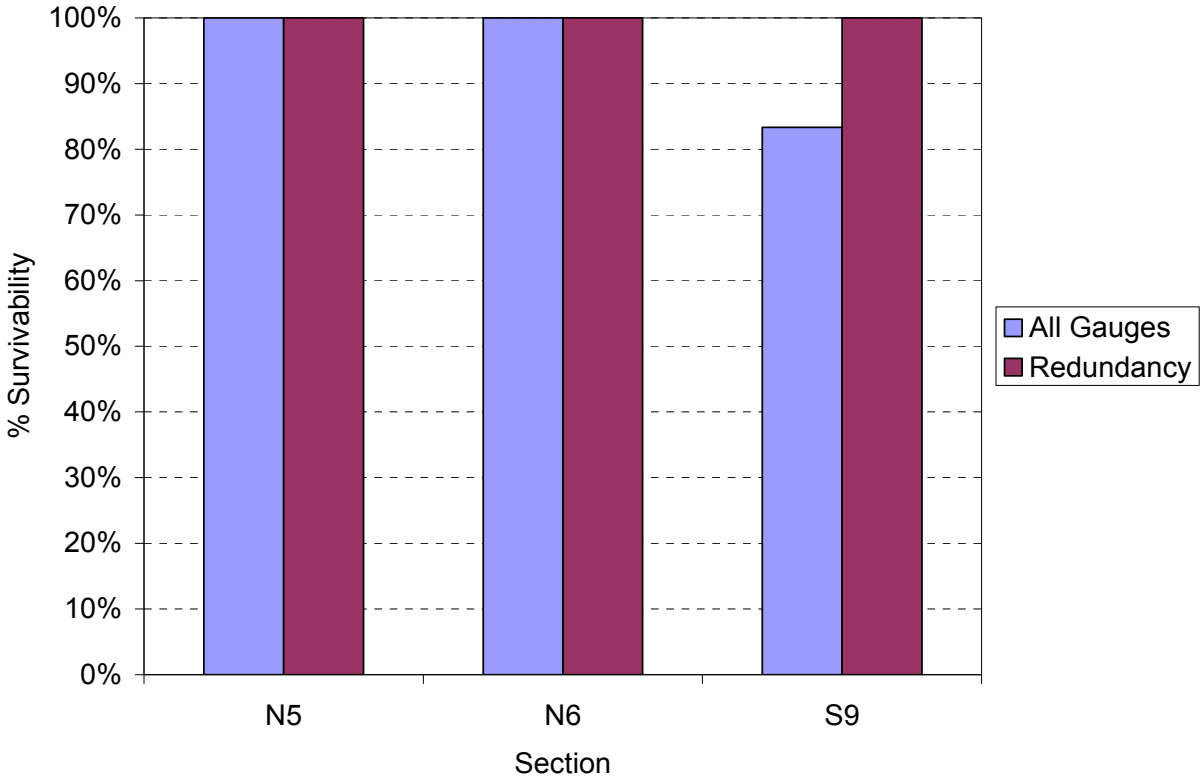

Figure 3.14 Asphalt Strain Gauge Survivability

4. LABORATORY TESTING ON BINDERS AND PLANT PRODUCED MIXTURES

During production of the mixtures, as described previously, samples of binder and mix were obtained for laboratory testing and characterization. The following subsections detail the tests conducted and results for each mixture and binder.

4.1 Compaction of Performance Testing Specimens from Plant-Produced Mixes

For the 2009 research cycle at the Test Track, a large amount of plant-produced mix was sampled to perform a wide range of laboratory performance tests. These mixtures were sampled in labeled 5-gallon buckets and sent to the NCAT laboratory for fabrication and testing.

The first step in the sample fabrication process was to verify the maximum theoretical specific gravity of each mix (G_{mm}) using the AASHTO T209-09 procedure. During construction of the Test Track, this test was performed on each mix as it was constructed. The results of these tests will be collectively termed "QC G_{mm}". A verification test was also performed on the re-heated mix at the NCAT lab. For sample fabrication, the QC G_{mm} value from the Test Track was used if the NCAT lab G_{mm} fell within the variability allowed by the multi-laboratory precision statement in section 13 of AASHTO T209-09. For most of the mixes produced during the 2009 Test Track reconstruction, the QC G_{mm} value was used. However, for those mixes where the Test Track G_{mm} and NCAT lab G_{mm} did not agree, as was the case for the Thiopave mixtures, the NCAT lab G_{mm} was used. Further investigation of these differences was warranted and is ongoing, but outside the scope of the report. The NCAT lab G_{mm} value was used since the G_{mm} was thought to be more representative of the re-heated material. A summary of the G_{mm} values used for

performance specimen fabrication, as well as the results for all G_{mm} tests conducted for this study, can be found in Table 4.1.

Table 4.1 Summary of G_{mm} and Laboratory Compaction Temperatures

Mix Description	Lab Compaction Temp, F	QC G_{mm}	Lab G_{mm}	G_{mm} Difference	G_{mm} for Lab Samples
Thiopave Base	250	2.518	2.495	0.023	2.495
Thiopave Intermediate	250	2.554	2.529	0.025	2.529
Control Base	290	2.540	2.538	0.002	2.540
Control Intermediate	310	2.556	2.543	0.013	2.556
Control Surface	310	2.472	2.464	0.008	2.472

For specimen fabrication, the mix was re-heated in the 5-gallon buckets sampled during production at approximately 20°F above the documented lay-down temperature at the Test Track. When the mix was sufficiently workable, the mix was placed in a splitting pan. A quartering device was then used to split out appropriate sized samples for performance testing. The splitting was done in accordance with the procedure in AASHTO R47-08. The individual samples of mix were returned to an oven set to 10-20°F above the target compaction temperature. Once a thermometer in the loose mix reached the target compaction temperature, the mix was compacted into the appropriately-sized performance testing specimen. No short-term mechanical aging (AASHTO R30) was conducted on the plant-produced mixes from the Test Track since these mixes had already been short-term aged during the plant production process. More discussion of specimen properties will be provided (sample height, target air voids, etc.) when the individual performance tests are discussed below.

A summary of the target compaction temperatures for this project are provided in Table 4.1. The Thiopave-modified mixtures were treated a little differently from the control mixtures. The target compaction temperature for these mixtures was 250°F. However, to achieve re-activation of the sulfur-modifier in the reheating process, these mixes were reheated to 285°F and thoroughly stirred prior to being allowed to cool to the compaction temperature. This was done on the advice of Shell Sulfur Solutions engineers.

4.2 Binder Properties

The virgin binders in the asphalt mixtures used in Sections S9, N5 and N6 were sampled at the plant for testing, except for the virgin binder (PG 76-22) used in the surface mix, which was mistakenly sampled. This PG 76-22 binder was extracted from the surface mixture, and the recovered binder was tested instead of the virgin binder mistakenly sampled at the plant. Testing of the virgin binder modified with Thiopave was not feasible. Recall that the Thiopave is added

to the aggregate/virgin binder/additive blend rather than independently with the binder/additive. This would require extraction and recovery from a mixture to perform binder testing. However, since the specific gravity of the sulfur (1.92) and virgin binder (1.03) are appreciably different, the extraction and recovery process does not yield a homogeneous sample sufficient for binder testing. All the binders used in the three sections were tested in the NCAT binder laboratory to determine the performance grade (PG) and high temperature creep-recovery properties. Testing results are described in the following sections.

4.2.1 PG Grading

The binders were tested and graded according to AASHTO M320. Detailed results are presented in Appendix C. Table 4.2 summarizes the true grade and performance grade of each binder. The results confirmed that all the binders used in the construction of the three sections were as specified in the mix designs.

Table 4.2 Grading of Binders

Mixture	True Grade	Performance Grade
Base Lifts of N5 and N6	69.1 – 24.8	64 – 22
Intermediate Lifts of N5 and N6	68.9 – 26.2	64 – 22
Base Lifts of S9	69.5 – 26.0	64 – 22
Intermediate Lifts of S9	78.6 – 25.5	76 – 22
Surface Lifts of S9, N5 and N6	81.7 – 24.7	76 – 22

Note: The first three binders were graded as PG 67-22 in the southeast.

4.2.2 Multiple Stress Creep Recovery (MSCR)

The AASHTO TP 70-09 test method was followed to determine the non-recoverable creep compliance of the binders. The same rolling thin film oven (RTFO) aged specimen utilized in dynamic shear rheometer (DSR) was also used in the MSCR test. Table 4.3 summarizes the MSCR testing results. Table 4.4 shows the acceptable non-recoverable creep compliance at 3.2 kPa and percent differences for varying levels of traffic as specified in AASHTO MP 19-10. Based on the MSCR test results, it can be concluded that the virgin binder used in the base layers of Sections N5 and N6 met the standard traffic "S" grade, and the other virgin binders met the heavy traffic level "H" grade. According to AASHTO MP 19-10, standard grade "S" is for traffic levels fewer than 10 million ESALs and normal-moving traffic (>70 km/h), and high grade "H" is for traffic levels of 10 to 30 million ESALs or slow moving traffic (20 to 70 km/h).

Table 4.3 Non-Recoverable Creep Compliance at Multiple Stress Levels

Mixture	Test Temperature	$J_{nr0.1}$ (kPa^{-1})	$J_{nr3.2}$ (kPa^{-1})	J_{nrdiff} (%)	Traffic Grade
Base Lifts of N5 and N6	64°C	1.86	2.09	12.4	S
Binder Lifts of N5 and N6	64°C	1.17	1.42	21.4	H
Base Lift of S9	64°C	1.68	1.95	16.1	H
Binder Lift of S9	76°C	0.84	1.15	36.9	H
Surface Lift of S9, N5 and N6	76°C	0.98	1.37	39.8	H

Table 4.4 Requirements for Non-Recoverable Creep Compliance (AASHTO MP 19-10)

Traffic Level	Max $J_{nr3.2}$ (kPa^{-1})	Max J_{nrdiff} (%)
Standard Traffic "S" Grade	4.0	75
Heavy Traffic "H" Grade	2.0	75
Very Heavy Traffic "V" Grade	1.0	75
Extremely Heavy Traffic "E" Grade	0.5	75

Note: The specified test temperature is typically the PG high temperature from AASHTO MP 19.

4.3 Dynamic Modulus Testing

Dynamic modulus testing was performed for each of the plant-produced mix types placed during the 2009 Test Track research cycle. Due to sampling limitations, if a particular mix design was placed in multiple lifts or sections, this mix was only sampled one time and tested as representative of that mix type.

The samples for this testing were prepared in accordance with AASHTO PP 60-09. The samples were compacted to a height of 170 mm and a diameter of 150 mm and prepared to meet the tolerances outlined in Table 4.5. The tolerances in Table 4.5 represent tolerances on the final sample that had been cut and cored from the interior of the larger SGC sample. Three samples were prepared for testing from each mix.

Table 4.5 Production Tolerances for Dynamic Modulus and Flow Number Specimens (AASHTO PP60-09)

Parameter	Tolerance
Average Diameter	100 to 104 mm
Standard Deviation of Diameter	≤ 0.5 mm
Height	147.5 mm to 152.5 mm
End Flatness	≤ 0.5 mm
End Perpendicularity	≤ 1.0 mm
Sample Air Voids	7 ± 0.5%

Dynamic modulus testing was performed in an IPC Global Asphalt Mixture Performance Tester (AMPT), shown in Figure 4.1. Dynamic modulus testing was performed to quantify the stiffness behavior of the asphalt mixture over a wide range of testing temperatures and loading rates (or frequencies). The temperatures and frequencies used for the Test Track mixes were those recommended by AASHTO PP 61-09. For this methodology, the high test temperature was dependent on the high PG grade of the base binder in the mixture. Table 4.6 shows the general outline of temperatures and frequencies used, while Table 4.7 shows the selection criteria for the high testing temperature. It should be noted, however, that the high test temperature could be reduced in the event that poor quality test data were collected. Data quality will be further defined below.

Figure 4.1 IPC Global Asphalt Mixture Performance Tester

Table 4.6 Temperatures and Frequencies used for Dynamic Modulus Testing

Test Temperature (^{o}C)	Loading Frequencies (Hz)
4.0	10, 1, 0.1
20.0	10, 1, 0.1
High Testing Temperature	10, 1, 0.1, 0.01

Table 4.7 High Test Temperature for Dynamic Modulus Testing

High PG Grade of Base Binder	High Test Temperature (^{o}C)
PG 58-XX and softer	35
PG 64-XX and PG 70-XX	40
PG 76-XX and stiffer	45

Dynamic modulus testing was performed in accordance with AASHTO TP 79-09. This testing was performed both confined and unconfined. The confined testing was conducted at 20 psi confining pressure and each compacted specimen was tested at all temperatures and frequencies in the confined mode before proceeding with unconfined testing. Test data were screened for data quality in accordance with the limits set in AASHTO TP 79-09. A summary of these data quality statistics is given in Table 4.8. Variability of dynamic modulus values at specific temperatures and frequencies were checked to have a coefficient of variation (COV) at or below 13%. All data were checked for reasonableness as well (reduction in moduli with increasing temperature, slower loading). Data with borderline data quality statistics were evaluated on a case by case basis.

Table 4.8 Dynamic Modulus Data Quality Threshold Values

Data Quality Statistic	Limit
Deformation Drift	No Limit in Direction of Applied Load
Peak-to-Peak Strain	75 to 125 microstrain (unconfined tests)
	85 to 115 microstrain (confined tests)
Load Standard Error	< 10%
Deformation Standard Error	< 10%
Deformation Uniformity	< 30%
Load Drift	< 2%
Phase Angle Uniformity	< 3°

The collected data were then analyzed for two specific purposes. First, the data were used to generate a master curve for each individual mix. The master curve uses the principle of time-temperature superposition to horizontally shift data at multiple temperatures and frequencies to a reference temperature so that the stiffness data can be viewed without temperature as a variable. This method of analysis allows for visual relative comparisons to be made between multiple mixes. An example of using the time-temperature superposition principle to generate a master curve is shown in Figure 4.2.

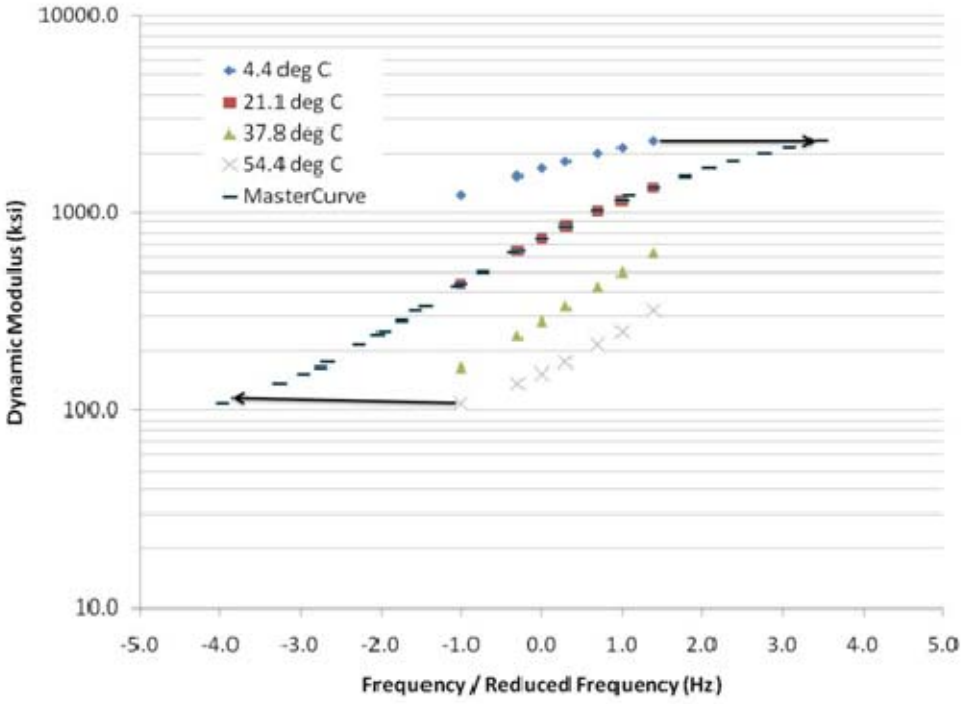

Figure 4.2 Example Master Curve Generation

Secondly, generation of the master curve also allows for creation of the dynamic modulus data over the entire range of temperatures and frequencies required for mechanistic-empirical pavement design using the MEPDG. By having an equation for the curve describing the stiffness behavior of the asphalt mix, both interpolated and extrapolated data points at various points along the curve can then be calculated. The temperatures and frequencies needed as an input for

the MEPDG are listed in Section 10.6.1 of AASHTO PP 61-09. Also, it must be noted that only unconfined master curve data should be entered into the MEPDG since calibration of the design system was originally based on unconfined master curves.

Data analysis was conducted per the methodology in AASHTO PP 61-09. The general form of the master curve equation is shown as Equation 4.1. As mentioned above, the dynamic modulus data were shifted to a reference temperature. This was done by converting testing frequency to a reduced frequency using the Arrhenius equation (Equation 4.2). Substituting Equation 4.2 into 4.1 yields the final form of the master curve equation, shown as Equation 4.3. The shift factors required at each temperature are given in Equation 4.4 (the right-hand portion of Equation 4.2). The limiting maximum modulus in Equation 4.3 was calculated using the Hirsch Model, shown as Equation 4.5. The P_c term, Equation 4.6, is simply a variable required for Equation 4.5. A limiting binder modulus of 1 GPa was assumed for this equation. Non-linear regression was conducted using the Solver function in EXCEL® to develop the coefficients for the master curve equation. Typically, these curves have an S_e/S_y term of less than 0.05 and an R^2 value of greater than 0.99. Definitions for the variables in Equations 4.1-4.6 are given in Table 4.9.

$$Log|E^*| = \delta + \frac{(Max - \delta)}{1 + e^{\beta + \gamma log f_r}} \tag{4.1}$$

$$log f_r = \log f + \frac{\Delta E_a}{19.14714}\left[\frac{1}{T} - \frac{1}{T_r}\right] \tag{4.2}$$

$$log|E^*| = \delta + \frac{(Max - \delta)}{1 + e^{\beta + \gamma\left[log f + \frac{\Delta E_a}{19.14714}\left[\frac{1}{T} - \frac{1}{T_r}\right]\right]}} \tag{4.3}$$

$$\log[a(T)] = \frac{\Delta E_a}{19.14714}\left[\frac{1}{T} - \frac{1}{T_r}\right] \tag{4.4}$$

$$|E^*|_{max} = P_c\left[4{,}200{,}000\left(1 - \frac{VMA}{100}\right) + 435{,}000\left(\frac{VFA * VMA}{10{,}000}\right) + \frac{1 - P_c}{\frac{\left(1 - \frac{VMA}{100}\right)}{4{,}200{,}000} + \frac{VMA}{435{,}000(VFA)}}\right] \tag{4.5}$$

$$P_c = \frac{\left(20 + \frac{435{,}000(VFA)}{VMA}\right)^{0.58}}{650 + \left(\frac{435{,}000(VFA)}{VMA}\right)^{0.58}} \tag{4.6}$$

Table 4.9 Master Curve Equation Variable Descriptions

Variable	Definition
|E*|	Dynamic Modulus, psi
δ,β, and γ	Fitting Parameters
Max	Limiting Maximum Modulus, psi
f_r	Reduced frequency at the reference temperature, Hz
f	The loading frequency at the test temperature, Hz
ΔE_a	Activation Energy (treated as a fitting parameter)
T	Test Temperature, ^oK
T_r	Reference Temperature, ^oK
a(T)	The shift factor at Temperature, T
$\|E^*\|_{max}$	The limiting maximum HMA dynamic modulus, psi
VMA	Voids in Mineral Aggregate, %
VFA	Voids filled with asphalt, %

The dynamic modulus results for both the Thiopave-modified and group experiment control sections at the Test Track are documented in the following paragraphs. Five plant-produced mix types were tested. Appendix D contains the complete dynamic modulus data set that is required for conducting an MEPDG analysis with these mixes. Tables 4.10 and 4.11 show the regression coefficients and fitting statistics for the individual master curves for the unconfined and confined tests, respectively

Table 4.10 Master Curve Coefficients – Unconfined

Mix ID	$\|E^*\|_{max}$, ksi	δ, ksi	β	γ	ΔE_A	R^2	Se/Sy
Control-Surface	3057.15	6.20	-0.799	-0.484	198757.5	0.995	0.050
Control-Intermediate	3189.49	8.86	-1.246	-0.472	198827.1	0.997	0.038
Control-Base	3177.54	6.52	-1.086	-0.522	178209.5	0.992	0.063
Thiopave-Intermediate	3104.14	22.11	-1.312	-0.555	193248.8	0.997	0.039
Thiopave-Base	3058.94	11.06	-1.053	-0.519	194778.4	0.996	0.042

Table 4.11 Master Curve Coefficients – 20 psi Confinement

Mix ID	$\|E^*\|_{max}$, ksi	δ, ksi	β	γ	ΔE_A	R^2	Se/Sy
Control-Surface	3057.15	62.92	-0.118	-0.560	191188.3	0.994	0.053
Control-Intermediate	3189.49	90.93	-0.491	-0.549	202747.7	0.997	0.039
Control-Base	3177.54	77.56	-0.321	-0.602	179802.0	0.994	0.056
Thiopave-Intermediate	3104.14	114.46	-0.787	-0.615	192773.0	0.991	0.066
Thiopave-Base	3058.94	84.38	-0.407	-0.556	207017.3	0.998	0.034

The master curve data are presented graphically in two ways for both the confined and unconfined data. Figures 4.3 and 4.5 (for unconfined and confined dynamic modulus, respectively) shows the dynamic modulus data on a log scale so as to better describe the relative stiffness of the mixes at higher temperatures and slower loading rates. Figures 4.4 and 4.6 (for unconfined and confined dynamic modulus, respectively) show the dynamic modulus data on an arithmetic scale so as to better show the relative stiffness of the different mixes at colder temperatures and faster loading rates.

Figure 4.3 shows that the control surface mix was the softest mix across the full range of temperatures and frequencies in an unconfined state. This mix was used in both Thiopave sections and the control section. The stiffest mix was the Thiopave-modified intermediate course followed by the control intermediate course with a polymer modified binder. The Thiopave-modified base course showed higher moduli at the high temperature, low frequency end of the spectrum than the control base course with unmodified binder. However, these mixes showed similar stiffness behavior at the intermediate temperatures and frequencies. Figure 4.4 shows the same results, but presented on an arithmetic scale for a different perspective.

Comparing the mixtures for both the confined and unconfined testing, it appears that the presence of confinement did not have a dramatic effect on the relative ranking of the mixtures in terms of modulus. Little effect was seen on the modulus values at the cold temperature, faster loading frequency portion of the curve. The relative rankings of the mixes remained the same at the high temperature, slow loading frequency end of the curve. However, the modulus magnitudes were increased due to the effects of confinement versus that of the unconfined specimens. This was particularly evident at the lower reduced frequencies (i.e., below 1 Hz). At the lowest reduced frequency, there was an approximate order of magnitude increase in the dynamic modulus for all mixtures.

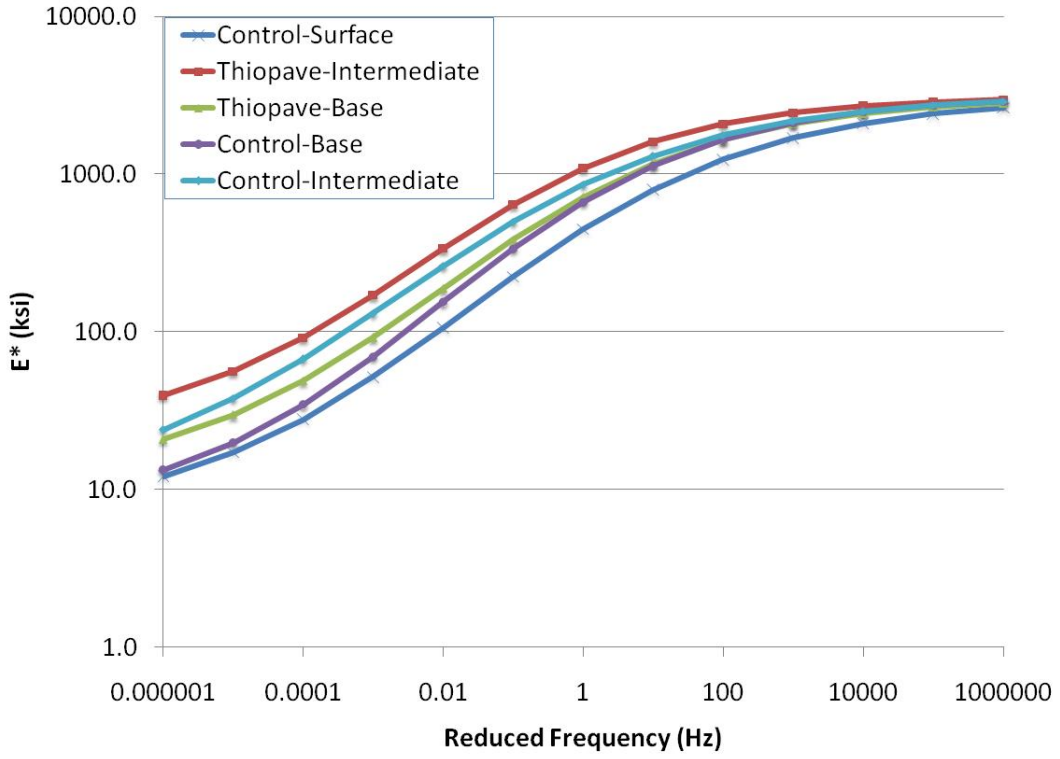

Figure 4.3 Unconfined Dynamic Modulus Testing Results (Logarithmic Scale)

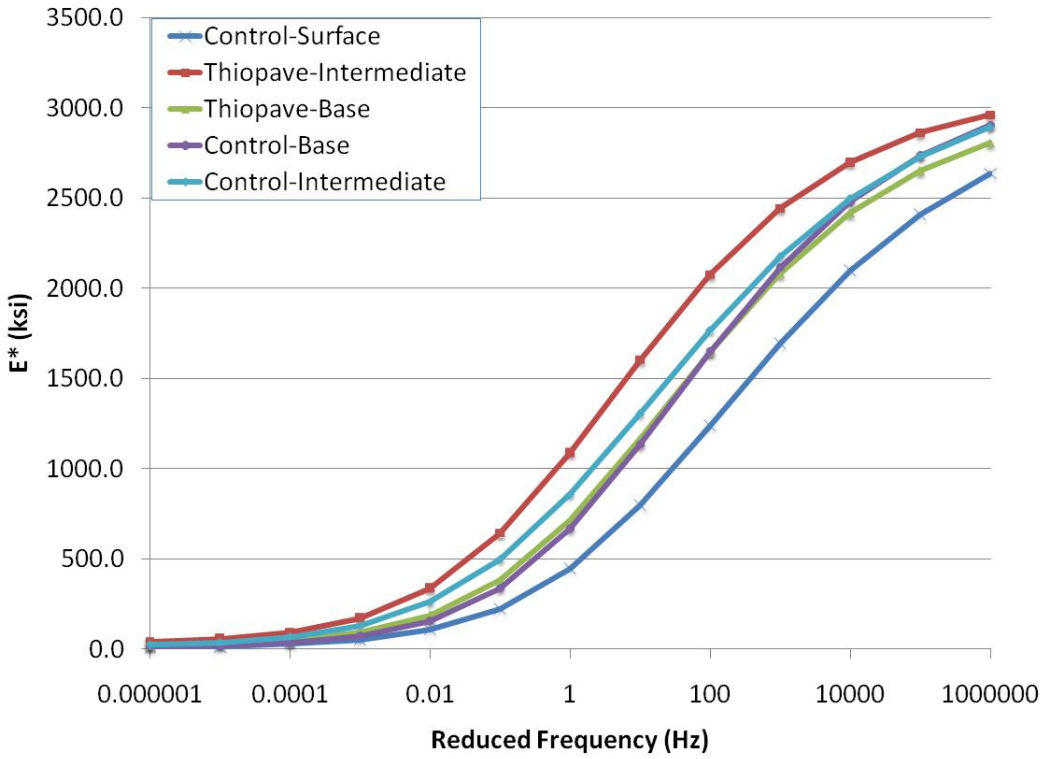

Figure 4.4 Unconfined Dynamic Modulus Testing Results (Arithmetic Scale)

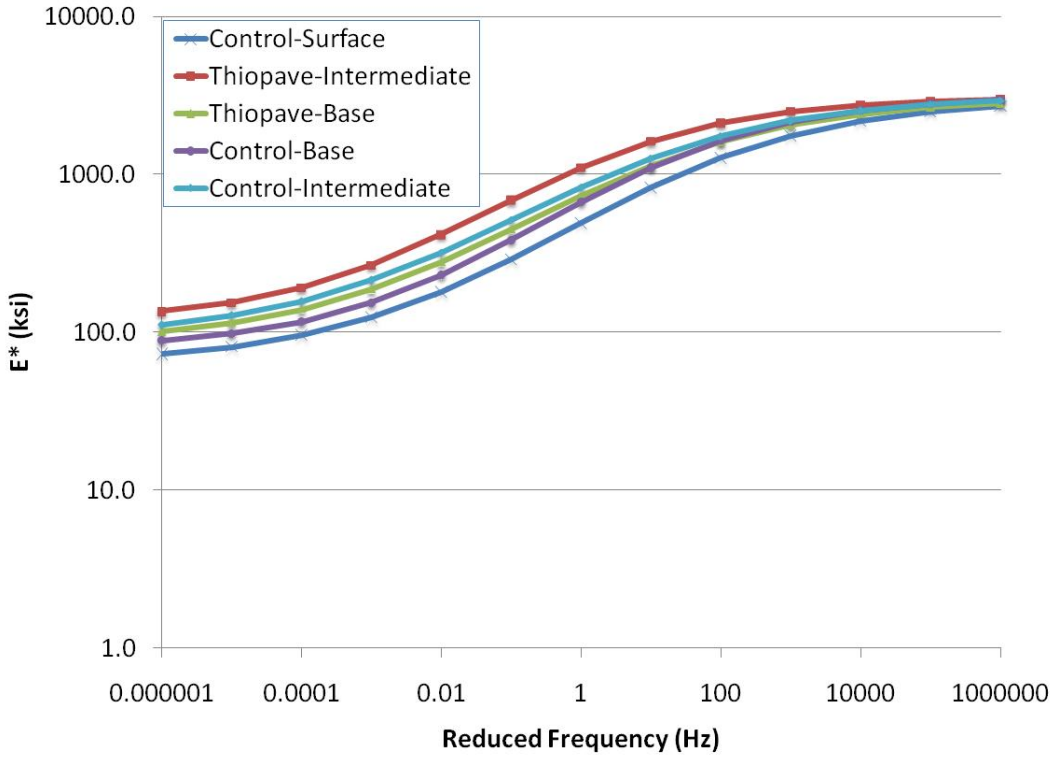

Figure 4.5 Confined Dynamic Modulus Testing Results (Logarithmic Scale)

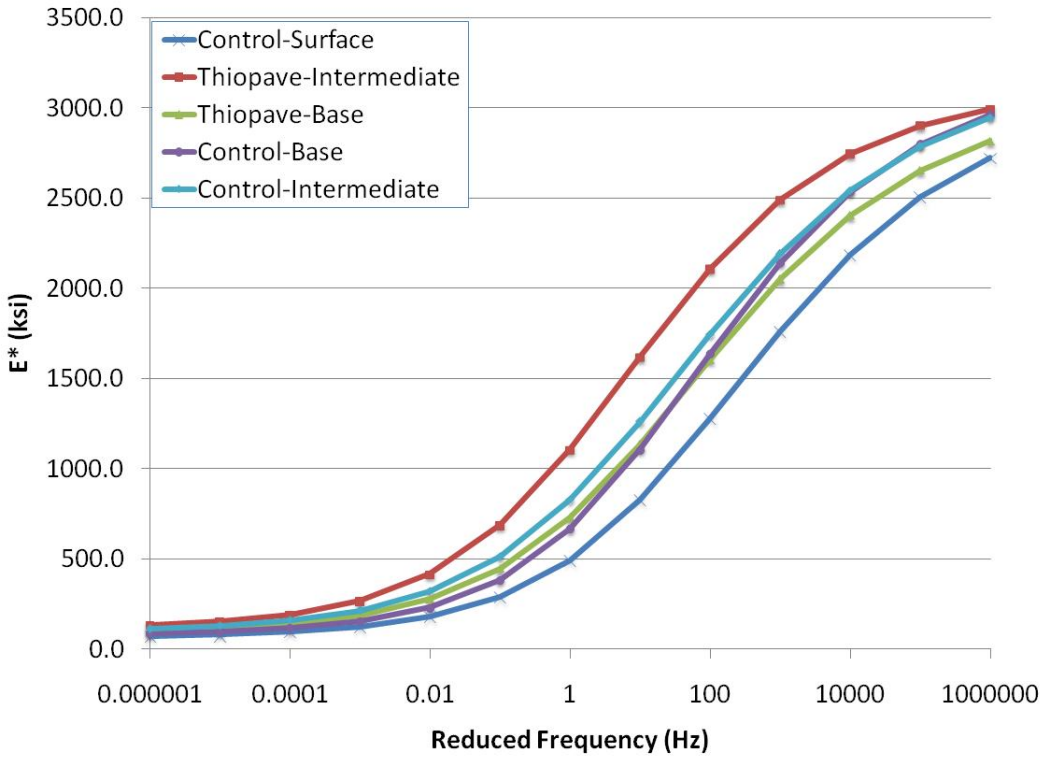

Figure 4.6 Confined Dynamic Modulus Testing Results (Arithmetic Scale)

4.4 Beam Fatigue Testing

Bending beam fatigue testing was performed in accordance with AASHTO T 321-07 to determine the fatigue limits of the 19.0 NMAS asphalt mixtures listed in Section 4.1. These were the base mixtures of the Thiopave and control sections. Six beam specimens were tested for each mix. Within each set of six, two beams each were tested at 200, 400, and 800 microstrain.

The specimens were originally compacted in a kneading beam compactor, shown in Figure 4.7, then trimmed to the dimensions of 380 ± 6 mm in length, 63 ± 2 mm in width, and 50 ± 2 mm in height. The beams were compacted to a target air void level of 7 ± 1.0 percent. Additionally, the orientation in which the beams were compacted (top and bottom) was marked and maintained for the fatigue testing as well.

The beam fatigue apparatus, shown in Figure 4.8, applies haversine loading at a frequency of 10 Hz. During each cycle, a constant level of strain is applied to the bottom of the specimen. The loading device consists of 4-point loading and reaction positions which allow for the application of the target strain to the bottom of the test specimen. Testing was performed at 20 ± 0.5°C. Data acquisition software was used to record load cycles, applied loads and beam deflections. The software also computed and recorded the maximum tensile stress, maximum tensile strain, phase angle, beam stiffness, dissipated energy, and cumulative dissipated energy at user-specified load cycle intervals.

Figure 4.7 Kneading Beam Compactor

Figure 4.8 IPC Global Beam Fatigue Testing Apparatus

At the beginning of each test, the initial beam stiffness was calculated by the data acquisition software after 50 conditioning cycles. AASHTO T 321-07 was used to define beam failure as a 50% reduction in beam stiffness in terms of number of cycles until failure. Normally, the test would be run to approximately 40% of initial stiffness, but as a factor of safety and to ensure a complete data set, the beams for this project were allowed to run until the beam stiffness was reduced to 25% of the initial stiffness. When testing occurred at 200 microstrain, two beams had not reached the failure point after 12,000,000 loading cycles. At this point, the test was terminated and the number of cycles until failure was extrapolated using a three-stage Weibull function. Past research has shown this to be the most efficient methodology for predicting the number of cycles to failure without running the beam past 12 million cycles (Prowell et al., 2010). Upon finding the cycles to failure at three different strain magnitudes, the fatigue endurance limit was calculated for each 19.0 mm mix design.

Using a proposed procedure developed under NCHRP 9-38 (Prowell et al., 2010), the endurance limit for each of the five mixes was estimated using Equation 4.7 based on a 95 percent lower prediction limit of a linear relationship between the log-log transformation of the strain levels (200, 400, and 800 microstrain) and cycles to failure. All the calculations were conducted using a spreadsheet developed under NCHRP 9-38.

$$\text{Endurance Limit} = \hat{y}_0 - t_\alpha s\sqrt{1+\frac{1}{n}+\frac{(x_0-\bar{x})^2}{S_{xx}}} \quad (4.7)$$

where:

$\hat{y}_o$ = log of the predicted strain level (microstrain)

t_α = value of *t* distribution for n-2 degrees of freedom = 2.131847 for n = 6 with $\alpha = 0.05$

s = standard error from the regression analysis

n = number of samples = 6

S_{xx} = $\sum_{i=1}^{n}(x_i-\bar{x})^2$ (Note: log of fatigue lives)

x_o = log (50,000,000) = 7.69897

$\bar{x}$ = log of average of the fatigue life results

A detailed summary of the bending beam fatigue test results for the plant-produced base layer mixes is presented in Table 4.12. Figure 4.9 compares the fatigue cracking resistance of the two mixtures determined based on AASHTO T 321-07 results. A power model transfer function ($\varepsilon = \alpha_1 N^{\alpha_2}$) was used to fit the results for each mixture. A summary of the model coefficients and R^2 values is given in Table 4.13. There was a significant difference between the magnitude of the intercept (α_1) and the slope (α_2) between the mixture and the Thiopave mixtures. These differences were 32.1 and 22.1%, respectively. The R^2 values for each of the mixes are above 0.97, showing a good model fit for the dataset.

Table 4.12 Bending Beam Fatigue Results

Mix	Microstrain Level	Beam #	Number of Cycles to Failure
Control Base	800	3	7,890
		6	4,260
	400	1	201,060
		4	216,270
	200	7	6,953,800
		5	2,165,480
Thiopave Base	800	2	8,840
		3	6,760
	400	5	398,100
		6	292,860
	200	1	24,700,000*
		4	54,400,000*

*Note: Failure point extrapolated based on three-stage Weibull function.

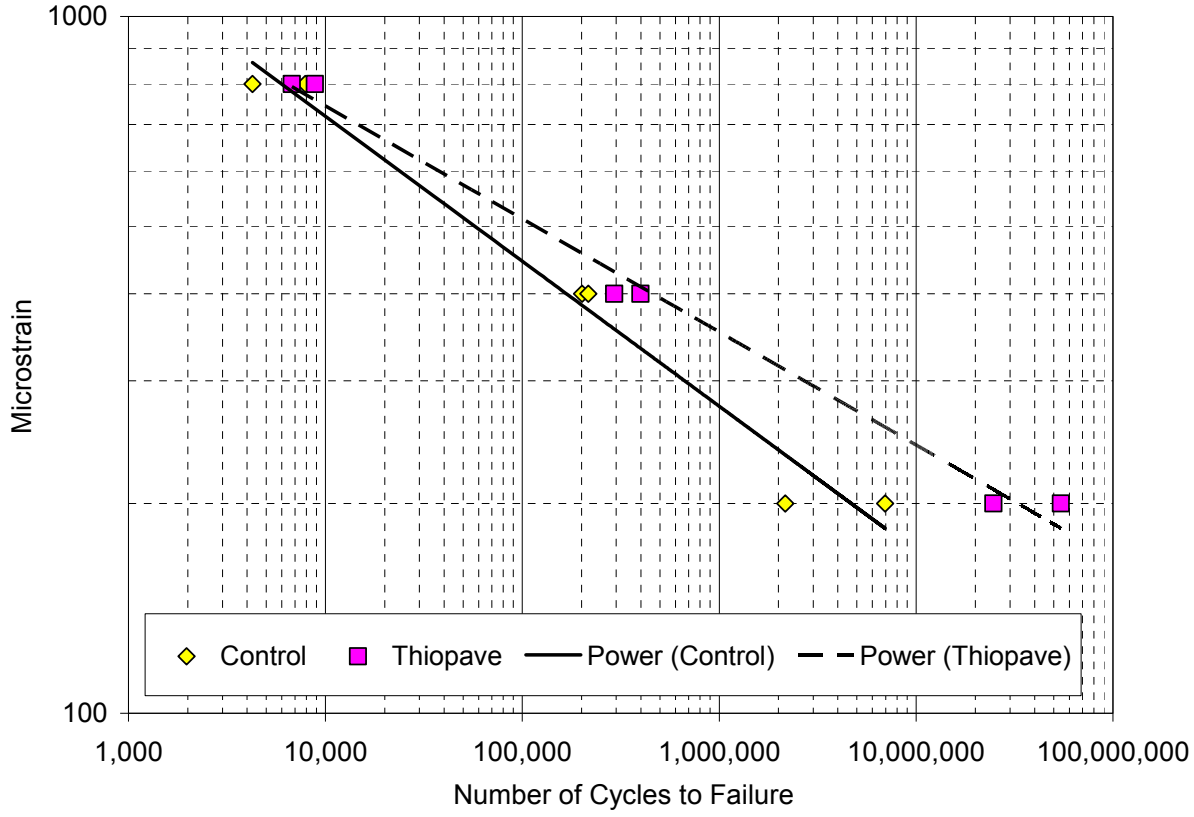

Figure 4.9 Comparison of Fatigue Resistance for Mixtures

Table 4.13 Fatigue Curve Fitting Coefficients (Power Model Form)

Mixture	AASHTO T321		
	α_1	α_2	R^2
Control Base	4886.3	-0.208	0.977
Thiopave Base	3318.6	-0.162	0.991

Table 4.14 shows that the percentage difference between the average fatigue life of the control mixture that of the Thiopave mixture at the three strain levels tested in this study, using the failure criteria (50% reduction in beam stiffness) defined by AASHTO 321. This information helps evaluate important aspects of the material behavior shown in Figure 4.9 as follows:

- At the highest tested strain level (800 με), the base Thiopave mixture exhibited longer fatigue life. The average fatigue life of the base Thiopave mixture was 28% longer than that of the base control mixture.
- At 400 με, the average fatigue life of the base Thiopave mixture with 2% air voids was 66% longer than that of the base control mixture.
- At 200 με, the base Thiopave mixture had an average fatigue life 767% longer than the control mixture. This percent increase should be viewed with some caution, however, since it was based on extrapolating at the lowest strain level.

Table 4.14 Percent Increase in Cycles to Failure for Thiopave versus Control Mixture

Strain Level	200 με	400 με	800 με
Percent Increase in Predicted Life	767%	65.6%	28.4%

It should be noted that the trends shown in Figure 4.9 and Table 4.14 were not evident during the preliminary laboratory investigation of these mixtures (Figure 1.4). This improved trend may be partially due to the lower than the design 30% Thiopave addition that was actually achieved during production. Lower Thiopave levels and increased binder content resulting from lower design air voids apparently achieves much better fatigue performance in the laboratory, which is the reason that this 2% air void mixture was selected for the bottom lift in the Thiopave sections.

Table 4.15 shows the 95 percent one-sided lower prediction of endurance limit for each of the two mixes tested in this study based on the number of cycles to failure determined in accordance with AASHTO T 321. The procedure for estimating the endurance limit was developed under NCHRP 9-38 (Prowell et al., 2010). Based on the results shown in Table 4.15, the 30% Thiopave mixture had a fatigue endurance limit 76% higher than the control mixture. Again, this may be attributed to the lower-than expected amounts of Thiopave in this mixture combined with increased asphalt content. The lower Thiopave and higher asphalt contents also resulted in lower moduli than expected, so this demonstrates the tradeoff between modulus and fatigue resistance/tolerance that is possible with the Thiopave mixtures when evaluating these options in the mix design.

Table 4.15 Predicted Endurance Limits

Mixture	% Base Binder	% Thiopave	% Total Binder	Endurance Limit (Microstrain)
Control Base	4.7	0.0	4.7	89
Thiopave Base	4.8	1.4	6.2	157

Note that percentages are of total mixture.

4.5 Asphalt Pavement Analyzer (APA) Testing

The rutting susceptibility of the Thiopave, base control and surface control mixtures were evaluated using the APA equipment shown in Figure 4.10. Often, only surface mixtures are evaluated using the APA. For this experiment, however, it was directed by the sponsor to test the surface mixture, in addition to each of the Thiopave mixtures. For comparison purposes, the base control mixture was also evaluated. The intermediate control mix was not sampled in sufficient quantities to allow for APA testing since it was not part of the original APA testing plan.

Testing was performed in accordance with AASHTO TP 63-09. The samples were prepared to a height of 75 mm and an air void level of 7 ± 0.5 percent. Six replicates were tested for each mix. The samples were tested at a temperature of 64^{o}C (the 98 percent reliability temperature for the high PG grade of the binder). Typically, these samples are tested at the high binder PG grade. However, for the Test Track a constant testing temperature for all mixes was desired to facilitate relative comparisons between the mixes. The samples were loaded by a steel wheel (loaded to 100 lbs) resting atop a pneumatic hose pressurized to 100 psi for 8,000 cycles. Manual depth readings were taken at two locations on each sample after 25 loading cycles and at the conclusion of testing to determine the sample rut depth (Table 4.16).

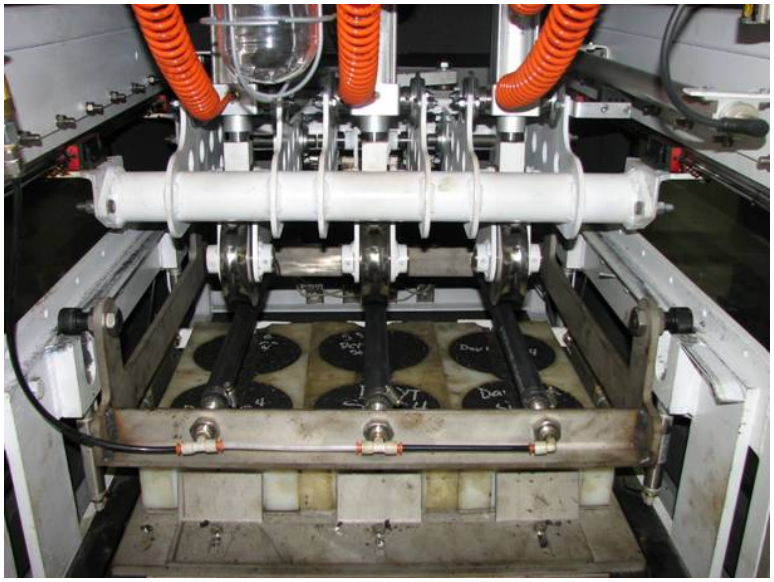

Figure 4.10 Asphalt Pavement Analyzer

Table 4.16 APA Test Results

Mixture	Average Rut Depth, mm	StDev, mm	COV,%	Rate of Secondary Rutting, mm/cycle
Control-Surface	3.07	0.58	19	0.000140
Control-Base	4.15	1.33	32	0.000116
Thiopave-Intermediate	2.00	0.68	34	0.000067
Thiopave-Base	4.07	1.36	34	0.000161

The APA is typically used as a "Go/No Go" type test to ensure mixtures susceptible to rutting are not placed on heavily trafficked highways. Past research at the Test Track has shown that if a mixture has an average APA rut depth less than 5.5 mm, it should be able to withstand 10 million equivalent single axle loads (ESALs) of traffic at the Test Track without accumulating more than 12.5 mm of field rutting. Considering this threshold, both Thiopave mixtures and the control mixtures are not suspected to fail in terms of rutting during the 2009 trafficking cycle. The APA test results are also appropriate for determining a rate of secondary rutting for each mixture. Rutting typically occurs in three stages: primary, secondary, and tertiary. Primary rutting develops during the early phases of pavement loading due to initial mixture consolidation (i.e., further compaction). Secondary rutting begins after initial consolidation with a gradual nearly linear increase in rut depth. Tertiary represents a shear flow condition. The confined state provided by the molds prevents the mixture from truly ever achieving tertiary flow. Therefore, once the mixture has overcome the stresses induced during primary consolidation, it is possible to determine the rate at which secondary rutting occurs.

This was determined in the APA by fitting a power function to the rut depths measured automatically in the APA during testing (Figure 4.11). The primary consolidation of a sample can be seen as the initial steep line when comparing rut depth to the number of cycles; however, as the slope of the line decreases, the samples move into secondary consolidation. The rate of rutting was determined by finding the slope of the power function at the 8000^{th} loading repetition. The results of this analysis are also given in Table 4.16.

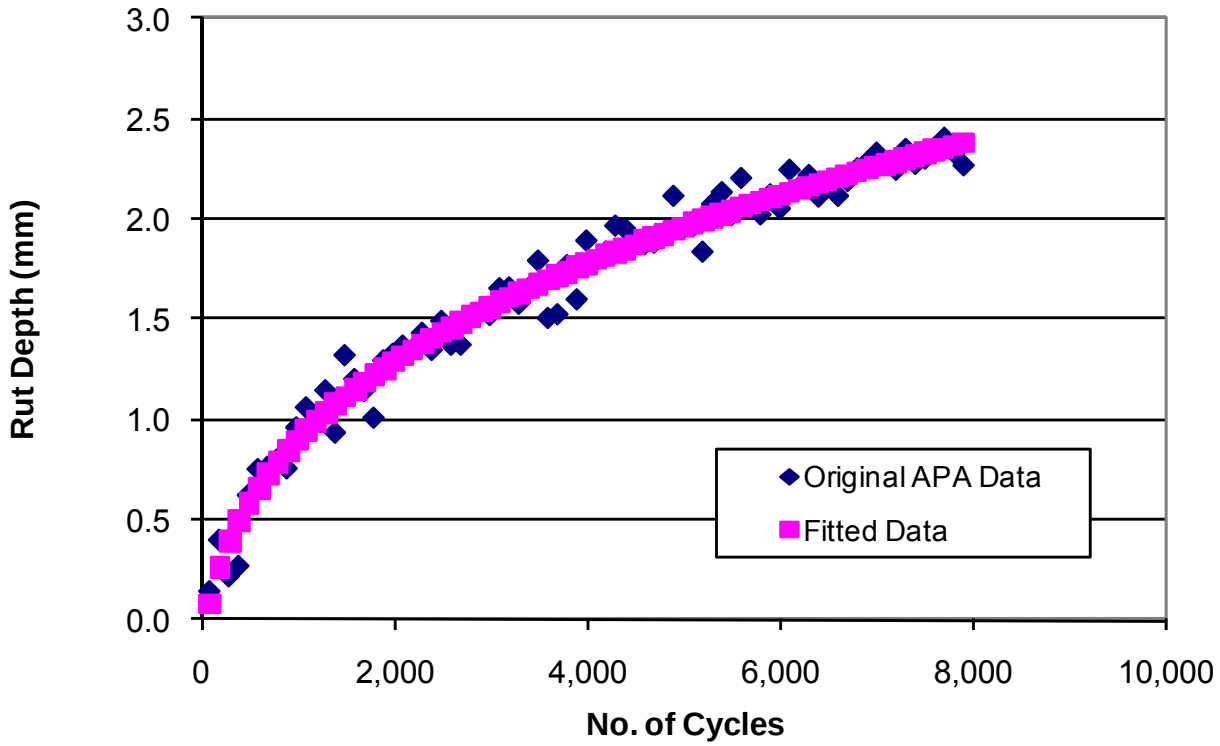

Figure 4.11 Rate of Rutting Plot

Of the four mixtures, the mix from N5-2 (Thiopave-intermediate) had the best, or smallest, rate of rutting. This mixture also had the lowest amount of total rutting in the APA. While the mix from N5-4 (Thiopave-base) had a lower total rut depth than the control base mix the APA, it had a higher rate of secondary consolidation. This suggests the Thiopave rich bottom base mix accrues rutting at a faster rate than the control base mix once initial consolidation occurs, which is to be expected. Overall, the relative rankings of the mixtures were as expected. The Thiopave intermediate mix with a higher design air voids and greater amount of Thiopave was more resistant to rutting than both the Thiopave rich-bottom and control mixtures.

5. FALLING WEIGHT DEFLECTOMETER TESTING AND BACKCALCULATION

Two phases of FWD testing were conducted on the sections. The first phase featured daily testing on each section from the time it was finished paving until it was opened to traffic. This was intended to track changes in modulus due to short term aging and curing. The second (and ongoing) phase was testing each section several times per month to track changes in modulus due to environmental changes, seasonal changes and potential changes due to pavement damage. Each of the phases is discussed in the following subsections.

The FWD device used for each phase was a Dynatest Model 8000 FWD (Figure 5.1). The configuration remained constant between testing phases. Nine sensors, as listed in Table 5.1, were used with a 5.91 in. radius split plate. Three replicates at four drop heights, listed in Table 5.2, were applied in each phase.

Figure 5.1 Dynatest Model 8000 FWD

Table 5.1 FWD Sensor Spacing

Sensor	Offset, in.
1	0
2	8
3	12
4	18
5	24
6	36
7	48
8	60
9	72

Table 5.2 FWD Drop Heights and Approximate Weights

Drop Height	Approximate Weight, lb	Replicates
1	6,000	3
2	9,000	3
3	12,000	3
4	16,000	3

5.1 Phase I FWD Testing – Short Term Testing

As noted in Table 3.6, the surface of S9 was completed on July 16, 2009 while the surfaces of N5 and N6 were completed on August 3, 2009. Since the traffic did not begin until August 28, 2009 there was an opportunity to conduct regular FWD testing on each section to study the short term aging and curing effect without traffic as a confounding factor. Recall from the introduction of this report (Figure 1.2) that there was a measurable increase in modulus from 1 to

14 days of curing for the Thiopave materials when tested for dynamic modulus in the laboratory. The objective of this testing was to evaluate whether a similar increase occurred in the field, as it could have important ramifications for when an agency may open a facility to traffic after paving.

Table 5.3 shows the surface completion date for each section followed by each date FWD testing was conducted. Section S9, having been completed earlier, experienced approximately 6 weeks of aging prior to traffic while N5 and N6 experienced about 3.5 weeks. Missing dates between surface completion and August 24 were weekend days, or when testing could not be completed due to equipment maintenance and/or time constraints.

On each test date, the between-wheelpath offsets at each of the four random locations were tested. Referring to Figure 3.2, these were locations 2, 5, 11 and 8. As mentioned previously, four drop heights with three replicates at each height were utilized at each location. Since the temperature probes had not yet been installed in the pavement sections, this analysis relied primarily on infrared-determined surface temperatures measured with a sensor on the FWD to estimate the mid-depth pavement temperatures. The mid-depth pavement temperature was needed to account for the different ambient conditions on a day-to-day basis and normalize the backcalculated moduli to a single reference temperature. Previous studies at the Test Track had found strong correlations between backcalculated AC modulus and mid-depth temperature (Timm and Priest, 2006; Taylor and Timm, 2009).

The procedure for predicting mid-depth temperature relied on data sets developed after the temperature probes had been installed. Using the hour of the day, which took into account the hourly angle of the sun, in addition to the measured temperature at the surface on an hourly basis, a regression equation was developed to predict mid-depth temperature from these two parameters. This regression equation was then used with the FWD-determined surface temperature and the hour in which the test was conducted to estimate the mid-depth temperature at the time of the FWD test. Approximately ten days of temperature data, as listed in Table 5.4, were used to develop the regression equations starting when probes were installed. Ten days were selected to provide a sufficiently accurate regression equation, but limit the time frame over which the predictions were made since the model did not consider seasonal changes (i.e., change in tilt of earth's axis over time).

Table 5.3 FWD Phase I Testing Dates

Date	N5	N6	S9
7/16/2009			S.C.
7/17/2009			FWD
7/18/2009			
7/19/2009			
7/20/2009			FWD
7/21/2009			FWD
7/22/2009			FWD
7/23/2009			FWD
7/24/2009	T.C.	T.C.	FWD
7/25/2009	FWD	FWD	
7/26/2009	FWD	FWD	
7/27/2009	FWD	FWD	FWD
7/28/2009	FWD	FWD	FWD
7/29/2009	FWD	FWD	FWD
7/30/2009	FWD	FWD	FWD
7/31/2009	FWD	FWD	FWD
8/1/2009			
8/2/2009			
8/3/2009	S.C.	S.C.	FWD
8/4/2009			FWD
8/5/2009	FWD	FWD	FWD
8/6/2009	FWD	FWD	FWD
8/7/2009	FWD	FWD	FWD
8/8/2009			
8/9/2009			
8/10/2009	FWD	FWD	FWD
8/11/2009			
8/12/2009	FWD	FWD	FWD
8/13/2009	FWD	FWD	FWD
8/14/2009	FWD	FWD	
8/15/2009			
8/16/2009			
8/17/2009	FWD	FWD	FWD
8/18/2009	FWD	FWD	FWD
8/19/2009	FWD	FWD	FWD
8/20/2009	FWD	FWD	FWD
8/21/2009	FWD	FWD	
8/22/2009			
8/23/2009			
8/24/2009	FWD	FWD	FWD
8/25/2009			
8/26/2009			
8/27/2009			
8/28/2009	Open to Traffic		

S.C.: Surface of section complete;
T.C.: Thiopave lifts complete
FWD: FWD testing conducted on this date

Table 5.4 Dates Used for Mid-Depth Temperature Regression

Section	Start Date	End Date
N5	8/21/2009	8/31/2009
N6	8/22/2009	8/31/2009
S9	8/26/2009	9/5/2009

A statistical model-fitting program, DataFit, was used to search for viable regression equations. Since the goal of this exercise was to generate accurate mid-depth temperature predictions from surface temperature measurements and the hour of day, the main criteria were to examine the model R^2 and range of residuals. The model form selected was:

$$T_{mid} = a + b * Hour + \frac{c}{T_{top}} + d * Hour^2 + \frac{e}{T_{top}^2} + f * \frac{Hour}{T_{top}} + g * Hour^2 + \frac{h}{T_{top}^2} + i * \frac{Hour}{T_{top}^2} + j * \frac{Hour^2}{T_{top}} \quad (5.1)$$

where:
T_{mid} = predicted mid-depth temperature, F
Hour = hour of day (0 to 24)
T_{top} = measured surface temperature, F
a,b,c,d,e,f,g,h,i,j = regression constants

Table 5.5 summarizes the regression constants, model R^2 and range of residuals for each test section. The model was judged sufficiently accurate based on the high R^2 values (exceeding 95%) and relatively low residuals (all were within ±5F). Figure 5.2 illustrates the measured versus predicted temperature for the three sections using this approach. The regression parameters listed in Table 5.5 were used with the FWD-measured surface temperature and hour-of-day from each specific test to determine the approximate mid-depth pavement temperature at the time of testing.

Table 5.5 Temperature Model Parameters

Parameter	N5	N6	S9
a	335.23	330.00	166.37
b	0.61	-2.13	3.31
c	-5.47E+04	-5.82E+04	-1.99E+04
d	0.35	0.59	0.52
e	4.60E+06	5.33E+06	2.32E+06
f	-785.97	-752.24	-1582.86
g	2.30E-05	-8.53E-04	-9.68E-04
h	-1.47E+08	-1.78E+08	-9.98E+07
i	5.76E+04	6.90E+04	1.01E+05
j	-27.16	-43.24	-37.50
R^2	0.99	0.97	0.95
Minimum Residual, F	-2.8	-4.3	-4.7
Maximum Residual, F	2.8	3.8	4.2

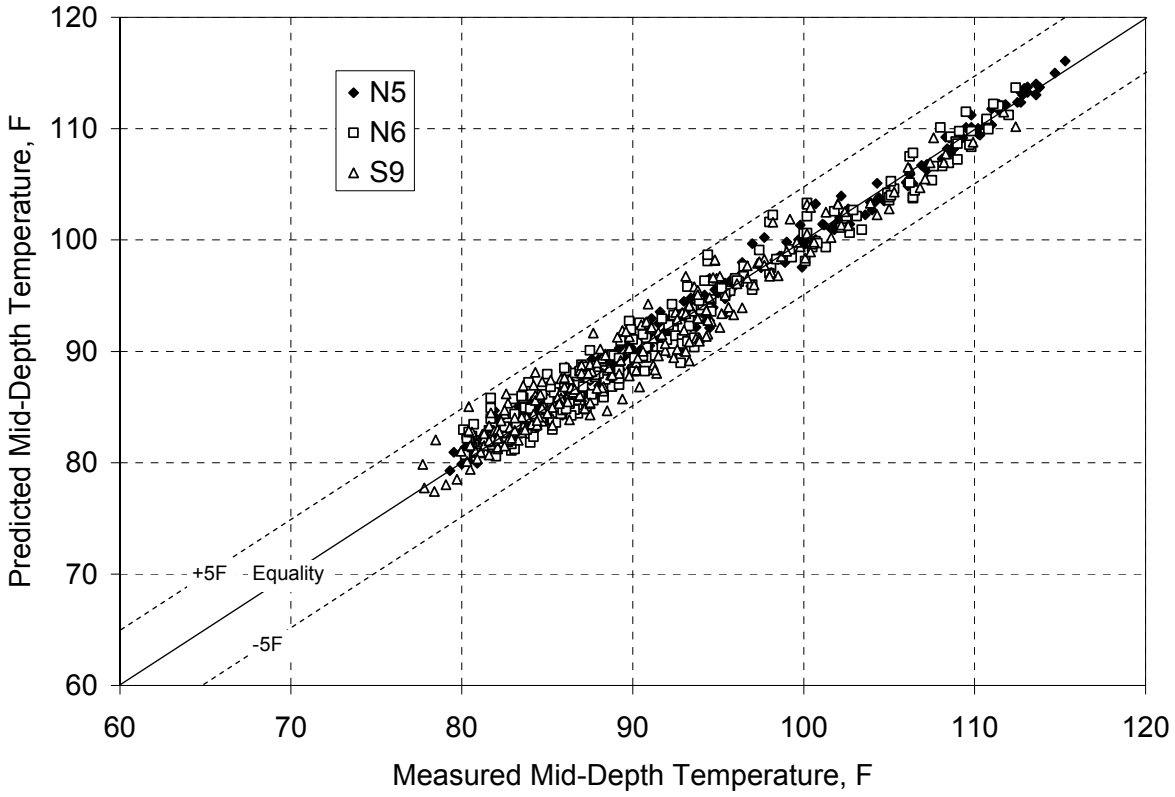

Figure 5.2 Measured vs. Predicted Mid-Depth Pavement Temperatures

Backcalculation of the deflection basins was conducted using EVERCALC 5.0. This backcalculation program had been used successfully in previous research cycles at the Test Track (Timm and Priest, 2006; Taylor and Timm, 2009). Based on results from previous backcalculation exercises (Timm and Priest, 2006; Taylor and Timm, 2009), using similar unbound aggregate base and subgrade materials, a three-layer system was established consisting of the entire depth of AC, over the aggregate base on top of the subgrade. While it may be ideal to backcalculate the moduli of the individual AC sublayers, this is not practically feasible because of the similar moduli of the AC materials which results in large errors and unrealistic moduli. Though all three layers were backcalculated, only the results from the asphalt concrete will be presented here since the focus was the short term aging of these materials. The base and subgrade materials are fully characterized in subsection 5.3. The backcalculated moduli presented below represent those results where the root-mean-square of the error (RMSE) in backcalculation was less than 3%.

During the short-term testing, there were two primary variables; time and temperature. The main goal of this investigation was to examine the time effect, so it was necessary to correct the backcalculated data for temperature. The procedure described above was used to estimate a mid-depth pavement temperature at the time of FWD testing. Laboratory dynamic modulus test data were used to establish a temperature-modulus relationship that enabled a temperature correction of the field data. It was necessary to use laboratory data since the field data included both time

and temperature while the lab data were tested over a range of temperatures within a single day which eliminated the time-effect as a confounding variable.

As described in Section 4, each mixture in each section was subjected to laboratory dynamic modulus testing over a range of temperatures and frequencies from which master-curves were generated. The master curves were used to generate a data set for each mixture from 1 to 10 Hz over a range of temperatures. This frequency range was somewhat arbitrary since there is not currently a widely accepted procedure to convert laboratory frequency to FWD-applied loading frequency. It should be noted, however, that similar results were obtained when all the frequencies were considered (0.1 to 25 Hz) as when frequency was limited to 1 to 10 Hz. Furthermore, since these data were intended to represent in situ conditions it was decided to use the test data generated under confined conditions only.

For each mixture, laboratory-determined E* versus temperature were plotted and fit with an exponential function:

$$E = \alpha_1 e^{\alpha_2 T} \quad (5.2)$$

where:
E = dynamic AC modulus, ksi
T = test temperature, F
α_1, α_2 = best-fit regression constants

Equation 5.2 has been used in previous Test Track research cycles to characterize the modulus-temperature relationship for both laboratory and field-determined moduli (Timm and Priest, 2006; Taylor and Timm, 2009). A temperature-corrected AC modulus (E_{Tref}) was determined from Equation 5.2 at a given reference temperature (T_{ref}) by dividing Equation 5.2 at T_{ref} by the same equation at the measured temperature (T_{meas}). After canceling terms and solving for E_{Tref}, the following equation was determined:

$$E_{T_{ref}} = E_{T_{meas}} e^{\alpha_2 \left(T_{ref} - T_{meas}\right)} \quad (5.3)$$

Equation 5.3 illustrates that the key variable in performing the temperature correction is the exponential regression coefficient, α_2. Figure 5.3 illustrates the best-fit equation for the base mixture in the control section (S9) while the exponential regression constants for each mixture are listed in Table 5.6. The regression constants were determined from test data at 1 and 10 Hz.

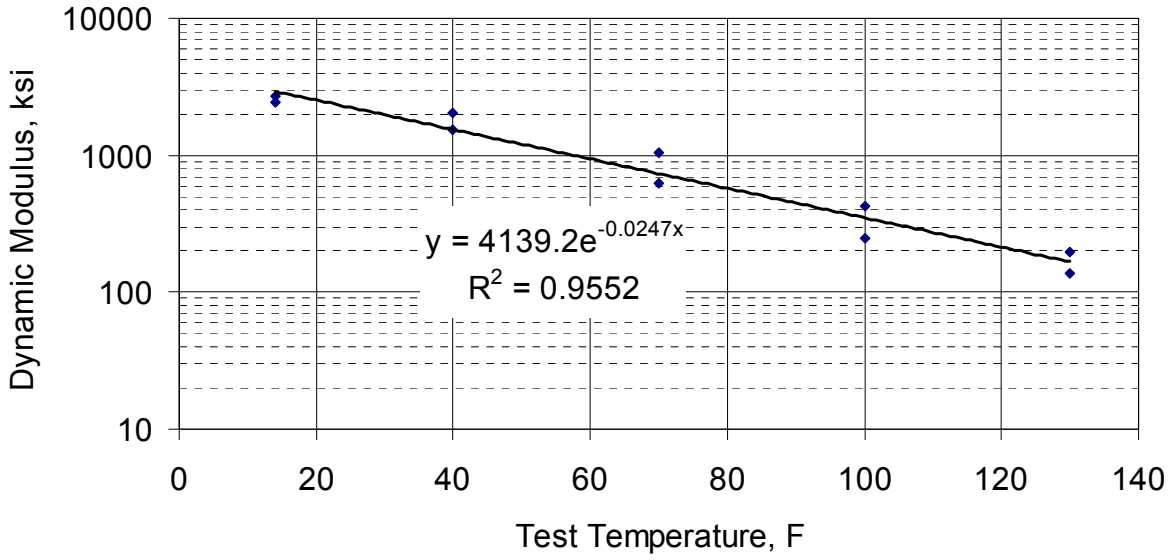

Figure 5.3 Laboratory E* vs. Temperature for Base Mixture in Control Section

Table 5.6 Best Fit Exponential Regression Constants for Laboratory E* Data (Confined Testing at 1 and 10 Hz)

Section-Lift	Exponential Regression Constant	Model R^2
S9-1	-0.0264	0.96
S9-2	-0.0236	0.96
S9-3	-0.0247	0.96
N5-1	-0.0264	0.96
N5-2	-0.0212	0.94
N5-3	-0.0212	0.94
N5-4	-0.0246	0.96
N6-1	-0.0264	0.96
N6-2	-0.0212	0.94
N6-3	-0.0246	0.96

A further complicating factor in using laboratory data to perform temperature corrections on backcalculated field data is that the backcalculated field moduli represent the entire depth of AC (all lifts) while the laboratory data are lift-specific. There is currently no widely-acceptable procedure for converting between lab and field data to overcome this issue. Therefore, a simple approach was taken whereby a weighted exponential coefficient was determined for each section based on the as-built lift thicknesses determined at each FWD station. The following equation was used to determine the average α_2 for each section listed in Table 5.6:

$$\alpha_2 = \frac{\sum_{i=1}^{n} \alpha_{2i} \cdot H_i}{\sum_{i=1}^{n} H_i} \quad (5.4)$$

Where:
α_2 = weighted average exponential coefficient
α_{2i} = exponential coefficient for lift i
H_i = as-built thickness of lift i, in.
i = lift number
n = number of lifts in section

The net result of all these mathematical manipulations of the lab and field data are shown in Figures 5.4 through 5.6 for sections S9, N5 and N6, respectively. In each figure, the uncorrected backcalculated AC modulus are plotted along with the temperature-corrected AC modulus using the procedure described above. The reference temperature was 90°F in all cases to represent actual measured temperatures during this testing phase. In each case, a best-fit regression equation was applied to both data sets (un-corrected and corrected) to demonstrate the effectiveness of the temperature-correction procedure. In each case, the temperature-corrected R^2 was below 0.07. This means that less than 7% of the variation in the data is due to temperature after the corrections were made. This was deemed sufficient for this investigation.

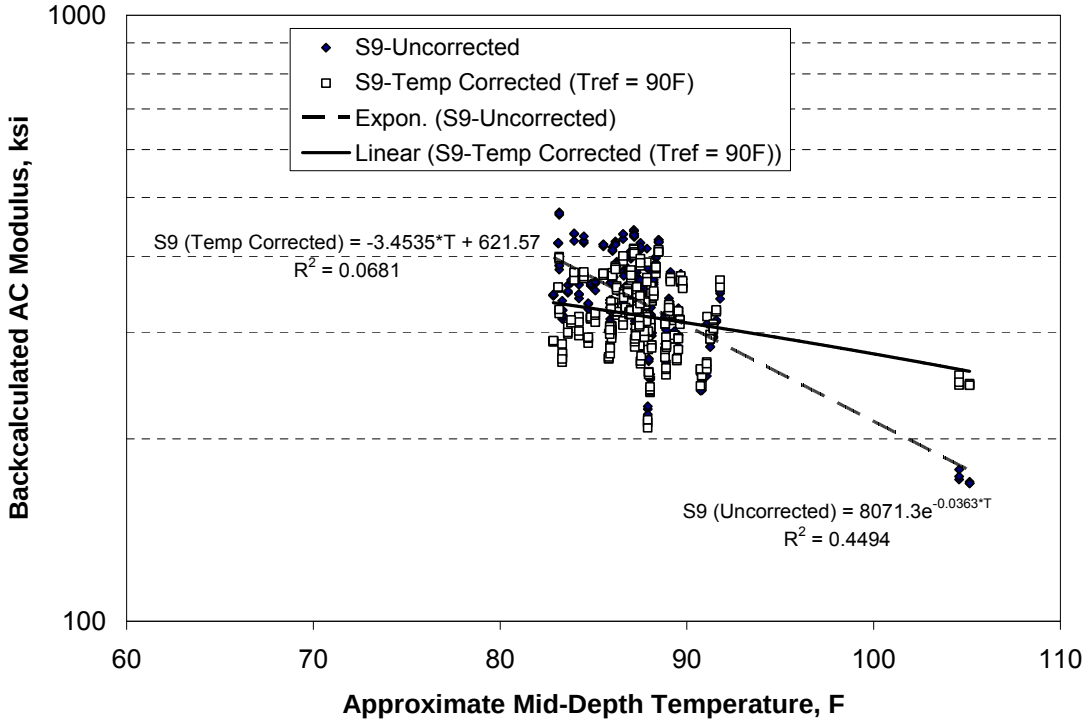

Figure 5.4 S9 Backcalculated AC Modulus (with and without Temperature Correction)

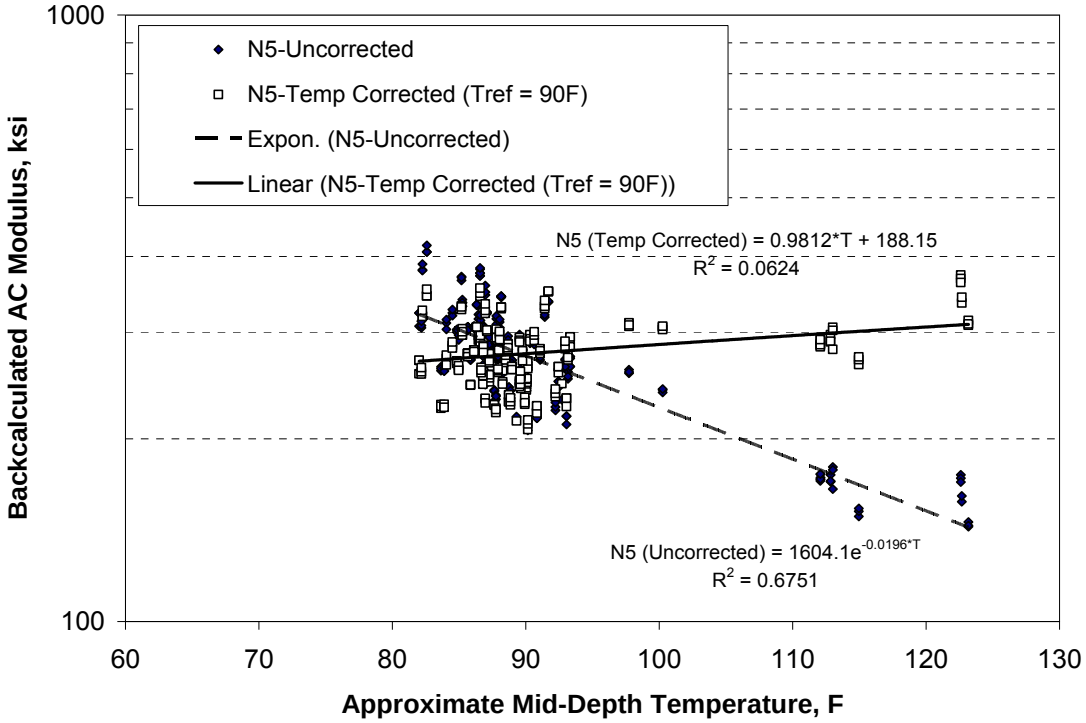

Figure 5.5 N5 Backcalculated AC Modulus (with and without Temperature Correction)

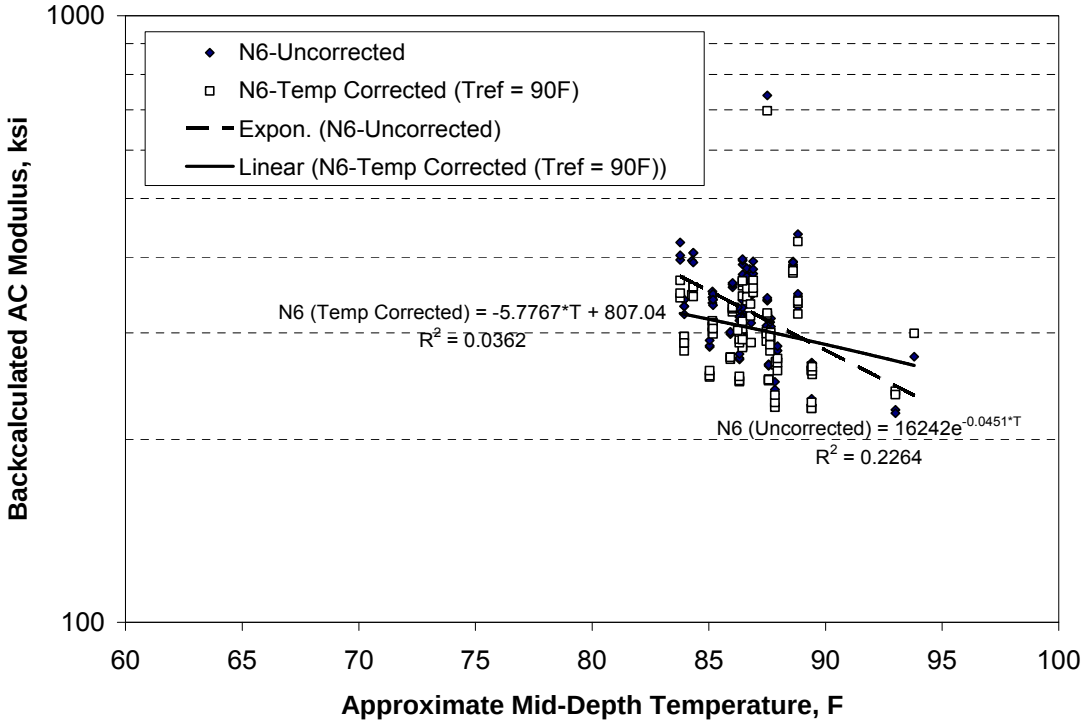

Figure 5.6 N6 Backcalculated AC Modulus (with and without Temperature Correction)

After the backcalculated AC moduli had been corrected to a reference temperature, it was possible to plot modulus versus test date. Figure 5.7 summarizes the data for each section with best-fit linear regression trendlines superimposed on the data. There was a slight increasing trend over time and it is interesting to note that the greatest slope and R^2 were achieved in the section with the greatest thickness of Thiopave (Section N5). In N5, the AC modulus increased by approximately 2,360 psi/day, though only about 25% of the variation in modulus was explained by the passage of time. Recall from the laboratory preliminary laboratory investigation (Section 1) that the modulus at 70F increased by about 350,000 psi over a two week period. Assuming a straight-line increase, this would be about 25,000 psi/day or about one order of magnitude greater than that measured in the field. Some of this observed difference in modulus increase with time may be related to the difference in material behavior between the 70F lab temperature and the reference 90F field temperature. Clearly, there are some major differences between lab measurements on the individual mixes and backcalculated composite AC moduli demonstrated by the much lower increase in modulus over time and the relatively low significance (R^2 less than 25%) of the "curing" time.

Some of the difference could be due to the lower-than-expected amounts of Thiopave replacement in the as-produced mixtures relative to the original mix design. Differences could also be due to how the mixtures were produced (lab versus asphalt plant). There could also be confounding factors related to the composite nature of the pavement where in Section N5 and N6 were topped with control mix. To examine this issue more closely, the data over just the first seven days for each section were plotted and fitted with straight lines. These data are shown in Figure 5.8 and represent the fully-complete control section (S9) and the Thiopave sections prior to placing the surface lift. The slopes of these lines are greater than those over the longer term, but the significance of time is still relatively low ($R^2 < 28\%$). Based on these data, it appears that the short-term curing effects are comparable between the control and Thiopave mixtures and that neither are approaching the effect observed in the laboratory-tested mixtures. Furthermore, it appears that the Thiopave material could be treated in the same manner as the control materials in terms of opening to traffic after construction.

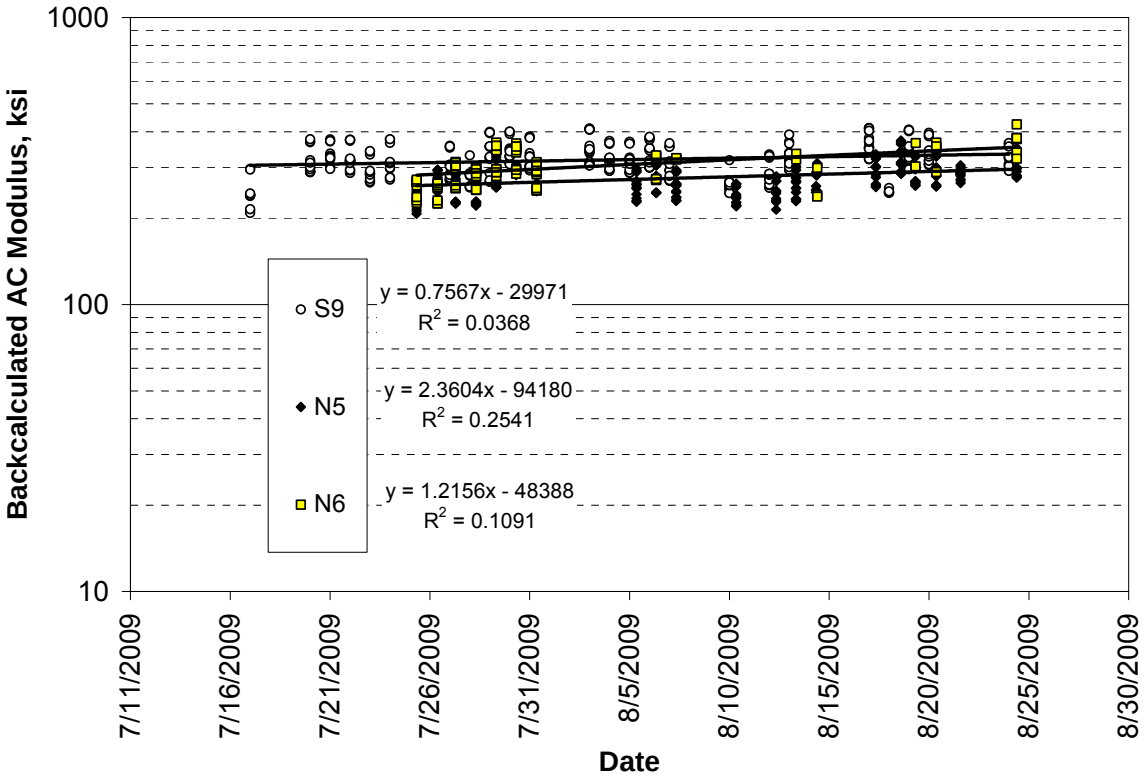

Figure 5.7 Temperature-Corrected AC Modulus vs. Date (T_{ref} = 90F)

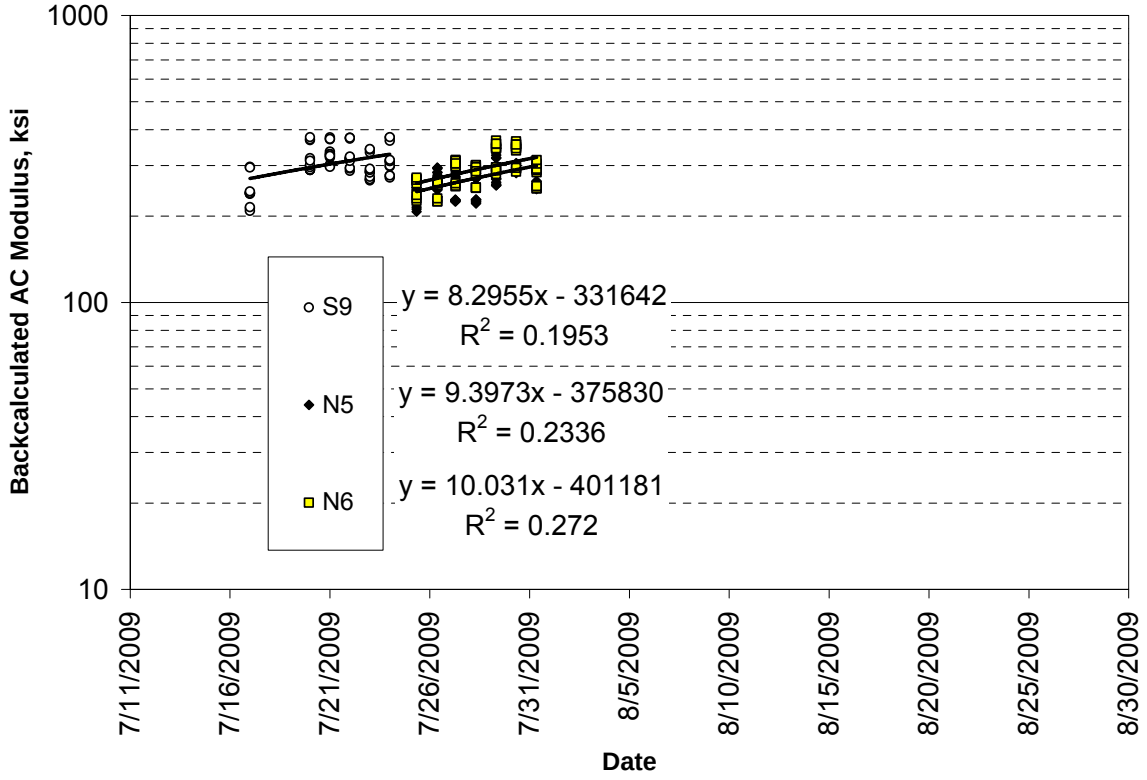

Figure 5.8 Temperature-Corrected AC Modulus in First Seven Days (T_{ref} = 90F)

5.2 Phase II FWD Testing – Ongoing Testing

The 2009 Test Track was opened to traffic on August 28, 2009. Beginning at that time, the control section was subjected to FWD testing three Mondays per month. The Thiopave sections were tested on corresponding alternating Mondays. This schedule was necessary because of time constraints and the need to test a total of sixteen sections within the structural experiment. The off-Monday within each month was used to perform relative calibration of the FWD equipment. Within each section, the twelve locations noted in Figure 3.2 were tested with three replicates at four drop heights. The data presented below only represent the results measured at the 9,000 lb load level. The test data range from August 28, 2009 through August 16, 2010.

Backcalculation was conducted using EVERCALC 5.0 using the same setup and constraints as used in the short-term backcalculation. Once again, the data presented below represent only those deflection basins that were below 3% RMSE.

Figures 5.9, 5.10 and 5.11 summarize the backcalculated results for the AC, granular base and subgrade, respectively. Data points within each plot represent the average backcalculated modulus across the entire test section at the 9000 lb load level. The seasonal effects of temperature on AC modulus are clearly evident in Figure 5.9 while the unbound materials were largely unaffected by seasonal temperature changes (Figures 5.10 and 5.11). These results are consistent with previous findings at the Test Track (Timm and Priest, 2006; Taylor and Timm, 2009).

Figure 5.10 shows relatively low granular base moduli in each of the test sections. Though these values may seem artificially low, these are consistent with findings from previous laboratory triaxial resilient modulus testing and values obtained from FWD evaluation at the Test Track on this crushed granite material (Timm and Priest, 2006; Taylor and Timm, 2009).

Figure 5.11 indicates good consistency in subgrade soil modulus between the two Thiopave sections on the north tangent while the soil on the south tangent control section was somewhat lower. This difference likely resulted from the construction history of the respective sections. Sections N5 and N6 were placed in test cells used previously for structural evaluations with relatively thin cross-sections. Therefore, in preparation for paving, N5 and N6 only required milling through the previous AC and granular base leaving the subgrade largely intact. This subgrade had been quarried and placed in 2003 from the lower cut of the West curve at the Test Track. Section S9 was placed in a cell that required deep milling (26 inches) of the AC followed by placement and compaction of newly quarried material from the upper hill area of the West curve at the Test Track. Slight differences in materials and duration of consolidation could be responsible for the differences in the subgrade moduli. With respect to structural modeling, the fact that they are different is not as critical as accurately quantifying the difference.

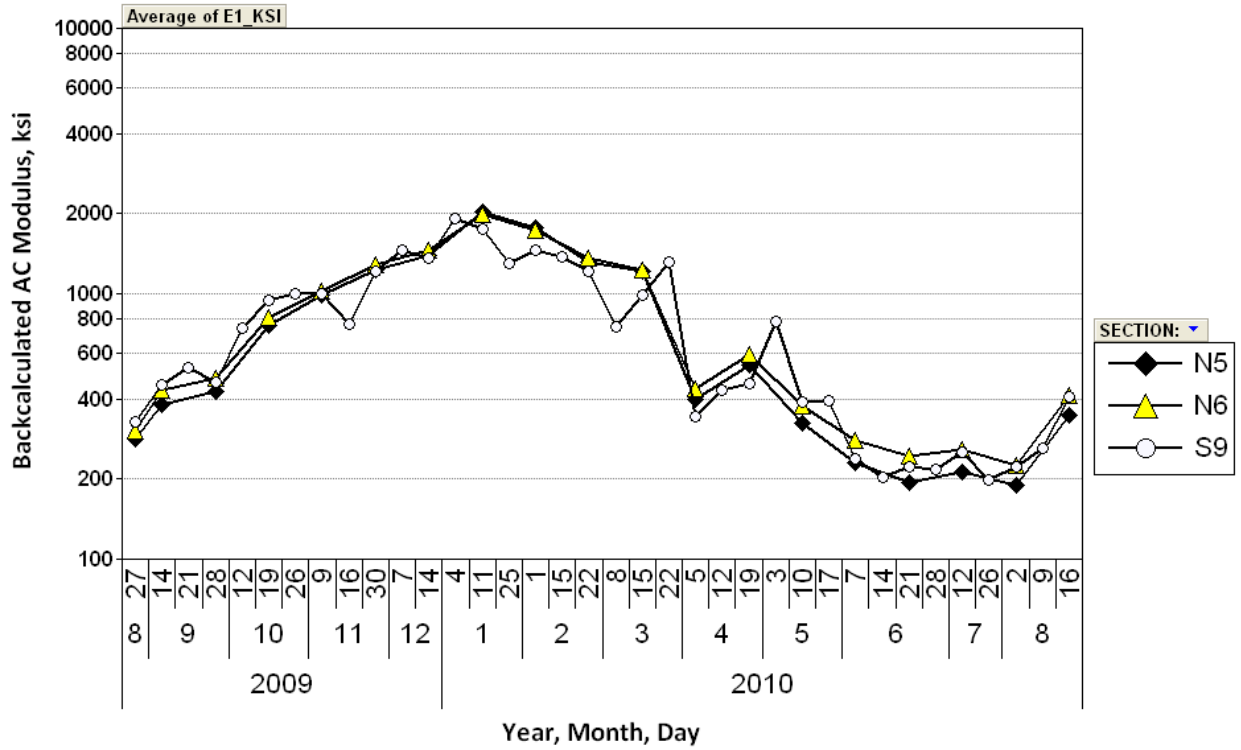

Figure 5.9 Backcalculated AC Modulus vs. Date

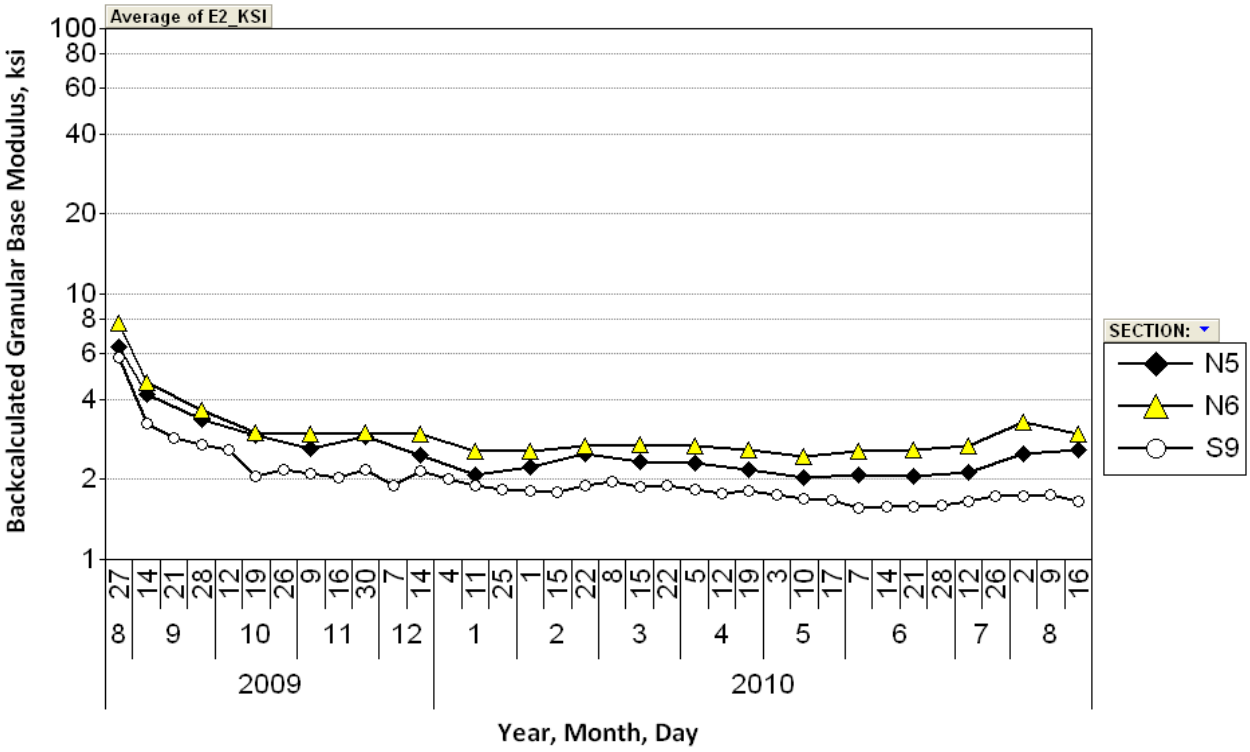

Figure 5.10 Backcalculated Granular Base Modulus vs. Date

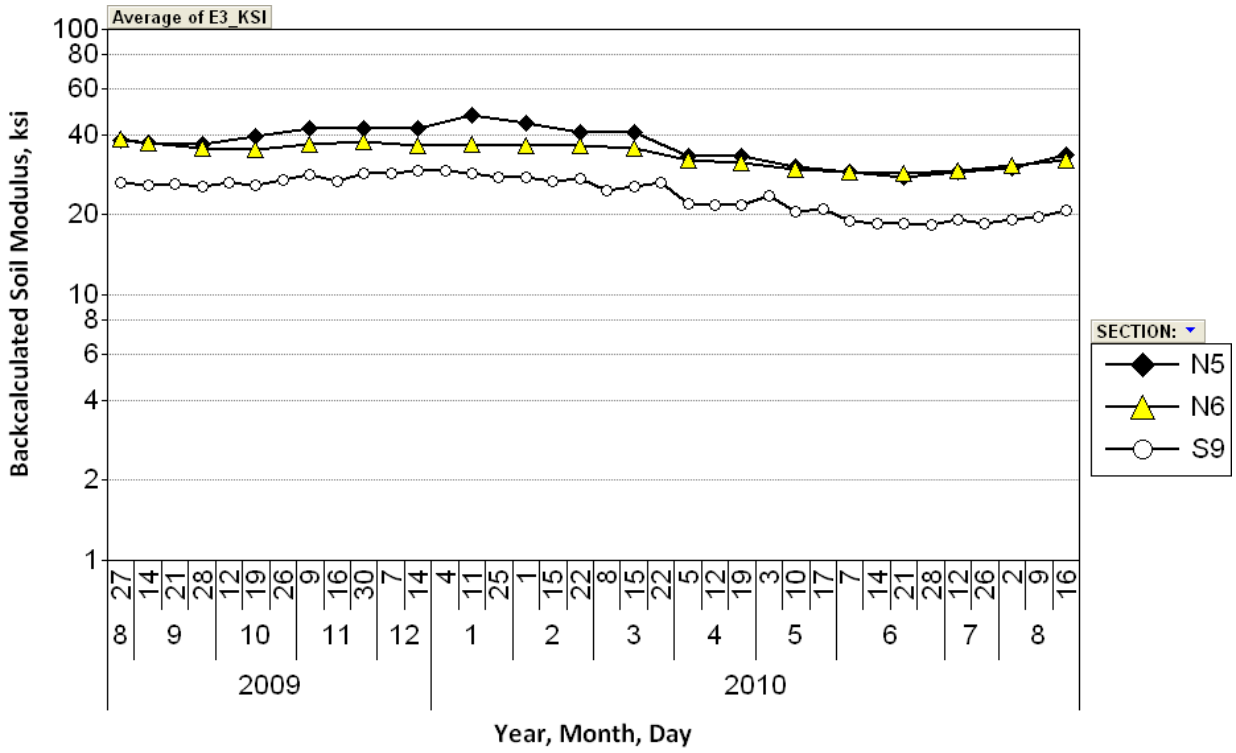

Figure 5.11 Backcalculated Subgrade Soil Modulus vs. Date

At the time of each FWD test, the mid-depth temperatures were recorded by embedded temperature probes in each section. Figure 5.12 plots the backcalculated AC modulus versus mid-depth temperature for each section in addition to best-fit exponential functions. Each data point in Figure 5.12 represents the AC modulus determined from the backcalculation of three deflection basins at the 9000 lb load level. Therefore, there is more scatter in the data than that shown previously in Figure 5.9. Despite the increased scatter, the change in AC modulus was well explained by change in mid-depth temperature ($R^2 > 0.92$). It is interesting to note that the three regression lines cross at approximately 70F. At cooler temperatures, the Thiopave sections appear to have higher moduli, while at warmer temperatures, the control section has the highest modulus. It should be pointed out that AC modulus determined through E* on individual mixtures did not necessarily show this same trend. However, it is important to keep in mind that some significant differences exist between laboratory E* testing and backcalculation of dynamic modulus. First, backcalculation considers the entire depth of AC that includes all the AC lifts in each section while E* testing considers each lift separately. Second, E* tests are conducted at uniform temperatures throughout the specimen while there are thermal gradients throughout the depth of AC in the field. Third, E* tests are conducted at fixed frequencies throughout the specimen. FWD tests in the field are actually tested under a frequency gradient that is derived from a mixture's proximity to the surface. Given these significant testing differences, one could expect to see differences between laboratory and field data.

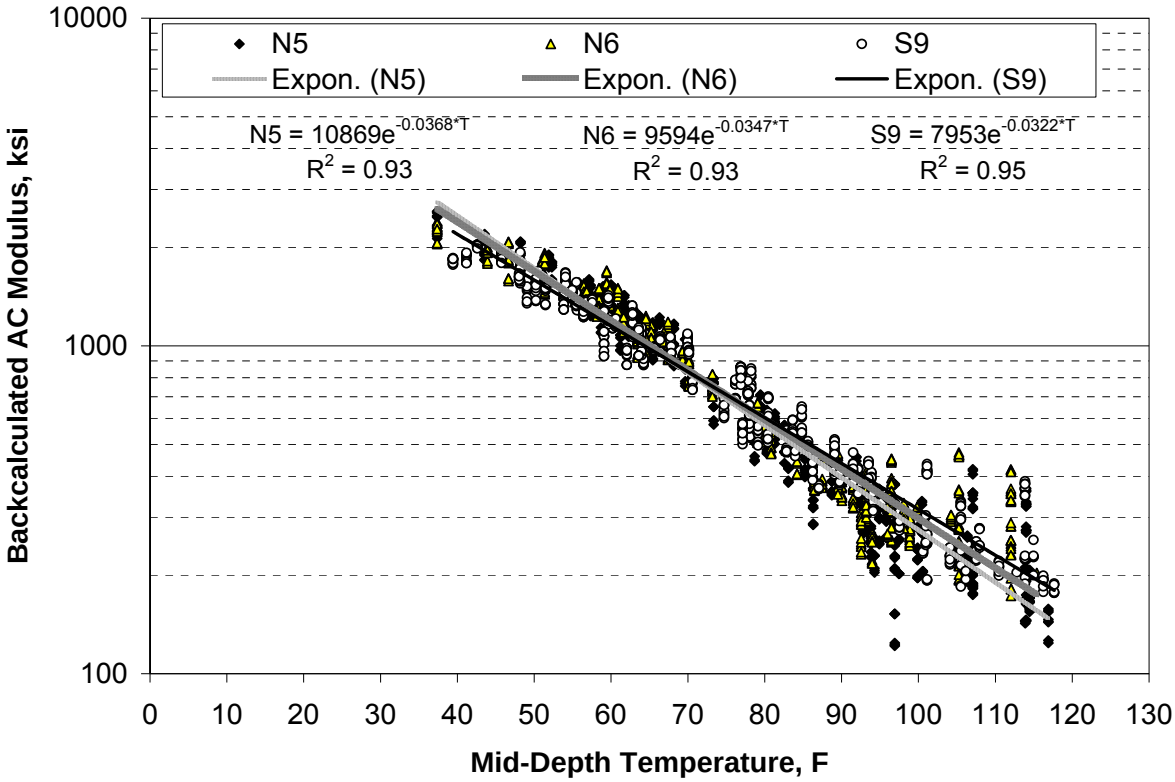

Figure 5.12 Backcalculated AC Modulus vs. Mid-Depth Temperature

To examine the differences between sections in backcalculated AC moduli over a range of temperatures, the moduli were temperature-corrected using the coefficients from Figure 5.12 in equation 5.3. Three reference temperatures were selected (50, 68 and 110F) that represented the range of FWD test temperatures. The results are summarized in Figure 5.13.

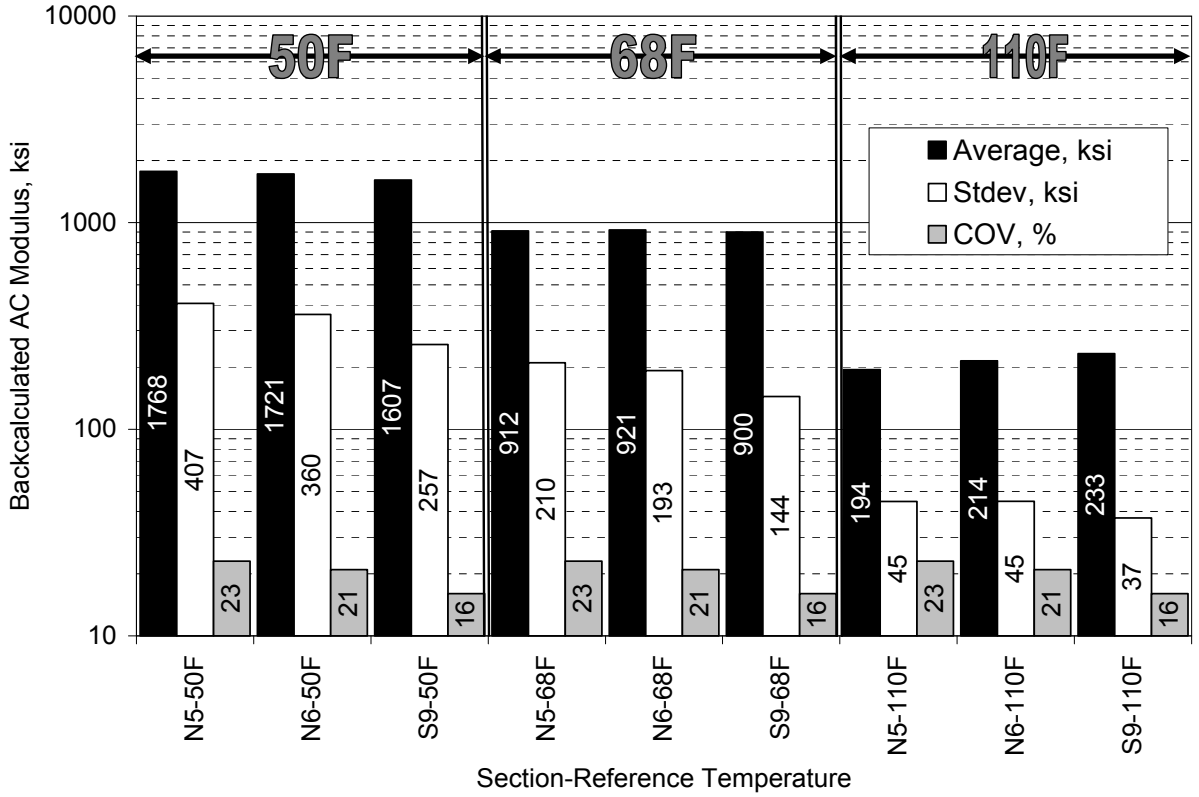

Figure 5.13 Backcalculated AC Modulus Corrected to Reference Temperatures

Figure 5.13 shows the average, standard deviation and coefficient of variation (COV) of each section's AC modulus at each reference temperature. In each case, the COV was less than 30%, which is a common benchmark for backcalculated AC modulus variability (Allen and Graves, 1994; Noureldin, 1994; Timm et al., 1999). Therefore, the AC moduli appear relatively consistent within each section.

Statistical testing was conducted using the Tukey-Kramer approach ($\alpha = 0.05$) to detect differences and sectional groupings with respect to AC modulus at each reference temperature. The Tukey-Kramer test is similar to the more commonly used ANOVA technique, but is able to determine statistical groupings. At 50F, all sections were statistically different with N5 having the largest amount of Thiopave and the highest modulus followed by N6 and S9. At 68F the average moduli between sections were not statistically distinguishable. At 110F, the differences in means were enough to distinguish between each section; N5 had the lowest modulus, followed by N6 and S9.

A final step in this analysis was to plot backcalculated AC modulus at 68F versus date to look for dramatic changes in AC modulus that would indicate possible pavement distress. Figure 5.14 shows relatively little change in modulus over time through the first year of testing. There did appear to be more erratic data in August 2010, but this is most likely due to the extreme temperatures tested (110 to 120F) rather than pavement distress at this point. Further monitoring through the end of the experiment will confirm or reject this hypothesis.

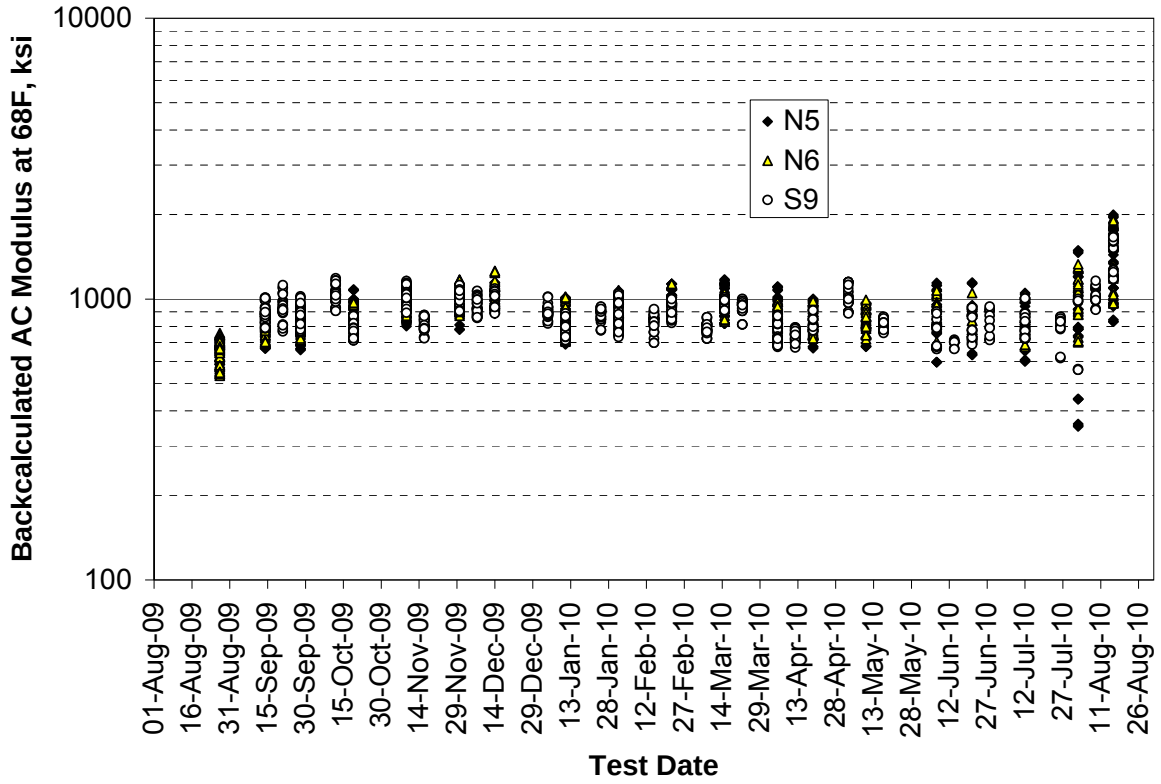

Figure 5.14 Backcalculated AC Modulus vs. Date at 68F

6. PAVEMENT RESPONSE MEASUREMENTS

As noted previously, traffic began on August 28, 2009. At that time, weekly pavement response measurements using the embedded asphalt strain gauges and earth pressure cells in the granular base and subgrade soil commenced. Weekly data collection consisted of collecting approximately fifteen truck passes (three passes of five trucks) in each section. The frequency of testing and number of trucks collected were consistent with previous data collection efforts at the Test Track which were shown to be sufficient to capture daily variability, seasonal variability and wheel wander effects (Timm and Priest, 2004; Priest and Timm, 2006). The response data in this report were gathered between August 28, 2009 and August 17, 2010.

Strain and pressure readings were acquired using a DATAQ DI-785 data acquisition system at a frequency of 1,000 samples/second/gauge. Raw signals were recorded in voltage versus time and customized processing templates developed in DaDISP were developed to clean the signals using a frequency filter, determine the peak responses for a given truck pass and convert the voltage output into engineering units of stress or strain, as appropriate. Figure 6.1 shows a sample truck pass over the aggregate base and subgrade soil earth pressure cells. The signals are in voltage versus time with peaks noted for each axle in the tractor-trailer combination. The processing scheme tabulates the peak responses, relative to the baseline, for each axle pass.

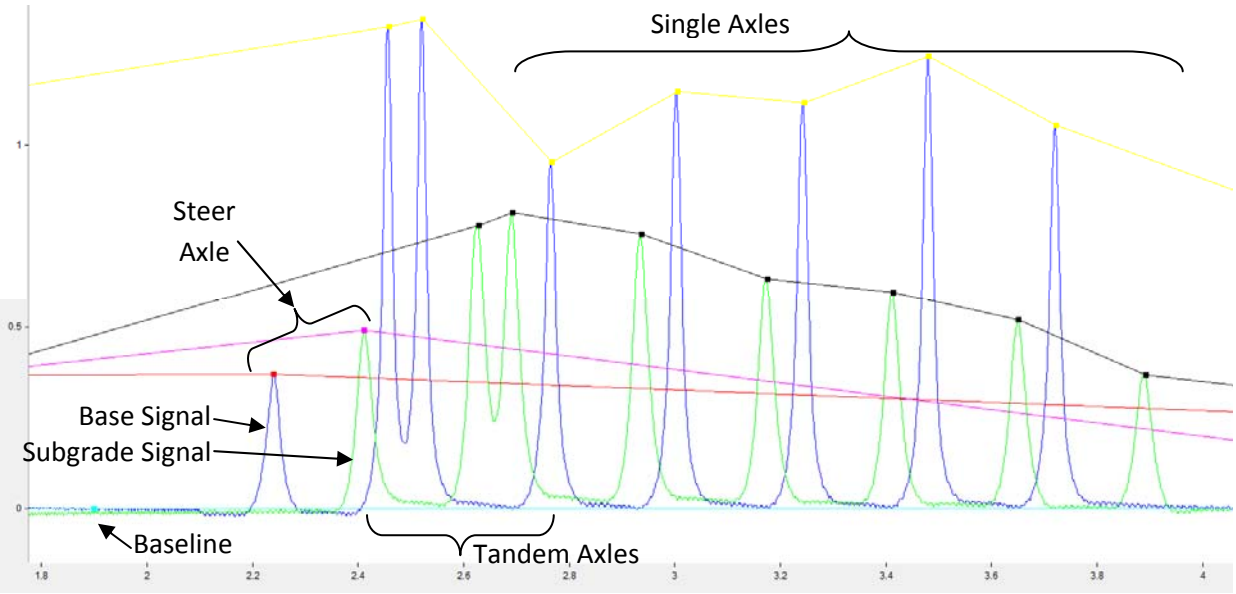

Figure 6.1 DaDISP Screen Capture of Pressure Measurements for Truck Pass

Figures 6.2 and 6.3 show typical strain response measurements in the longitudinal and transverse directions, respectively. The longitudinal measurements (Figure 6.2) usually have compressive strain as the axle approaches the gauge followed by peak tensile response when the axle is directly over the gauge. Finally, the pavement again goes into compression as the axle departs. This cyclic effect is seen throughout each of the axle passes in Figure 6.2.

Transverse strain responses (Figure 6.3) were distinctly different than the longitudinal strain measurements. The processing scheme was the same as that described above, but the signals typically were unilaterally compressive or tensile without the strain reversal seen in the longitudinal measurements. Full explanation of this behavior has been documented previously (Timm and Priest, 2008).

For each truck pass on each gauge, maximum (tensile) and minimum (compressive) responses, in addition to the amplitude (maximum-minimum) for each axle were recorded relative to the baseline. An Access database system was used to archive the data from which the "best-hit" response on a given day was determined on an axle-type basis. The "best-hit" represents the 95th percentile reading on a particular test day from all the readings made under a particular axle type. For example, on a typical day there could be 450 longitudinal strain readings made under single axles in a particular section (6 longitudinal gauges∗5 trucks∗3 passes/truck∗5 single axles/truck = 450 strain readings). The 95th percentile of these 450 readings represented the "best-hit" response for longitudinal strain The 95th percentile was used in previous research cycles at the Test Track (Willis and Timm, 2009) and was found to reasonably represent the true best-hit but guard against erroneously-high readings. This same approach was used for all axle types and the other measurements (base pressure, subgrade pressure and transverse strain).

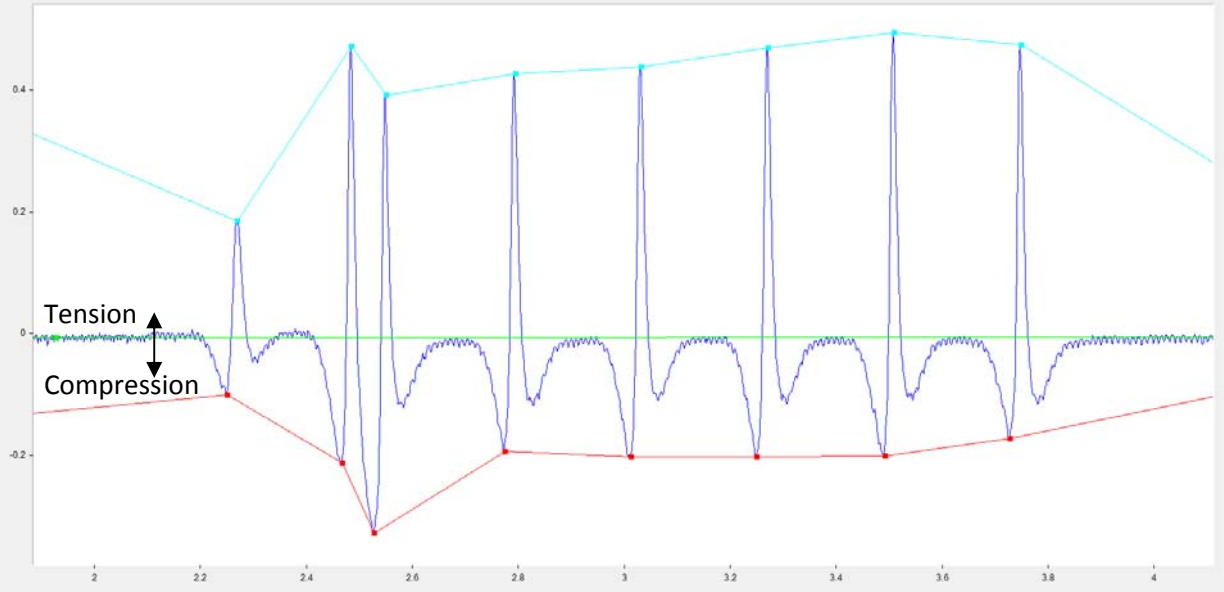

Figure 6.2 DaDISP Screen Capture of Longitudinal Strain Measurements

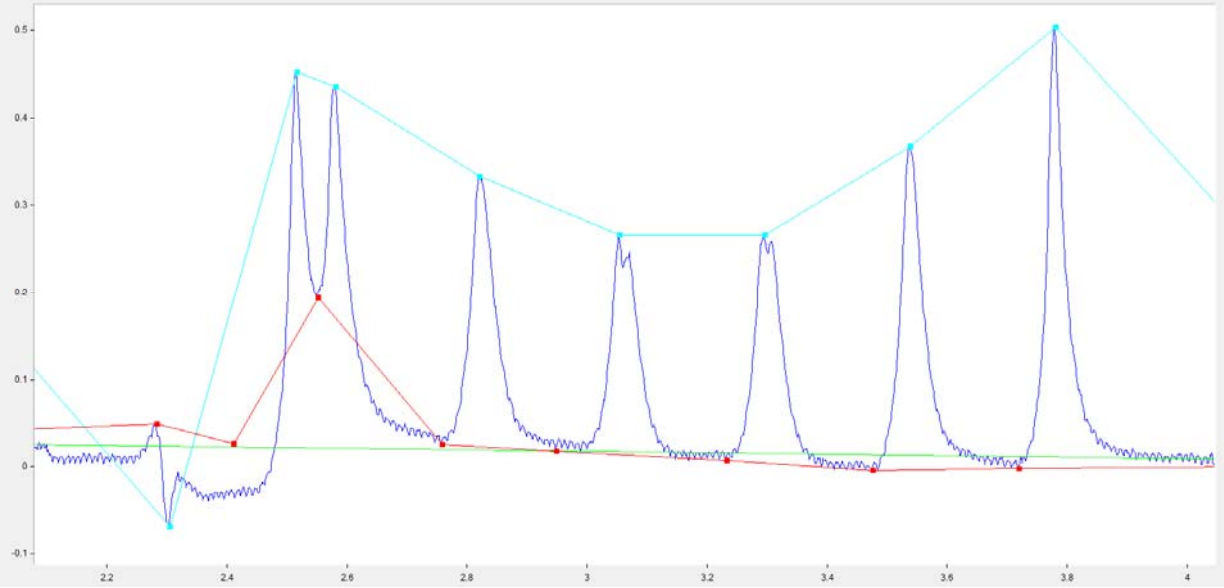

Figure 6.3 DaDISP Screen Capture of Transverse Strain Measurements

After collecting, processing and archiving the data, there were a number of analyses conducted. The following subsections examine seasonal trends in pavement response, temperature effects on pavement response, responses normalized to particular reference temperatures, responses over time at a normalized temperature and distributions of pavement response.

6.1 Seasonal Trends in Pavement Response

As discussed above, there are four primary measured pavement responses: longitudinal strain in the AC, transverse strain in the AC, vertical pressure in the aggregate base and vertical pressure in the subgrade soil. Figures 6.4 through 6.7 plot these responses versus test date for the single axle loadings only, though similar trends were observed with the other axle types. Each data

point in each plot represents the "best-hit" on that particular test date. The seemingly large fluctuation between consecutive test dates is a product of alternating collection times between morning and afternoon on a week-to-week basis. This ensures that a fuller range of temperatures are sampled during a particular season.

In each plot, the seasonal trends are clearly evident with lower responses during the cooler months and increased responses during warmer months. Though there are section-to-section differences, each exhibits a similar trend with respect to seasonal changes. On any particular date, Section N5 typically had the lowest pavement responses. This is owed primarily to the 2 in. thickness advantage over the other two sections. Sections N6 and S9, built to approximately the same AC thickness had much more similar pavement responses. These trends are more evident when responses are examined relative to temperature as shown in the next subsection.

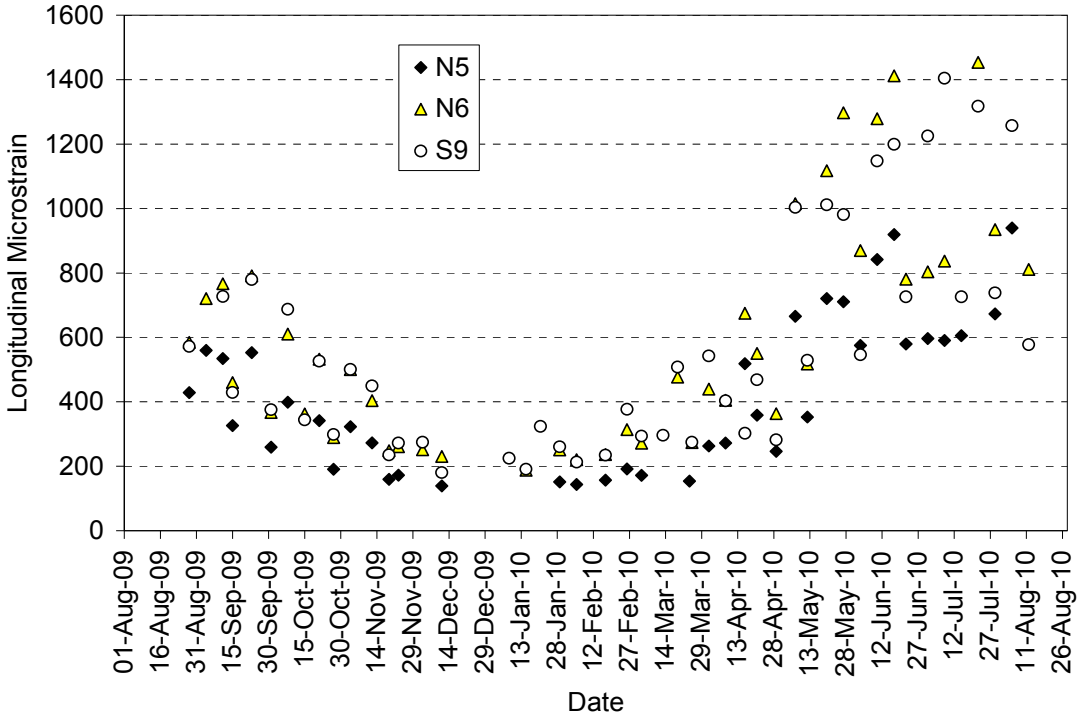

Figure 6.4 Longitudinal Microstrain Under Single Axles

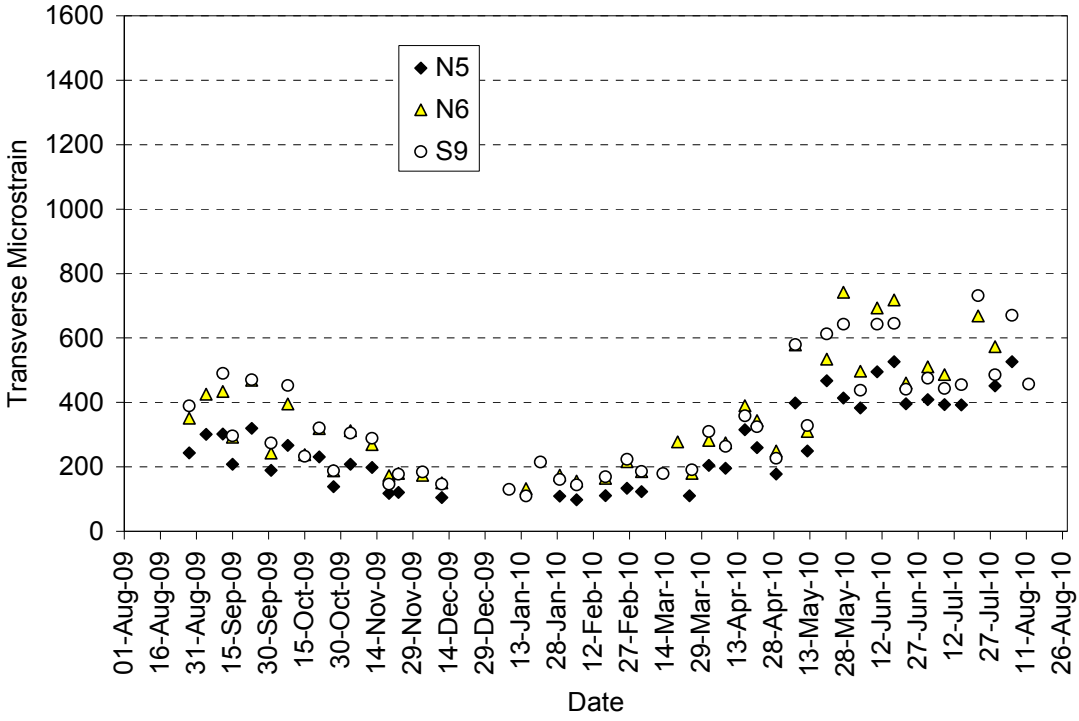

Figure 6.5 Transverse Microstrain Under Single Axles

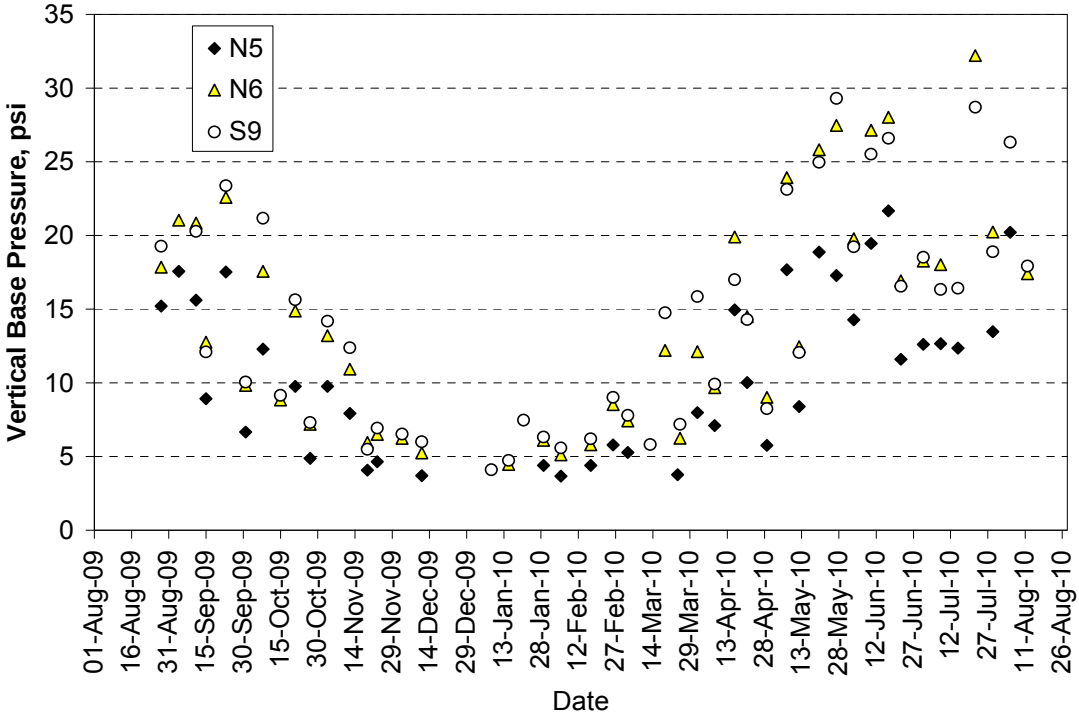

Figure 6.6 Aggregate Base Pressure Under Single Axles

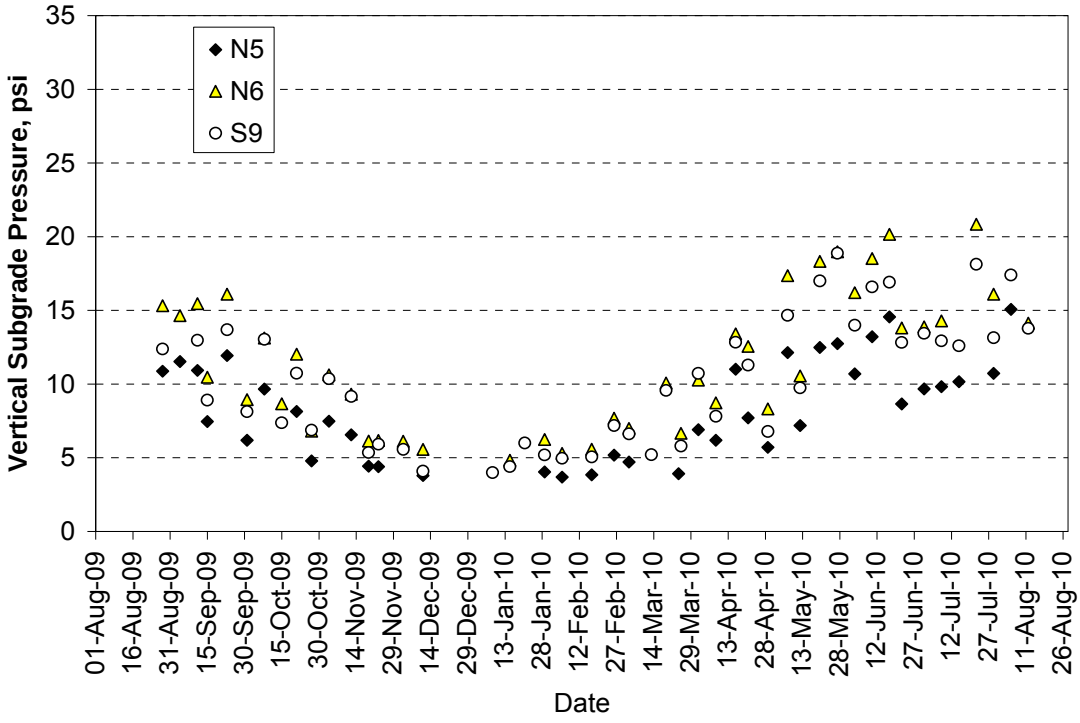

Figure 6.7 Subgrade Pressure Under Single Axles

6.2 Pavement Response vs. Temperature

The data presented in Figures 6.4 through 6.7 were the best-hit pavement responses on a particular test date. These data were replotted in Figures 6.8 through 6.11 against their corresponding mid-depth pavement temperature. Exponential regression equations, much like those determined for the backcalculated AC moduli, were best-fit to each data set in Figures 6.8 through 6.11 representing single axles. Additional equations were developed for each of the axle types, the results of which are presented in Table 6.1. In total, 36 sets of regression parameters were determined (3 sections∗4 responses∗3 axle types = 36). In 32 of 36 equations, the R^2 exceeded 90%. Three of the remaining four equations had R^2 exceeding 80%. The poorest fit was for the aggregate base pressure in S9 under steer axle loading (R^2 = 68%). Clearly, mid-depth temperature is a strong predictor of each of the measured pavement responses.

It is important to note that the sections followed similar exponential trends. This indicates similar response under dynamic axle loading such that the materials (control vs. Thiopave) can be modeled in a similar fashion. S9 (Control) and N6 (Thiopave), having approximately the same thickness, yielded very similar responses across the temperature spectrum. The exception was the vertical pressures measured in the subgrade which were consistently higher for the N6 relative to S9. Recall from Figure 3.5 that the aggregate base thickness in N6 was on average approximately 0.8 inches thinner than the base in S9. Therefore, it is reasonable and expected that N6 would have slightly greater subgrade stresses. The notable distinction between the thinner sections (N6, S9) and N5 is due primarily to the 2 inch thickness advantage of this section.

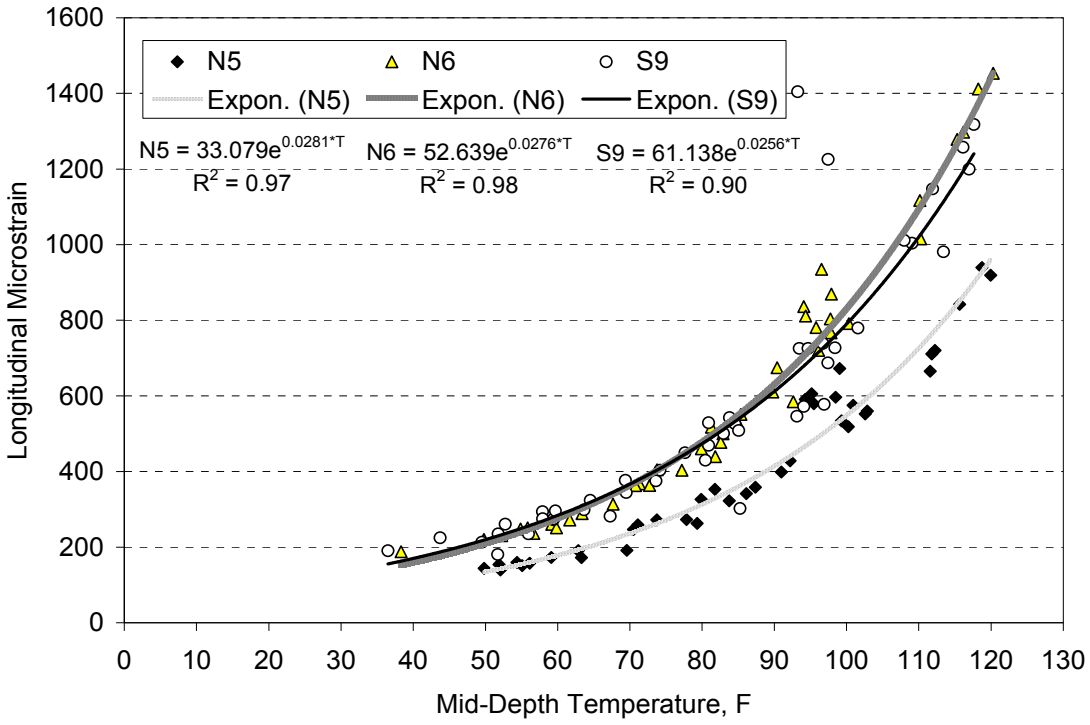

Figure 6.8 Longitudinal Strain vs. Mid-Depth Temperature Under Single Axles

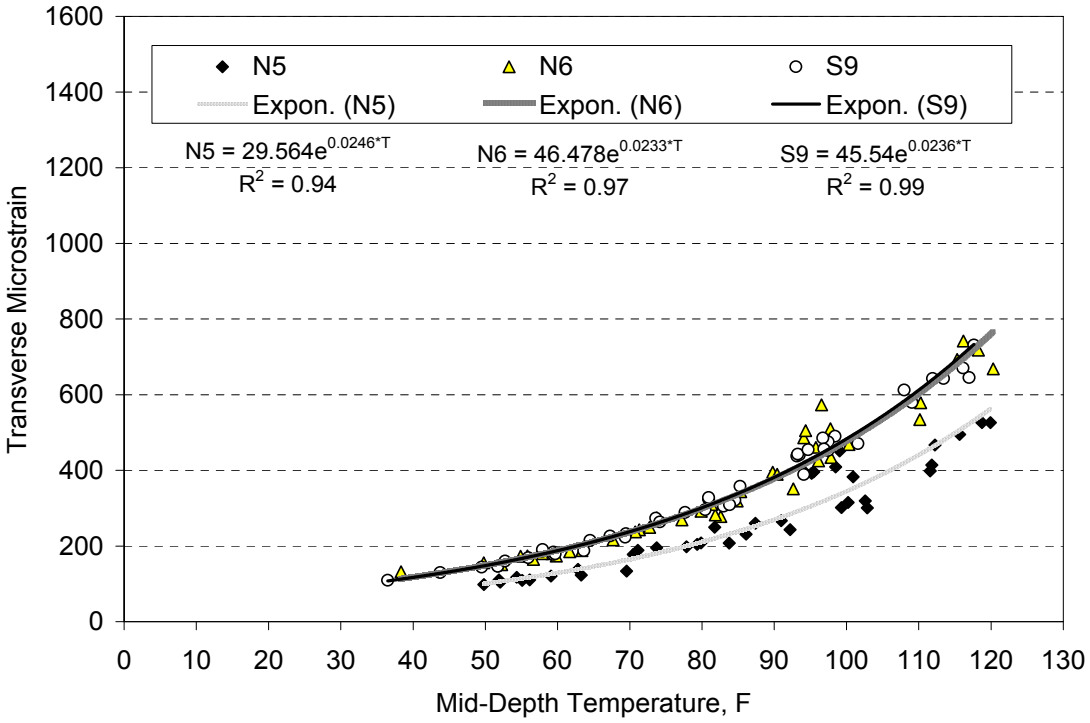

Figure 6.9 Transverse Strain vs. Mid-Depth Temperature Under Single Axles

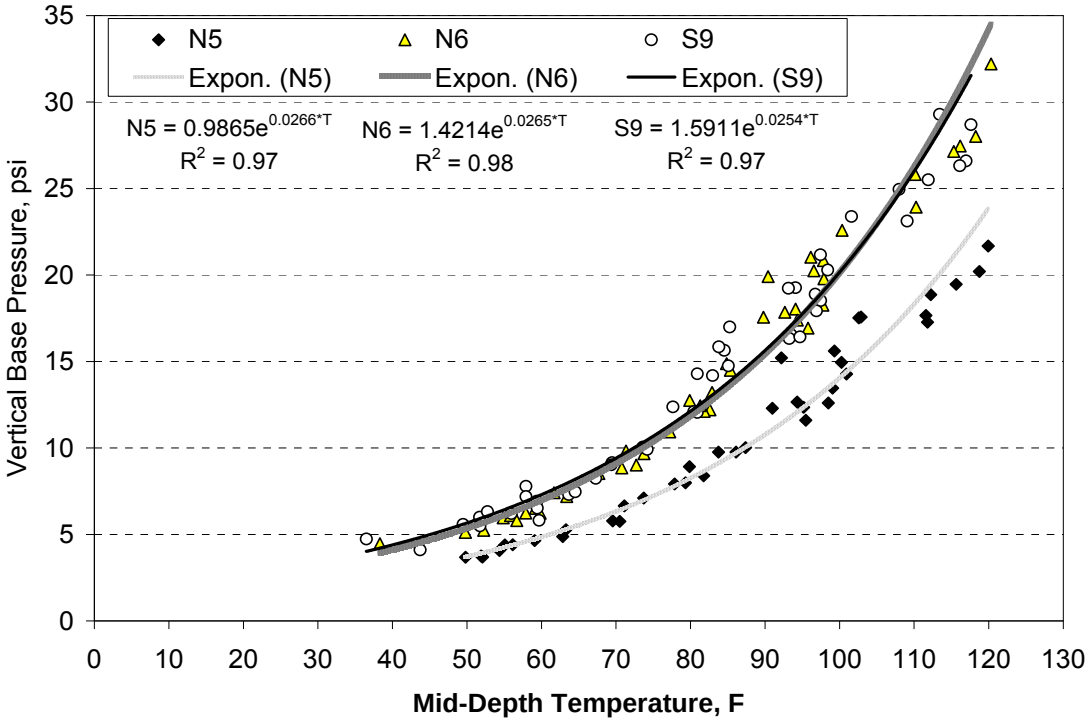

Figure 6.10 Base Pressure vs. Mid-Depth Temperature Under Single Axles

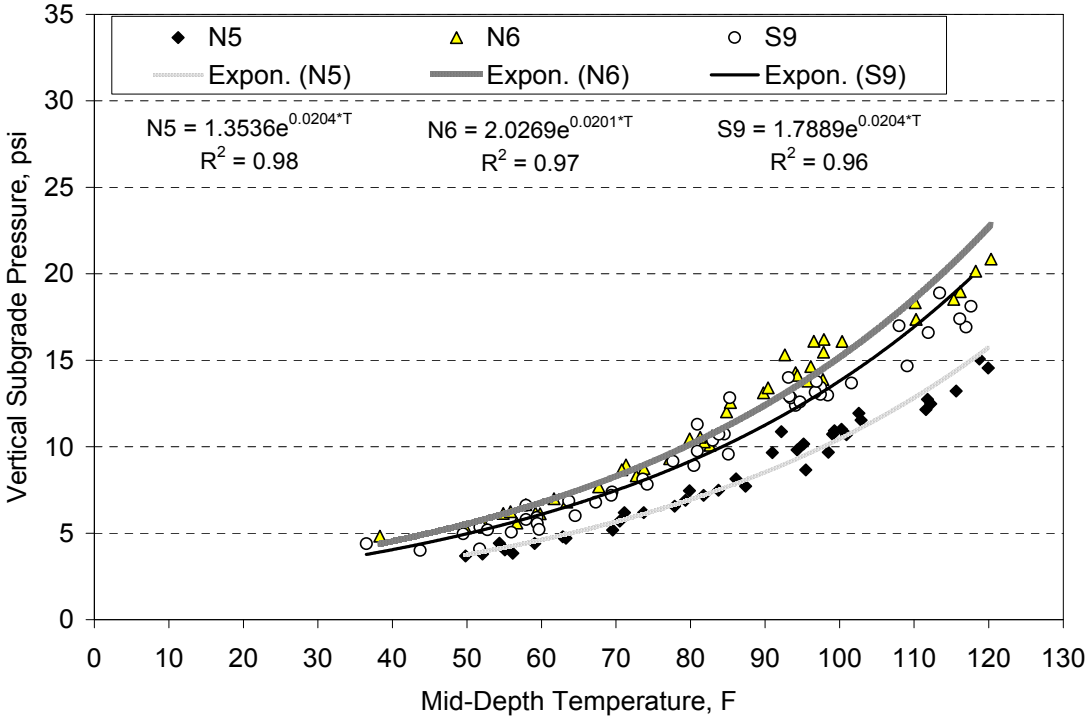

Figure 6.11 Subgrade Pressure vs. Mid-Depth Temperature Under Single Axles

Table 6.1 Pavement Response vs. Temperature Regression Terms

		Longitudinal Strain			Transverse Strain			Base Pressure			Subgrade Pressure		
Section	Axle	k_1	k_2	R^2	k_1	k_2	R^2	k_1	k_2	R^2	k_1	k_2	R^2
N5	Steer	13.790	0.033	0.98	15.376	0.032	0.88	0.296	0.033	0.97	0.474	0.026	0.97
	Single	33.079	0.028	0.97	29.564	0.025	0.94	0.987	0.027	0.98	1.354	0.020	0.98
	Tandem	23.662	0.032	0.97	30.985	0.024	0.93	1.254	0.025	0.98	1.748	0.018	0.97
N6	Steer	21.825	0.033	0.98	22.298	0.032	0.98	0.414	0.034	0.98	0.675	0.026	0.96
	Single	52.639	0.028	0.98	46.478	0.023	0.97	1.421	0.027	0.98	2.027	0.020	0.97
	Tandem	46.248	0.029	0.98	51.235	0.021	0.95	1.847	0.024	0.97	2.532	0.018	0.96
S9	Steer	26.675	0.029	0.87	26.878	0.030	0.96	0.698	0.025	0.68	0.701	0.023	0.82
	Single	61.138	0.026	0.90	45.540	0.024	0.99	1.591	0.025	0.97	1.789	0.020	0.96
	Tandem	46.970	0.028	0.91	43.669	0.023	0.98	1.799	0.024	0.95	2.234	0.018	0.95

6.3 Pavement Responses Normalized to Reference Temperatures

To characterize statistical differences in pavement response between sections, temperature corrections were applied to each data set (longitudinal strain, transverse strain, base pressure, subgrade pressure) at 50, 68 and 110F. Temperature-corrected responses were determined according to:

$$response_{T_{ref}} = response_{T_{meas}} e^{k_2\left(T_{ref} - T_{meas}\right)} \quad (6.1)$$

Where:
$response_{Tref}$ = response at T_{ref}
$response_{Tmeas}$ = response at T_{meas}
T_{ref} = mid-depth reference temperature (50, 68, 110F)
T_{meas} = mid-depth measured temperature, F
k_2 = section, axle and response-specific regression constant from Table 6.1

The average, standard deviation and coefficient of variation were determined at each reference temperature. Tukey-Kramer statistical tests (α=0.05) were conducted on each data set to establish groupings with the results discussed below. Only results for the single axles are presented here, though similar trends were noted amongst the other axles.

6.3.1 Longitudinal Strain Responses

Figure 6.12 summarizes the temperature-corrected longitudinal strain measurements under single axles. The data show relatively good consistency with COV's less than 23%. Tukey-Kramer testing indicated no differences between S9 (7"-Control) and N6 (7"-Thiopave) at each reference temperature. This is important since Tukey-Kramer testing indicated statistically-different backcalculated AC moduli at the coldest (50F) and warmest (110F) reference temperatures with no difference in AC modulus at 68F. Evidently, the statistical differences in AC modulus were not sufficient to statistically impact the longitudinal strain responses. Section N5 (9"-Thiopave) was statistically lower than the other sections at each of the reference temperatures as one would expect for the thickest of the three sections.

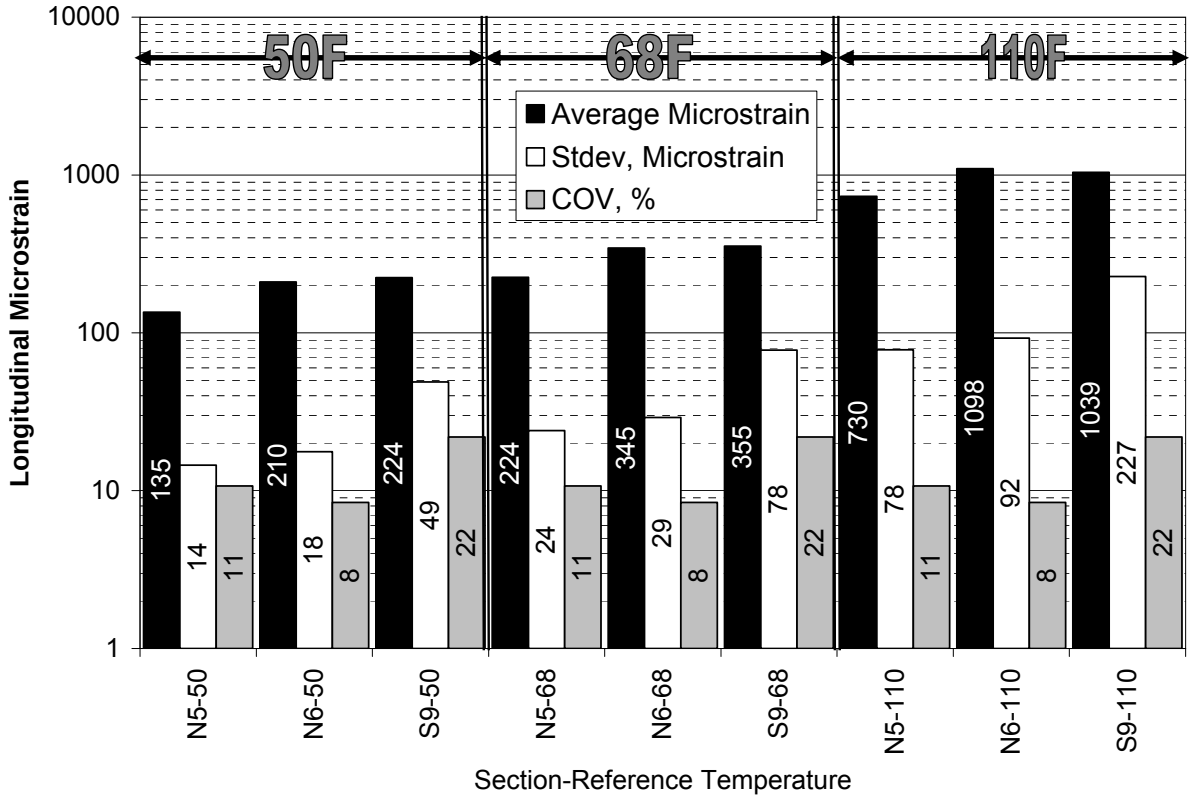

Figure 6.12 Longitudinal Strain Under Single Axles at Three Reference Temperatures

After one year of testing, there has been no fatigue cracking evident. However, preliminary fatigue estimates can be made for comparison purposes to evaluate relative performance estimates using the strain data in Figure 6.12 with the fatigue transfer functions developed previously. Table 6.2 lists the measured average strain at 68F and the corresponding predicted fatigue life using the transfer functions presented in Table 4.13. It is important to note that despite N6 and S9 having statistically equivalent strain levels at 68F, the improved fatigue characteristics of the Thiopave-modified base mixture yields an improvement of approximately 3.9 times in the predicted fatigue life over the control section. The improved fatigue characteristics combined with increased thickness in section N5 increases the predicted fatigue life by a factor of 54 over the control section.

Table 6.2 Predicted Fatigue Life at 68F

Section	Average Microstrain at 68F	Predicted Fatigue Life – Cycles to Failure at 68F
N5	224	15,827,114
N6	345	1,132,838
S9	355	293,097

6.3.2 Transverse Strain Responses

Figure 6.13 summarizes the transverse strains under single axle loadings. As found in previous studies (Timm and Priest, 2008), the transverse strains were generally lower than their longitudinal counterparts. Also, the transverse strains were somewhat more consistent than longitudinal with COV's below 14%. The Tukey-Kramer findings were identical to the longitudinal strain findings; no differences were noted between S9 and N6, with N5 statistically lower at all temperatures. The average strain levels in S9 and N6 were remarkably similar with, at most, 8 με separating the sections.

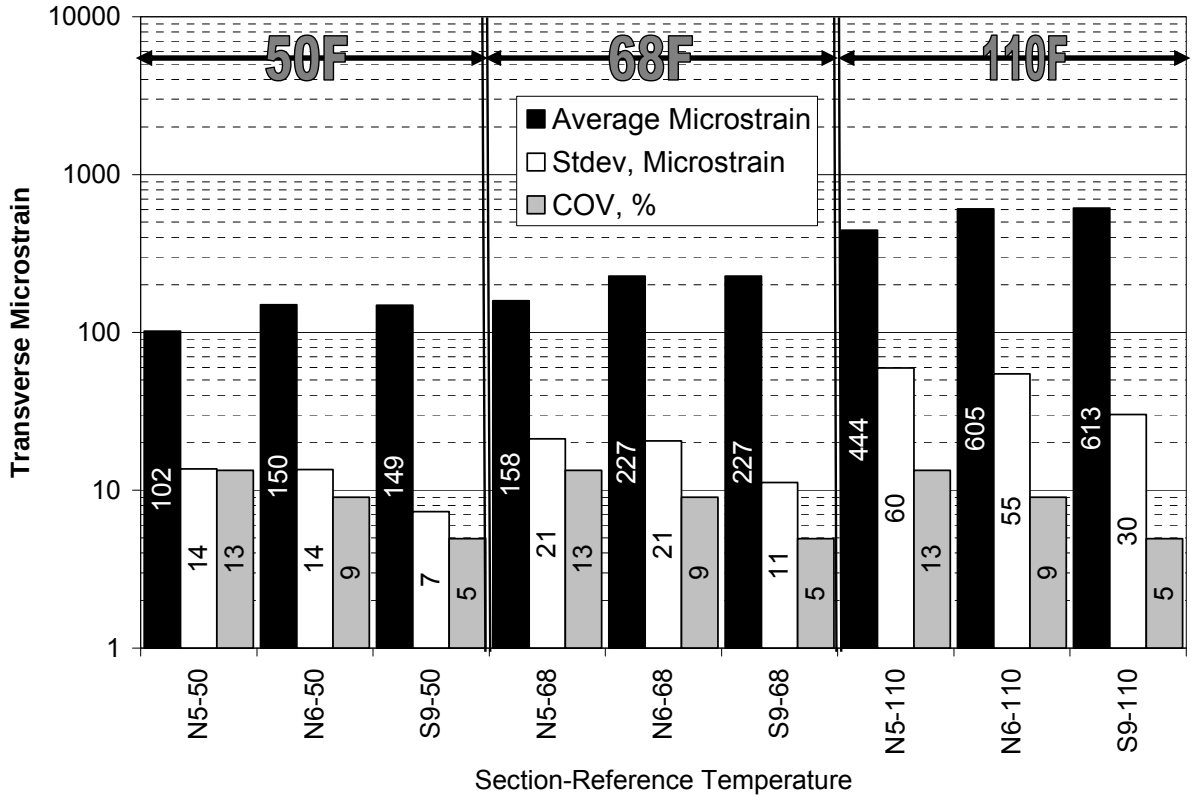

Figure 6.13 Transverse Strain Under Single Axles at Three Reference Temperatures

6.3.3 Aggregate Base Vertical Pressure Responses

Figure 6.14 summarizes the vertical pressures in the aggregate base under single axle loadings. These data are even less variable than the strain measurements with COV's below 11%. At 50F, the mean values for each section are statistically different, though one could argue the practical significance of 0.3 psi between N6 and S9. At 68 and 110F, N6 and S9 are grouped while N5 is statistically lower due to its increased AC thickness.

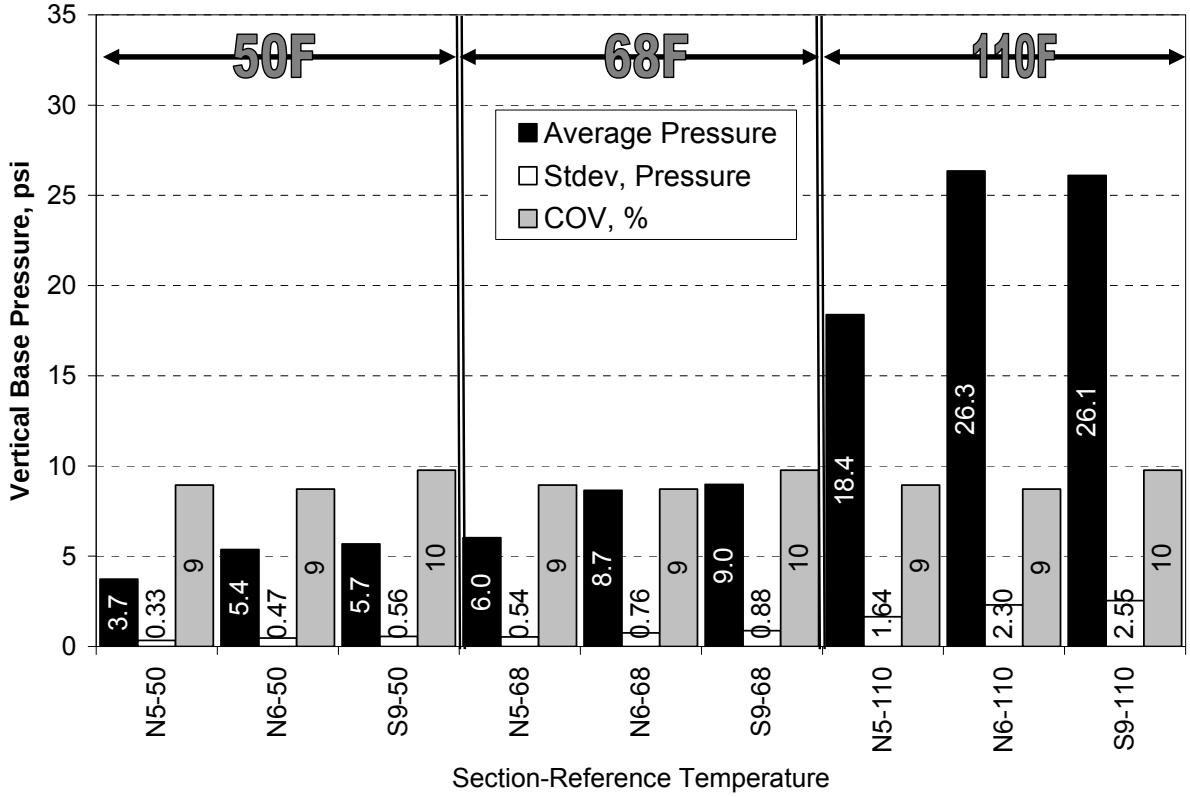

Figure 6.14 Base Pressure Under Single Axles at Three Reference Temperatures

*6.3.4 Subgrade Vertical Pressure Response***s**

The temperature-corrected vertical pressures in the subgrade are plotted in Figure 6.15. These measurements were less variable than those presented above with all COV's less than 10%. Statistically, all the mean values in Figure 6.15 are statistically significantly different.

As noted previously, the aggregate base in S9 is slightly thicker than N6, so one would expect lower stresses in the subgrade. Though statistically different, one could again argue the practical significance of less than 2 psi difference between S9 and N6.

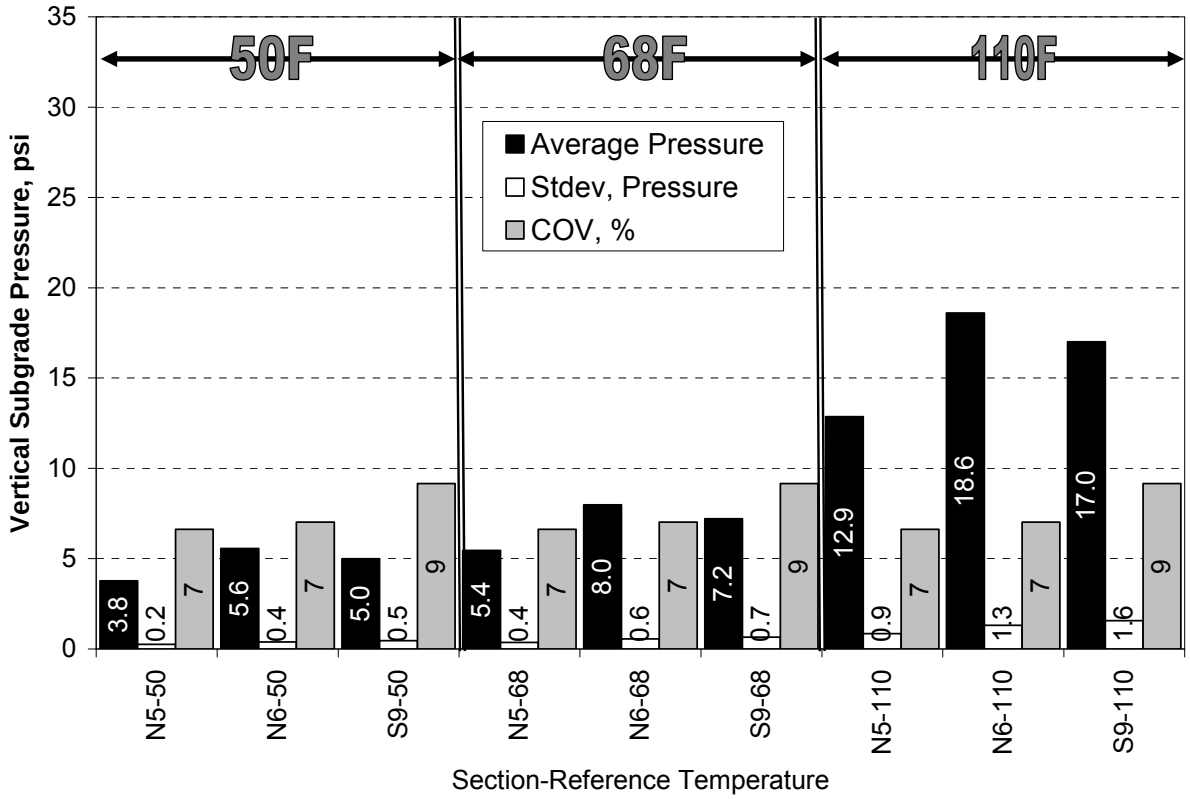

Figure 6.15 Subgrade Pressure Under Single Axles at Three Reference Temperatures

6.4 Pavement Response Over Time at 68F

Responses corrected to 68F were plotted against test date, as done with the backcalculated AC moduli data, to look for signs of distress in the response measurements. Figures 6.16 through 6.19 show relatively constant measurements over time, which is consistent with the AC moduli versus time presented earlier. Both data sets indicate no cracking after one year of testing. The two outliers seen in Figure 6.16 were further investigated. No justification could be found, other than their non-conformance to the general trend, to remove them from the data set so they were left in-place.

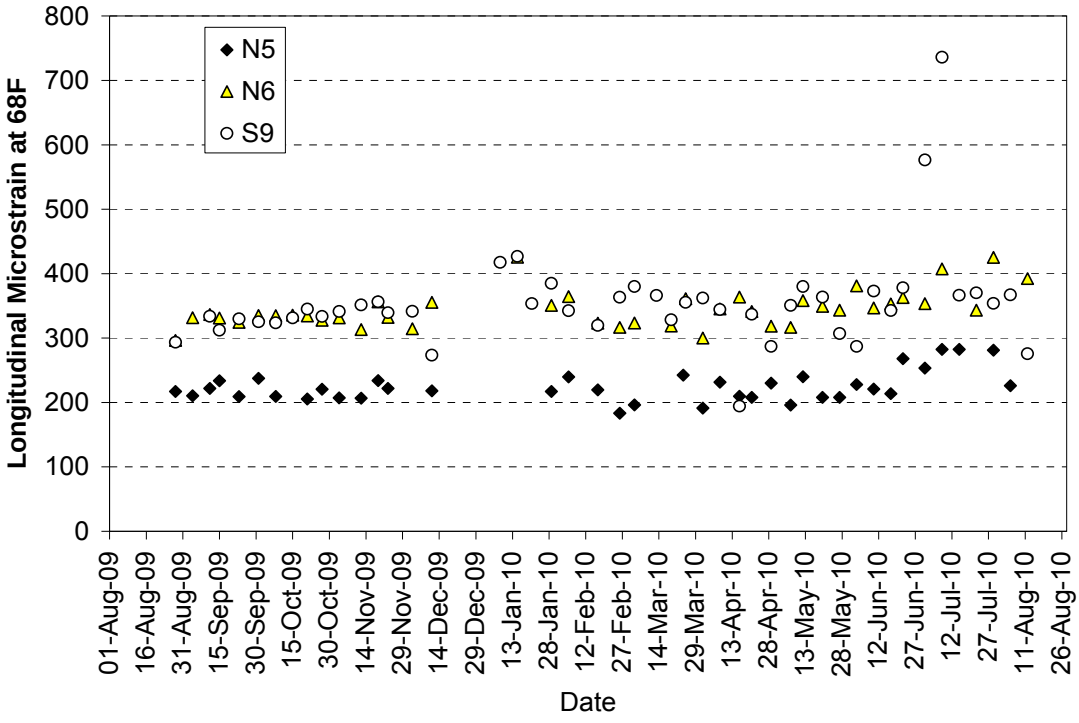

Figure 6.16 Longitudinal Microstrain Under Single Axles vs. Date at 68F

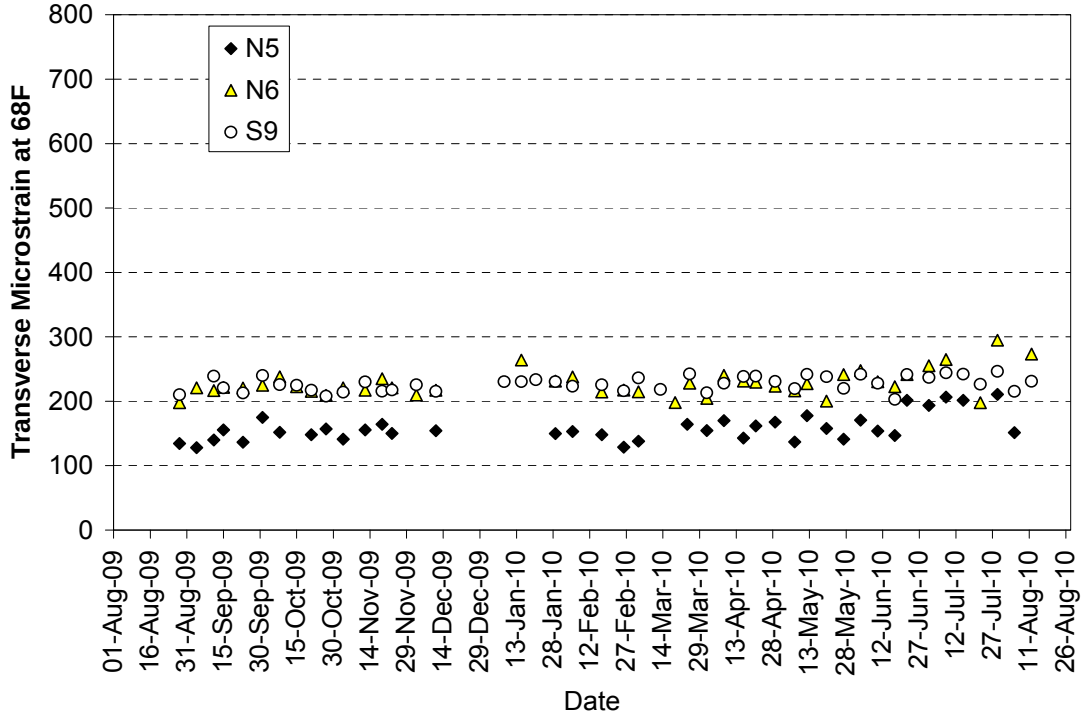

Figure 6.17 Transverse Microstrain Under Single Axles vs. Date at 68F

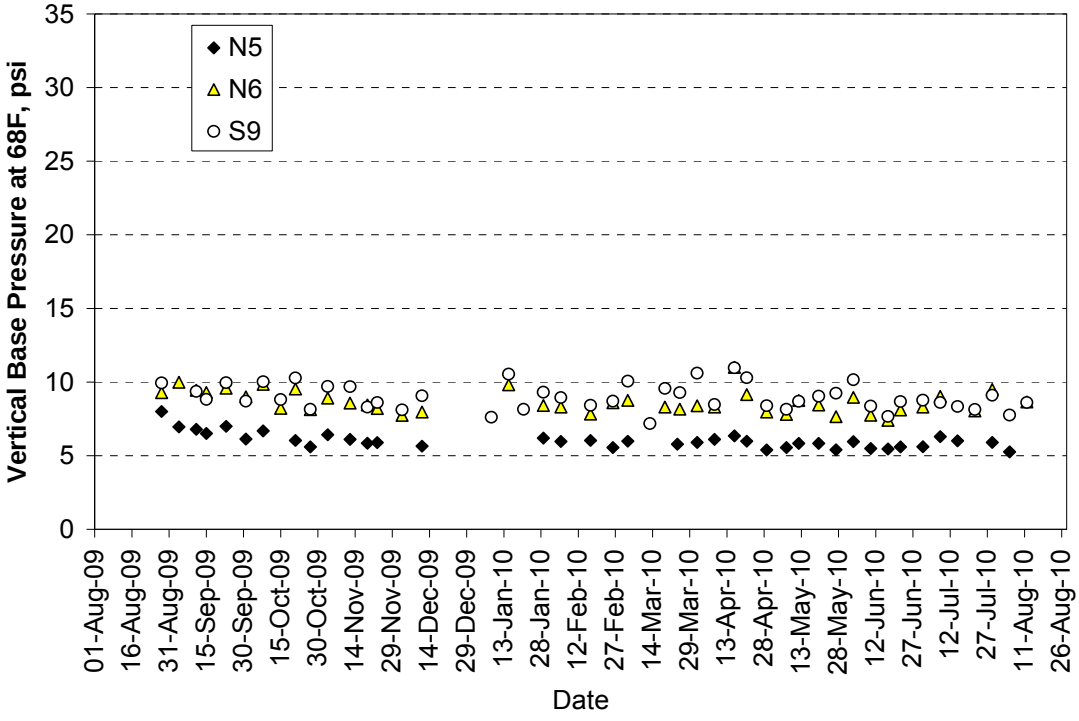

Figure 6.18 Base Pressure Under Single Axles vs. Date at 68F

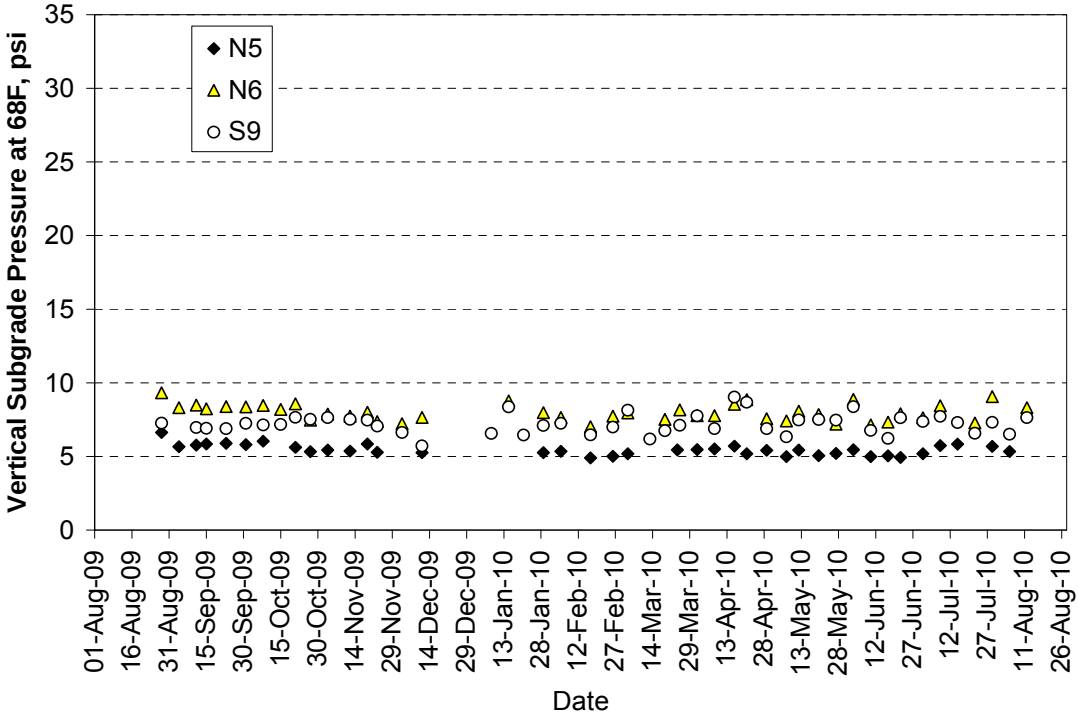

Figure 6.19 Subgrade Pressure Under Single Axles vs. Date at 68F

6.5 Strain Distributions

The response measurements presented thus far represent a weekly data collection cycle. However, the trucks operated on a 16-hour schedule 5 days per week. During this time, detailed trucking records were kept so that the number of laps made by each truck during each hour of operation could be determined. Also, minute-by-minute mid-depth temperature readings were collected and aggregated into hourly averages for a continuous hourly record of pavement temperature. These two databases (temperature versus time and traffic versus time) were combined, with the response versus temperature equations previously established (Table 6.1), to create pavement response distributions from August 28, 2009 through August 28, 2010.

Figures 6.20 through 6.23 summarize the distributions for longitudinal strain, transverse strain, vertical base pressure and vertical subgrade pressure, respectively. In each graph, the left vertical axis represents the percentage of readings at each response level (probability density functions (PDF)). The right vertical axis represents the cumulative percentage below each response level (cumulative density functions (CDF)). It is important to note that these distributions represent the cumulative effect of all axle types during trafficking and are the most complete representation of structural responses exhibited by these sections. In effect, they are the best representation of the cumulative response distributions that would have been obtained if each and every axle pass had been recorded and processed.

In all cases, the PDF's appear to have a nearly log-normal distribution with relatively long tails in the higher response ranges. It is also interesting to note that each PDF appears to have a major peak at approximately the 20^{th} percentile. For example, for section N6 in Figure 6.20, the peak PDF frequency is 5% at 240 με which corresponds to the 20^{th} percentile on the CDF scale. Peaks for the other sections and responses also occur approximately at the 20^{th} percentile. A secondary peak also appears in each plot, for each section, between the 70^{th} and 80^{th} percentiles. These peaks are the product of the environmental and loading conditions at the Test Track. The fact that each distribution contains these characteristic peak values lends confidence to the data acquisition, processing and post-processing analysis.

With the exception of vertical subgrade stress (Figure 6.23), the response distributions are very similar between S9 and N6 as one would expect given the data presented above. Also, as expected, there was a significant decrease in response resulting from the increased thickness of N5. The increased subgrade stresses in N6 relative to S9 result from the thinner aggregate base in N6, as discussed above.

The strain and pressure magnitudes are also important in each of the figures. Recall from Figure 1.8 that the expected 90^{th} percentile strain generated using PerRoad in the preliminary analysis of the control section was approximately 375 με. The 90^{th} percentile measured strains in Figure 6.20 are on the order of 1000 με for N6 and S9. These discrepancies certainly warranted further investigation as discussed below.

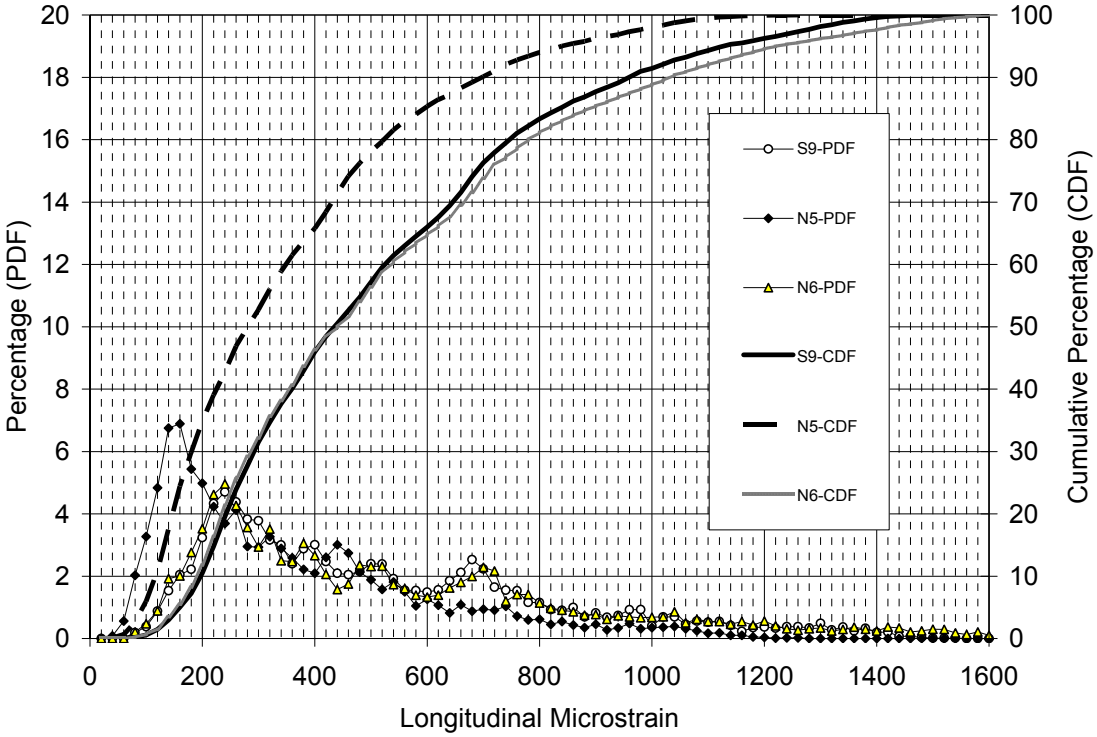

Figure 6.20 Longitudinal Strain Distributions

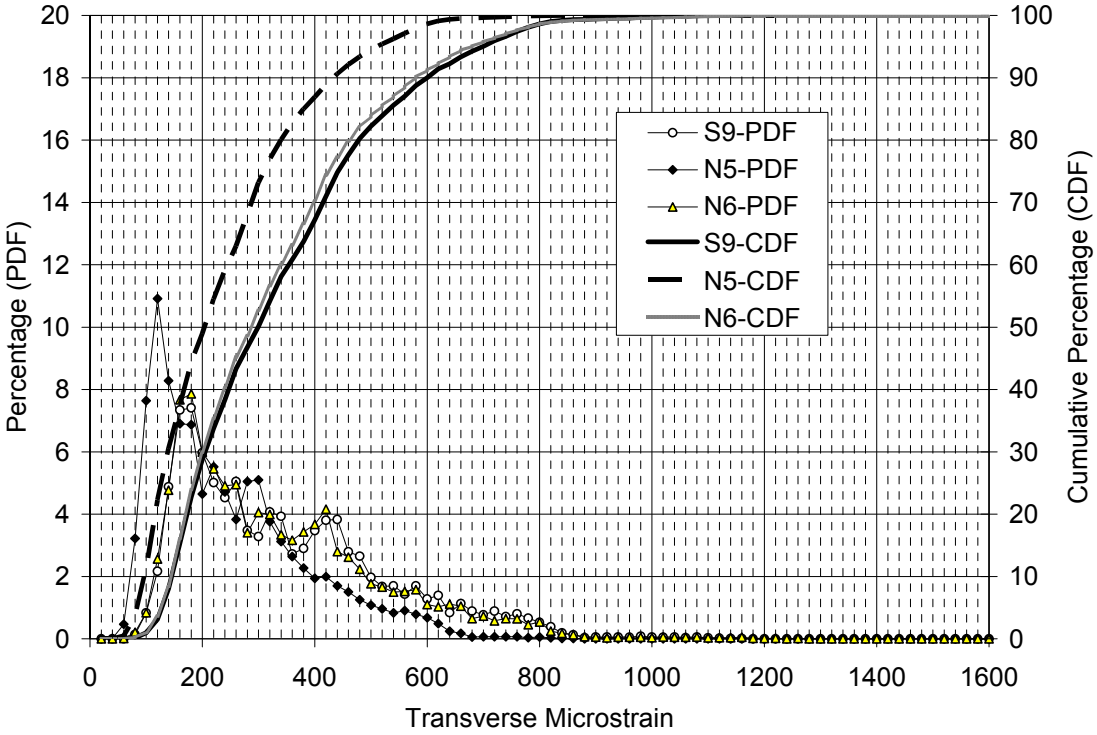

Figure 6.21 Transverse Strain Distributions

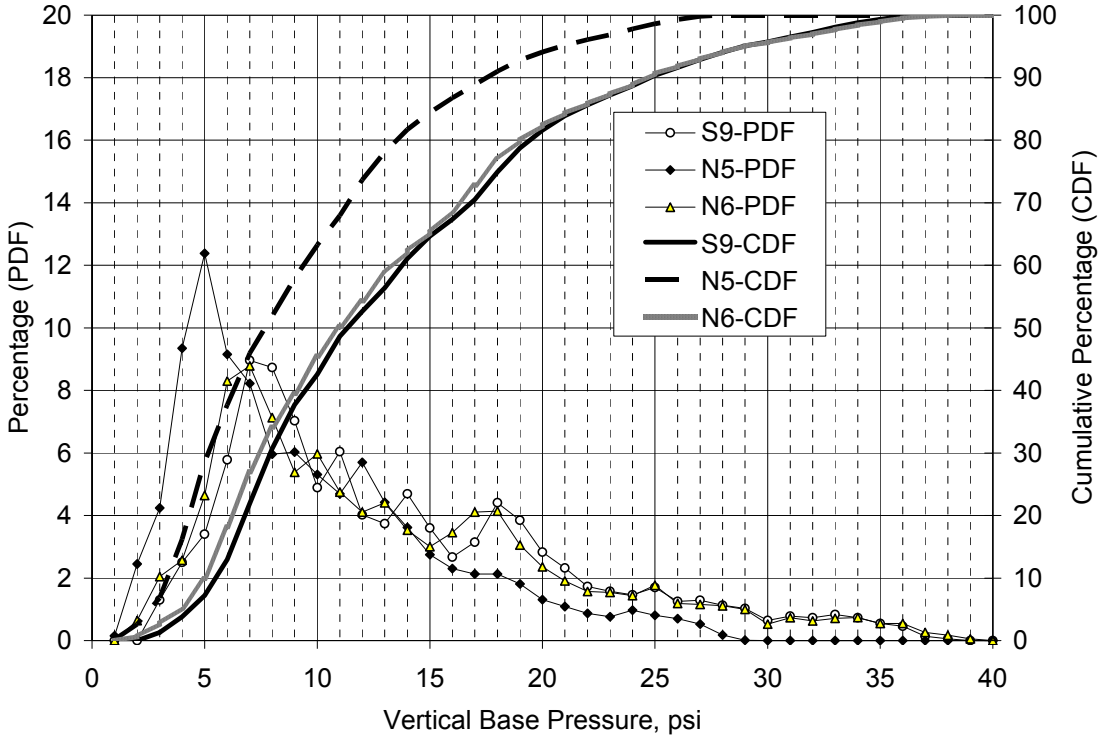

Figure 6.22 Base Pressure Distributions

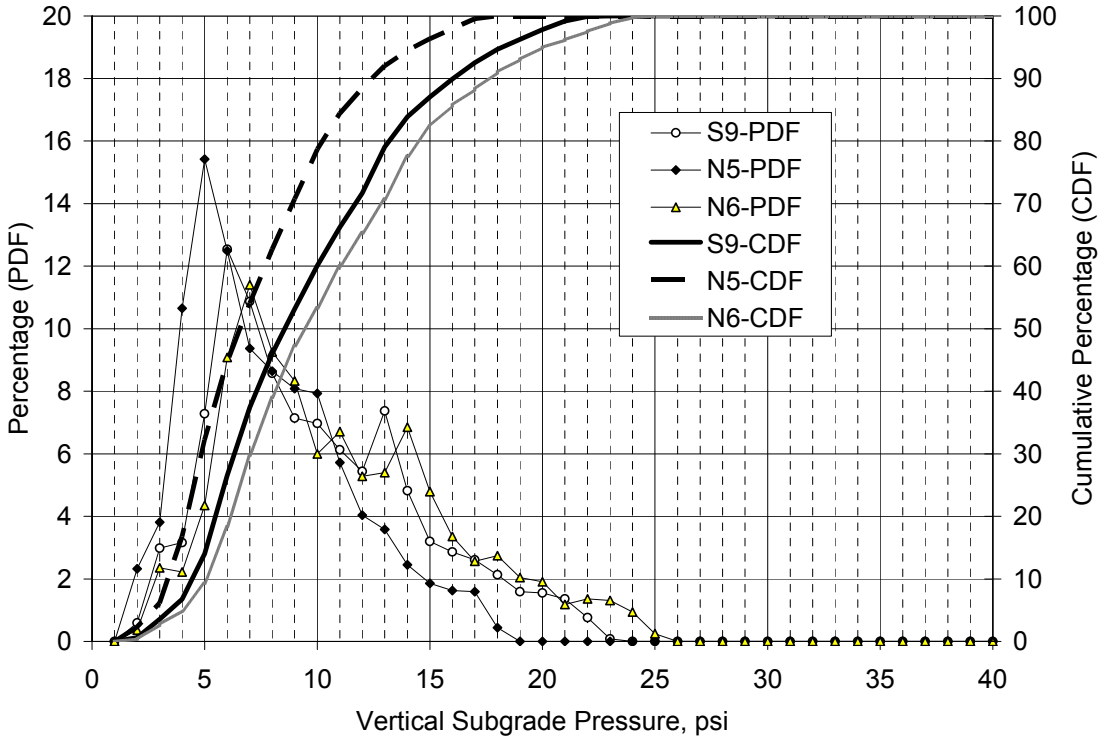

Figure 6.23 Subgrade Pressure Distributions

6.5.1 Predicted and Measured Pavement Response Distributions

The pavement response percentiles presented in Figures 1.8 and 1.9 were based on PerRoad simulation of hypothetical cross-sections using either previously-developed dynamic modulus data (in the case of the control mixtures) or dynamic moduli obtained during the first phase of this study (Timm et al., 2009) (for the Thiopave mixtures). During these simulations, temperature data collected at the Test Track between 2006 and 2008 were used to determine the asphalt moduli assuming a frequency of 10 Hz. Furthermore, the subgrade and base moduli used in simulation were based on values obtained from Section S11 of the 2006-2009 Test Track.

The data presented in Figures 6.20 through 6.23, on the other hand, represent measured pavement responses of in-place sections between August 2009 and August 2010. Given the differences between what was actually built versus that which was previously simulated, it is expected that these responses would not completely match. However, as noted above, the differences here are quite large (375 με versus 1000 με, in the case of asphalt strain). So, the question naturally arises whether theoretical predictions using PerRoad can be made using section-specific as-built information that better match the measured pavement response distributions. This is an important question for future modeling of these materials in modern pavement design and analysis methodologies.

When using PerRoad, or any pavement simulation tool, a decision must be made regarding characterizing the modulus of the materials. In the simulations summarized in Figure 1.8 and 1.9, the decision was made to use dynamic modulus data at 10 Hz. While this worked well for comparison between sections, there are other options available such as using backcalculated moduli to represent in situ conditions, using dynamic modulus data at other frequencies and using dynamic modulus data from confined and unconfined testing. As demonstrated below, each data set results in different response levels since the moduli change with each change in test condition. Furthermore, it has been observed at the Test Track that slippage between layers can occur (Willis and Timm, 2006; Willis and Timm, 2007). The simulations presented below include both fully-bonded and fully-slipped layer interfaces. Table 6.3 summarizes the PerRoad scenarios considered in this analysis. When considering the 5 sources of AC moduli data, 3 test sections and fully-bonded versus fully slipped interfaces, a total of 30 (5x3x2) PerRoad simulations were conducted as described below. The goal of these simulations was to identify the set of conditions that best-matched the measured pavement responses and determine if these conditions were reasonable.

Table 6.3 PerRoad AC Simulation Conditions

Case	AC Layers	AC Modulus
1	1	Backcalculated
2	3	E* from 10 Hz – Confined
3	3	E* from 10 Hz – Unconfined
4	3	E* from 1 Hz – Confined
5	3	E* from 1 Hz – Unconfined

Table 6.3 shows that two general approaches were taken. The first was to simulate the pavement cross section with one composite AC layer using the backcalculated asphalt modulus versus temperature equations from Figure 5.12. Mid-depth measured temperature data were used to

determine the spectrum of moduli for each test section. These data, in addition to backcalculated granular base and subgrade moduli were entered into PerRoad to simulate the respective test sections. The second approach was to use the laboratory-generated dynamic modulus data of the plant-produced mixtures to subdivide the AC into three lifts having lift-specific modulus-temperature relationships. E* data generated at 10 Hz and 1 Hz in addition to confined and unconfined testing were considered. Measured temperatures at the top, middle and bottom of each AC cross section were interpolated to represent the mid-depth of each AC lift and generate a spectrum of moduli for each lift in each section. These data, in addition to the backcalculated granular base and subgrade moduli were entered into PerRoad for simulation. Modulus variability for each pavement layer based on backcalculation was entered into PerRoad while the thicknesses of each lift were held constant and represented the surveyed depths in the middle of the instrumentation array.

The following graphs are presented in groups of three. Each plot contains the section-specific measured cumulative pavement response distribution for each respective response (longitudinal AC strain, base pressure and subgrade pressure). Transverse strain was not included since PerRoad only outputs the maximum horizontal strain, which corresponds to longitudinal strain. These are the same distributions presented in Figures 6.20, 6.22 and 6.23 above. Added to each plot are the PerRoad-simulated response distributions for each section representing fully-bonded and fully-slipped interfaces. Each group of three graphs corresponds to the cases listed in Table 6.3.

6.5.1.1 Simulations Based on Backcalculated AC Moduli

As shown in Figures 6.24, 6.25 and 6.26, using backcalculated AC moduli in PerRoad, whether in a full slip or full bond condition, underestimates the measured pavement responses in all cases. Clearly, the composite AC moduli determined under FWD loading, are too high to represent the pavement cross sections under actual traffic loading.

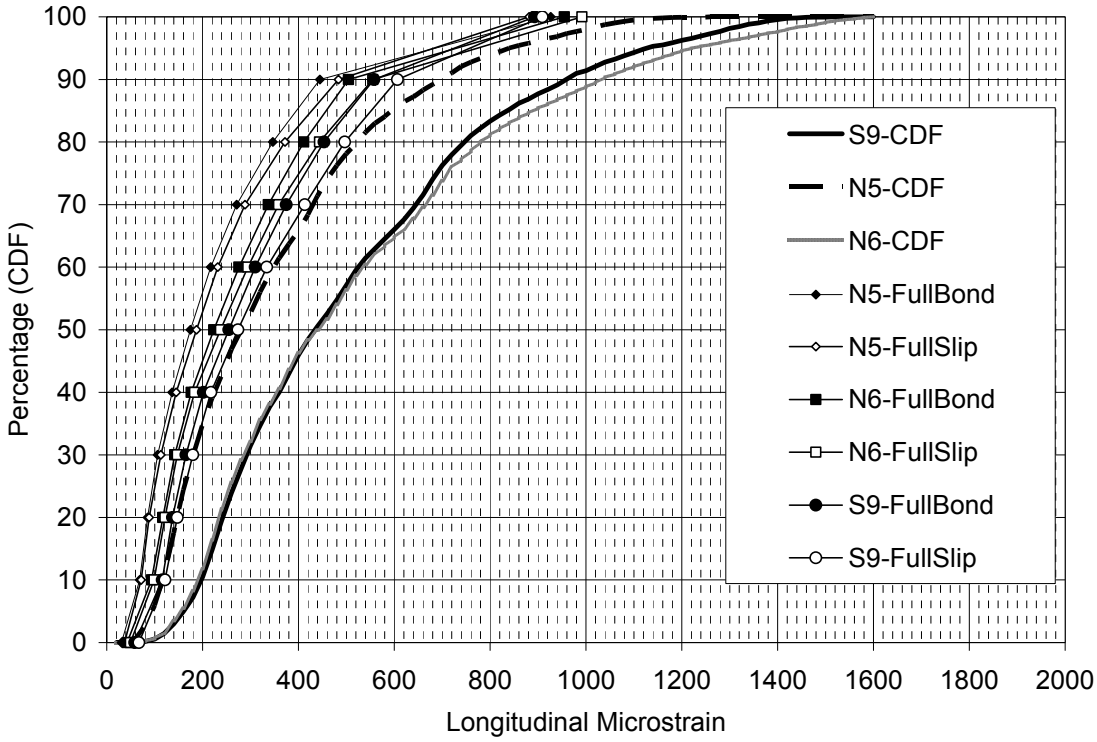

Figure 6.24 Measured and Predicted Strain – Backcalculated

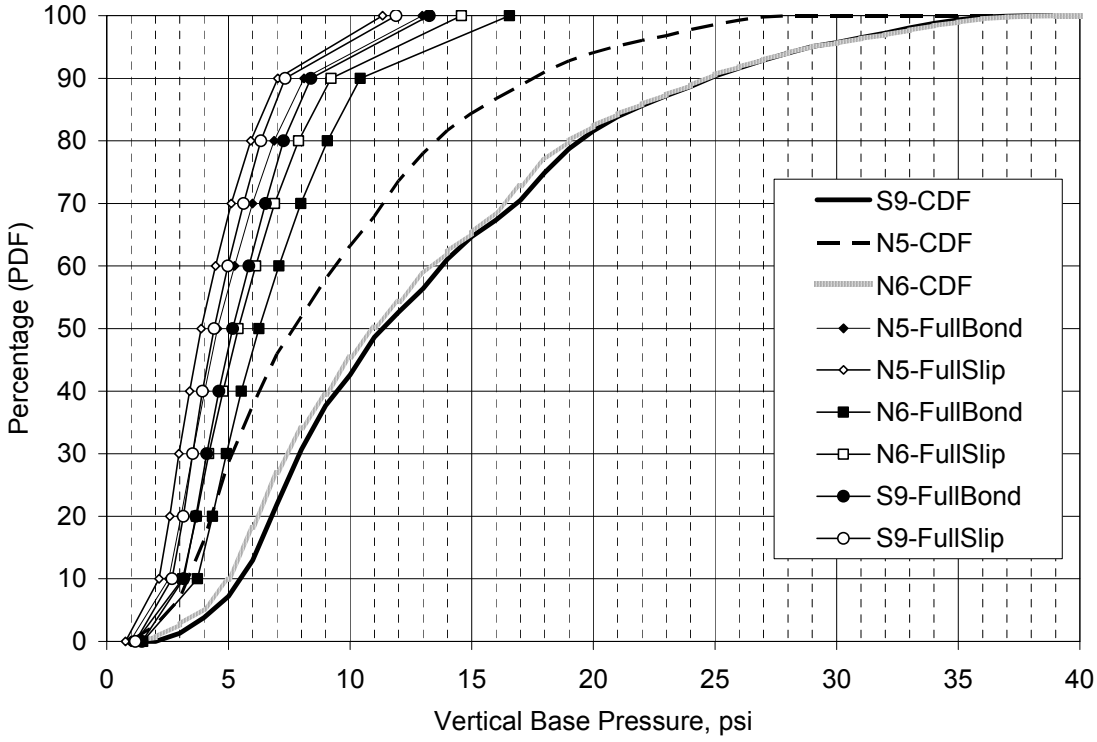

Figure 6.25 Measured and Predicted Base Pressure – Backcalculated

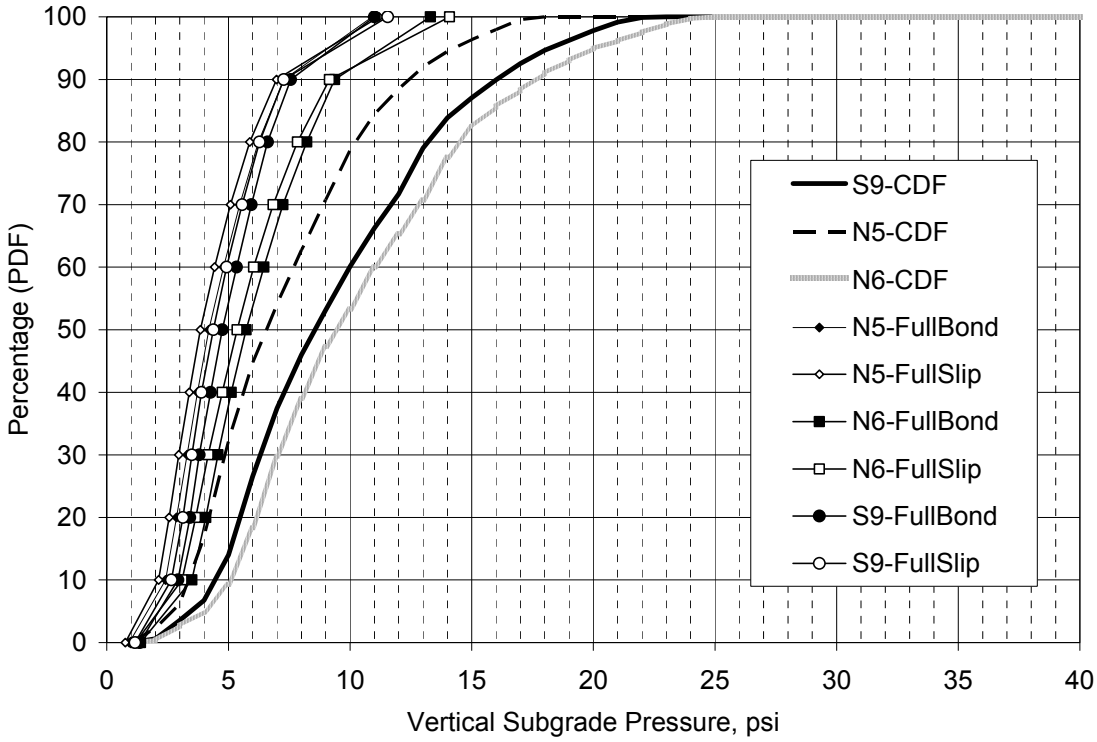

Figure 6.26 Measured and Predicted Subgrade Pressure – Backcalculated

6.5.1.2 Simulations Based on AC E* Moduli at 10 Hz - Confined

Figures 6.27, 6.28 and 6.29 show that using E* (10 Hz –Confined) plant-produced mixture data for each lift to characterize the AC layer moduli increases the magnitude of pavement responses, but still does not provide a good comparison between measured and predicted at the higher percentages. This is especially true under fully-bonded conditions. This condition, as noted previously, was essentially the same condition used in the preliminary analyses presented in Figure 1.8. Debonding the layers increases the responses significantly, but still under predicts the AC strain and aggregate base pressure. A closer match was achieved for the subgrade pressures under debonded conditions.

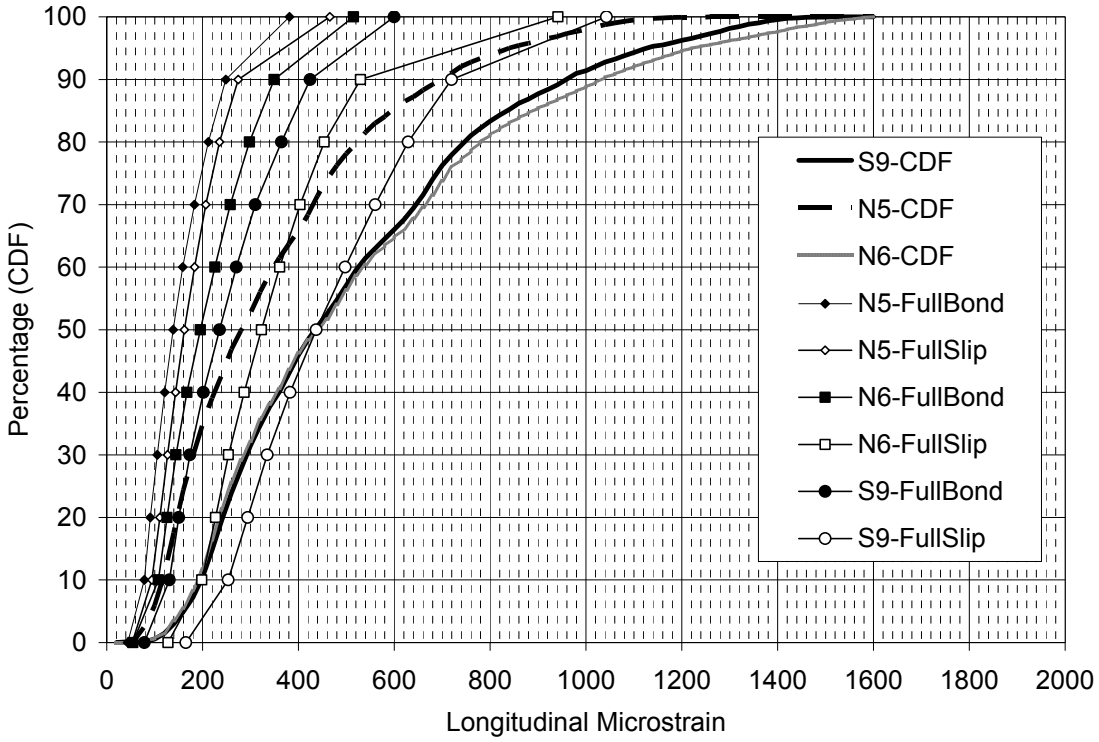

Figure 6.27 Measured and Predicted Strain–10Hz–Confined

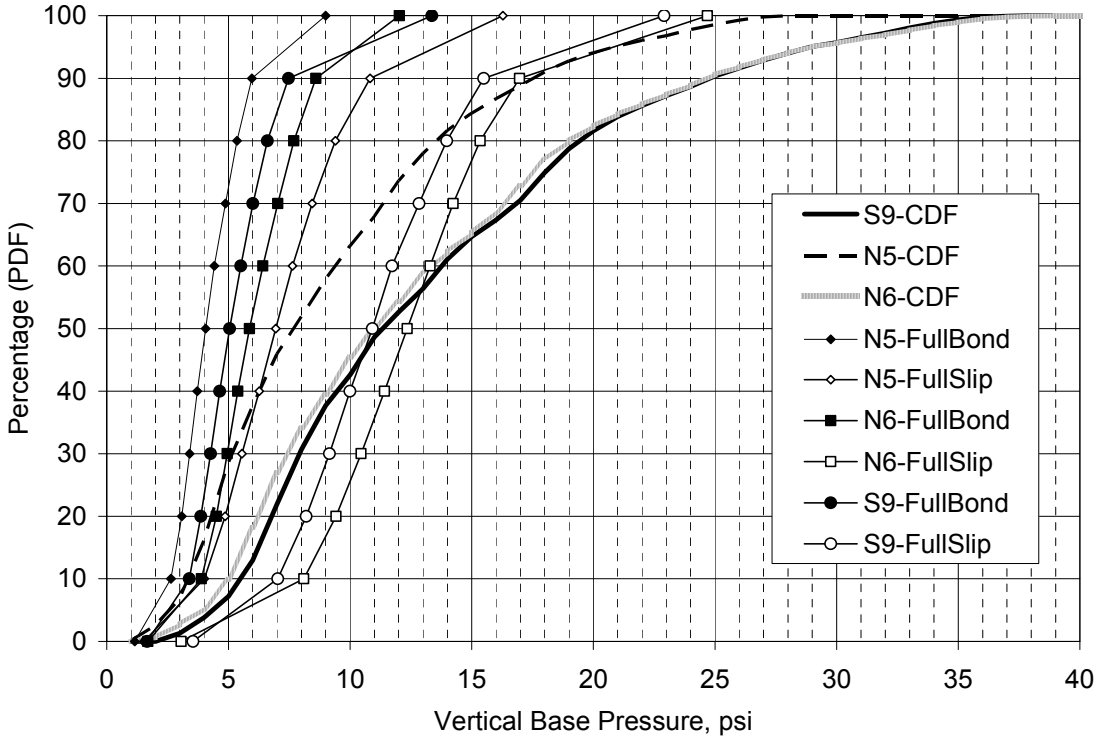

Figure 6.28 Measured and Predicted Base Pressure–10Hz–Confined

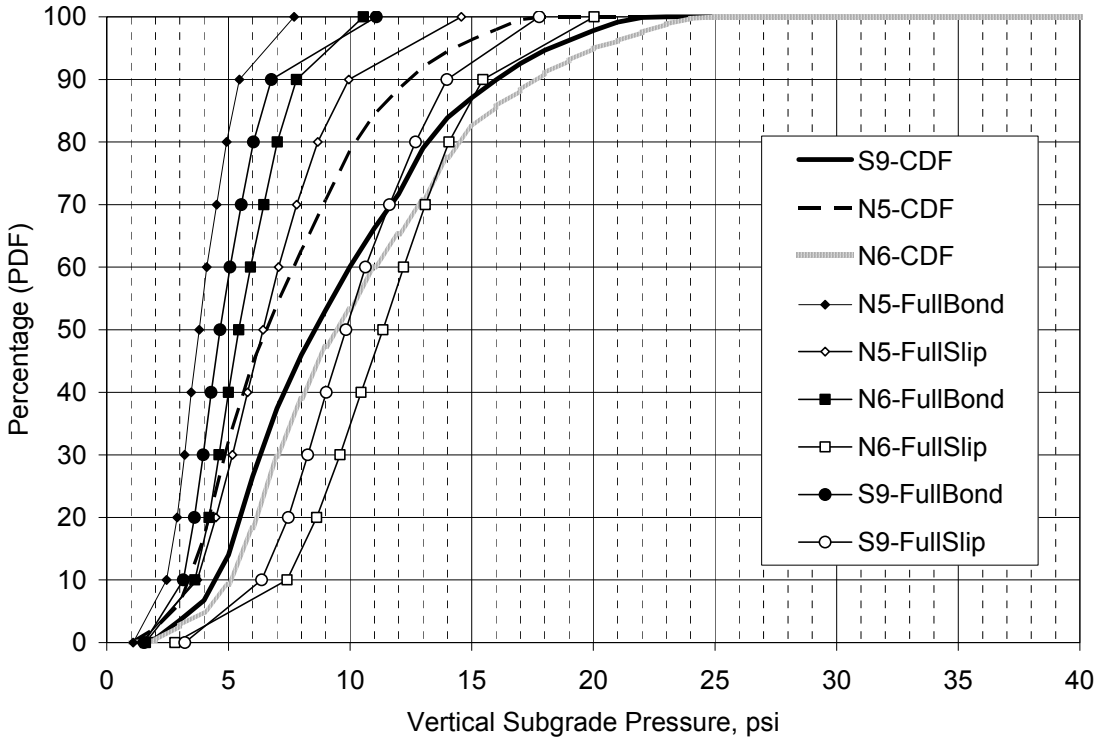

Figure 6.29 Measured and Predicted Subgrade Pressure–10Hz–Confined

6.5.1.3 Simulations Based on AC E* Moduli at 10 Hz - Unconfined

Recall from the discussion of the E* data (Section 4.3) that the state of confinement during E* testing significantly changes the dynamic modulus of the plant-produced mixtures. This is evident in Figures 6.30 through 6.32 where the pavement responses are increased due to decreased modulus in the unconfined state. The best match in AC strain (Figure 6.30) was obtained for the control section in an unbonded state. However, the strains in the Thiopave sections, even when unbonded, were still grossly under-predicted at the higher percentiles. Very little difference was noted between fully-bonded and fully-unbonded states for the thick Thiopave section (N6). For the base and subgrade pressure responses, the fully-unbonded condition came much closer to simulating the field measured responses.

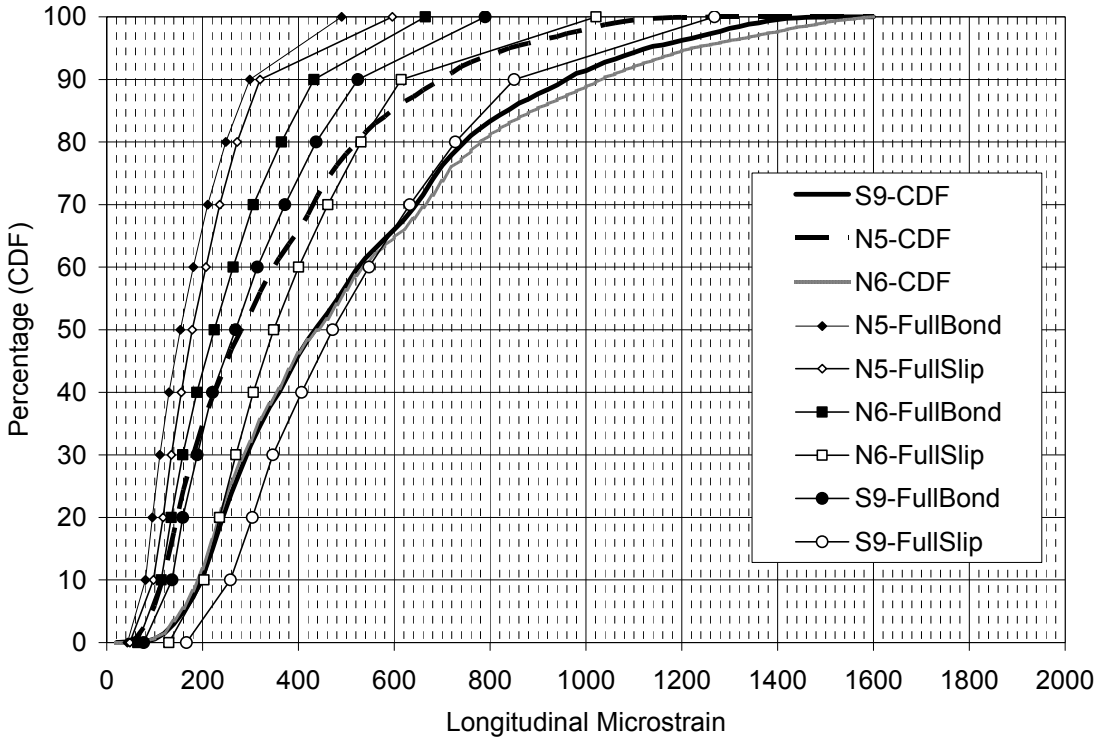

Figure 6.30 Measured and Predicted Strain–10Hz–Unconfined

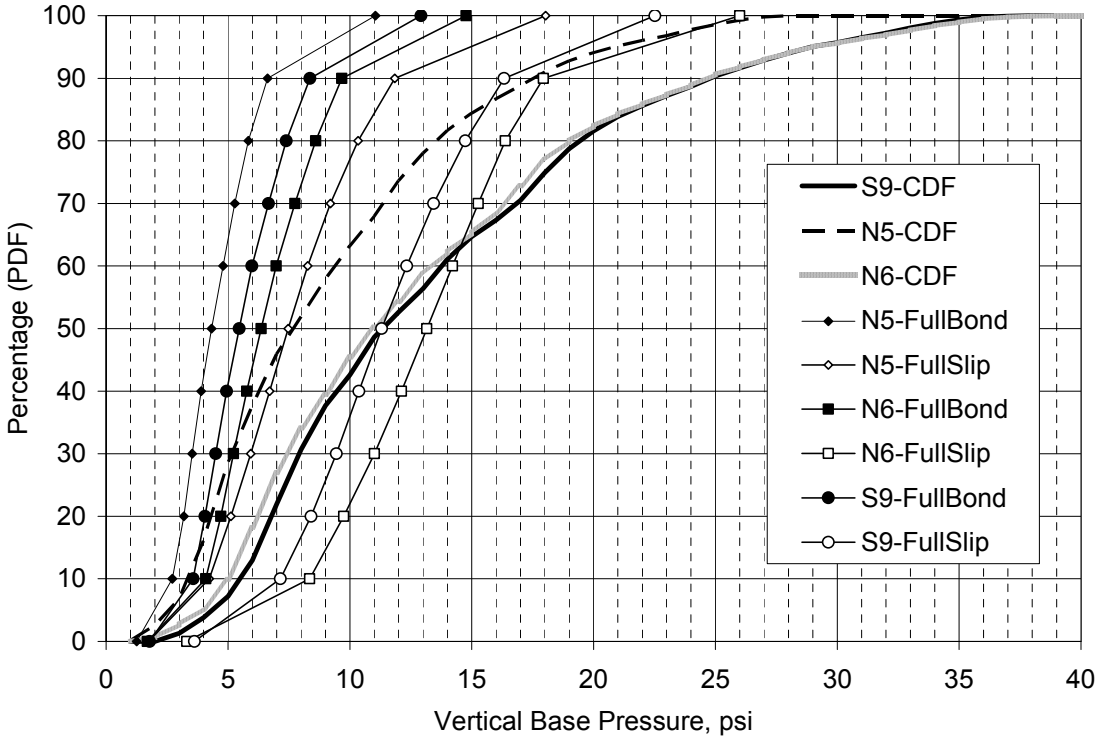

Figure 6.31 Measured and Predicted Base Pressure–10Hz–Unconfined

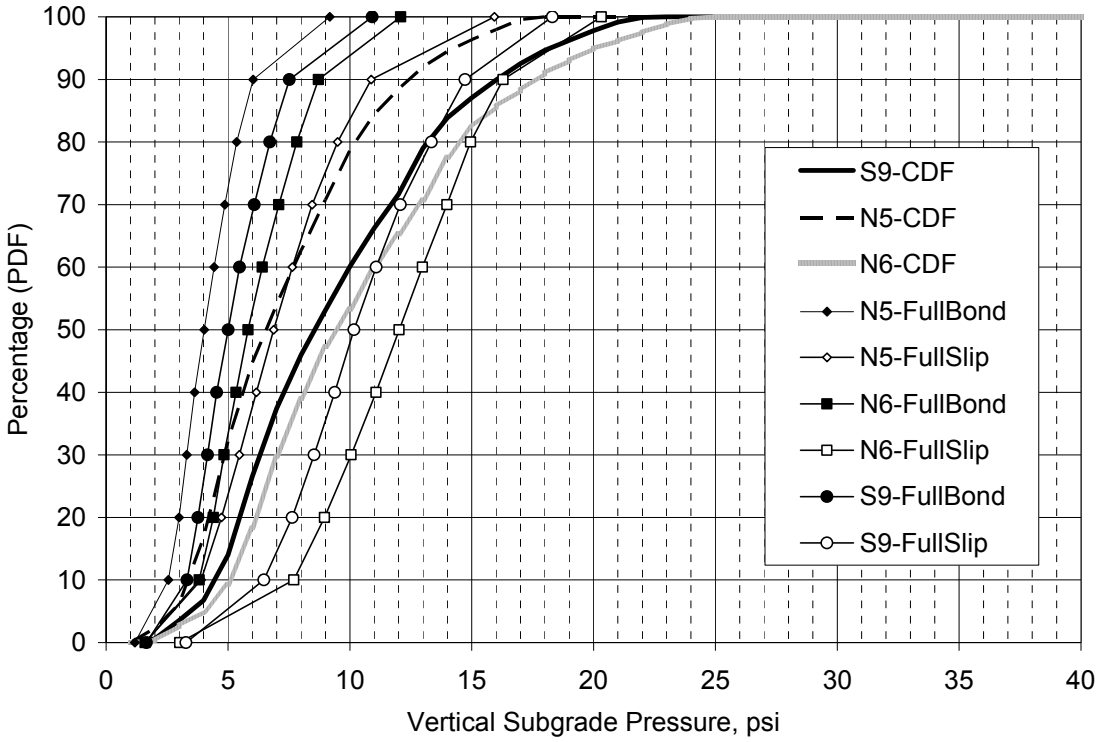

Figure 6.32 Measured and Predicted Subgrade Pressure–10Hz–Unconfined

6.5.1.4 Simulations Based on AC E* Moduli at 1 Hz - Confined

Using E* data from 1 Hz testing of the plant-produced mixtures in a confined state results in even higher pavement responses as shown in Figures 6.33 through 6.35. Better matches were obtained at the lower percentiles, but in a fully-bonded state, the higher percentiles were still under predicted. Fully debonding the layers had mixed results. For example, in the case of AC strain (Figure 6.33) in the control section, fully-debonded resulted in a fair match at the higher percentiles and over prediction below the 90th percentile.

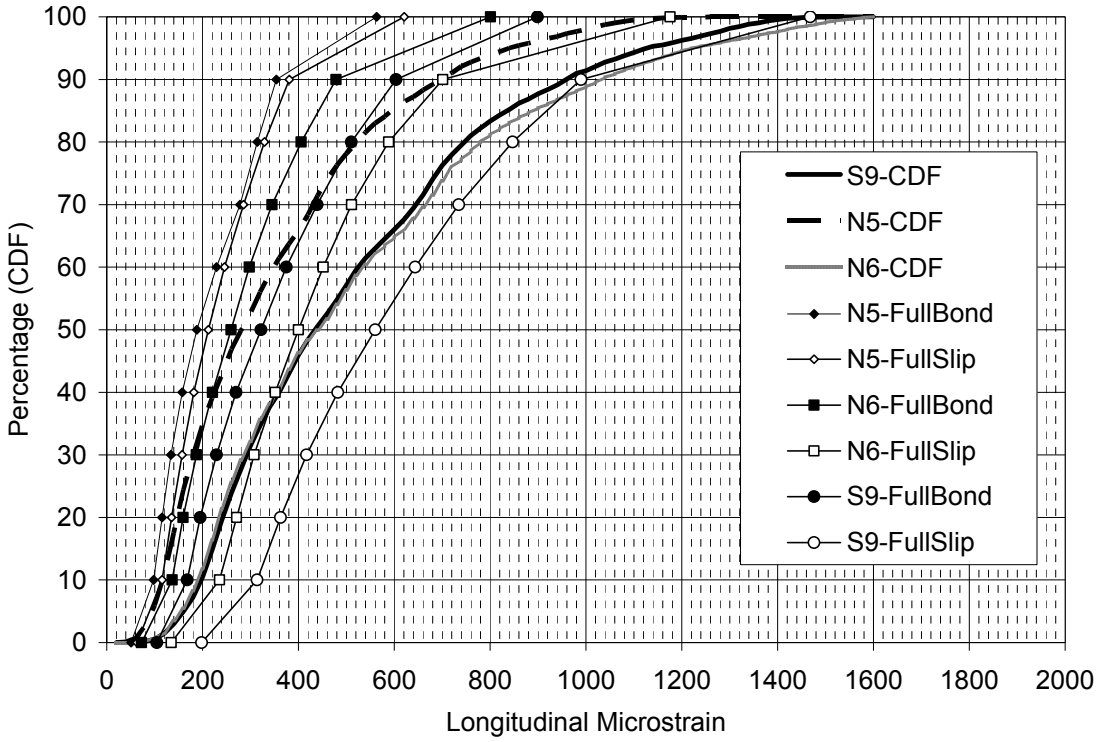

Figure 6.33 Measured and Predicted Strain–1Hz–Confined

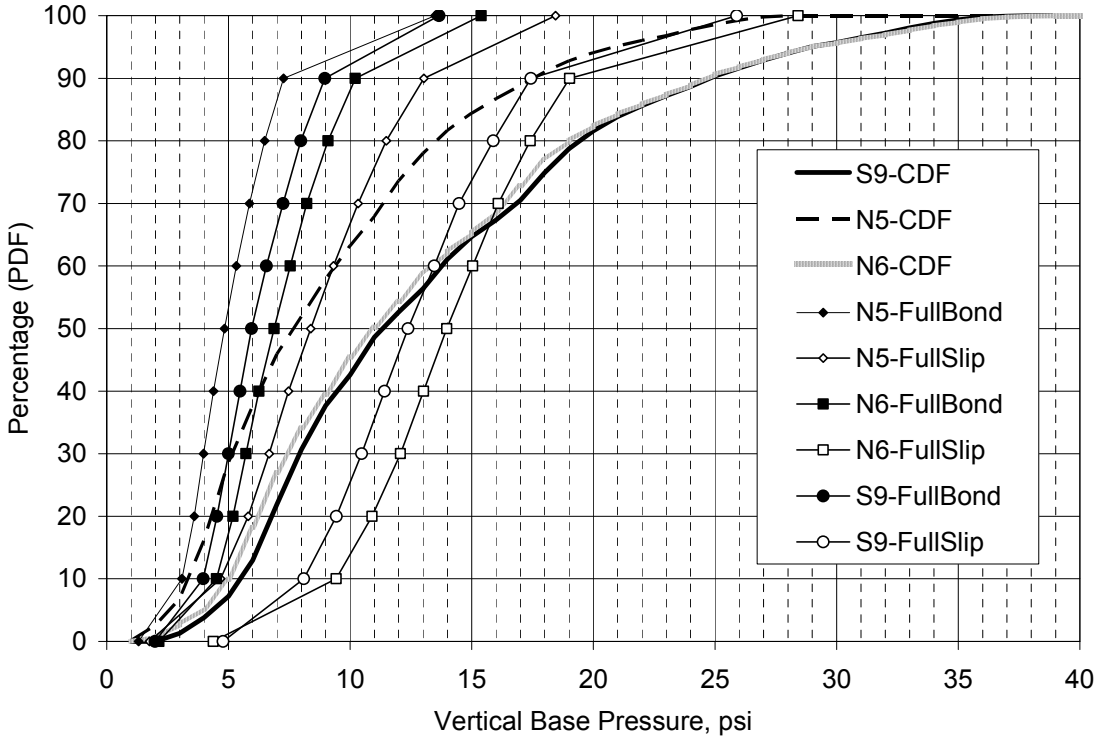

Figure 6.34 Measured and Predicted Base Pressure–1Hz–Confined

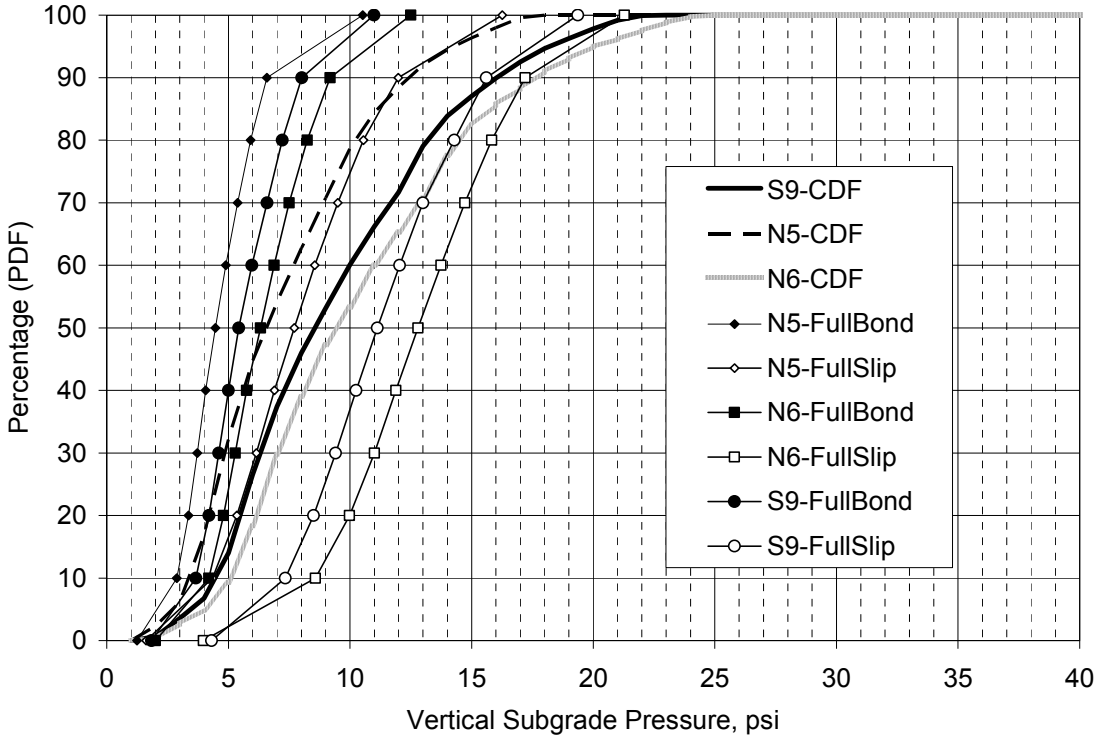

Figure 6.35 Measured and Predicted Subgrade Pressure–1Hz–Confined

6.5.1.5 Simulations Based on AC E* Moduli at 1 Hz - Unconfined

The simulations with the lowest AC moduli data of the plant-produced mixtures were represented by the 1 Hz testing in an unconfined state. Figure 6.36 shows a remarkably good match between measured and predicted AC strains for S9 in a fully-bonded state. A gross over prediction was achieved for S9 when fully debonded. Section N6 was under predicted when fully bonded and provided a reasonably close prediction in a fully-unbonded condition. The AC strain in N5 was under predicted at the higher percentiles in both fully bonded and debonded conditions. Interestingly, Figure 6.37 shows general over prediction of base pressures when using a fully bonded condition and general under prediction when fully debonded. This was also the case for subgrade pressures (Figure 6.38).

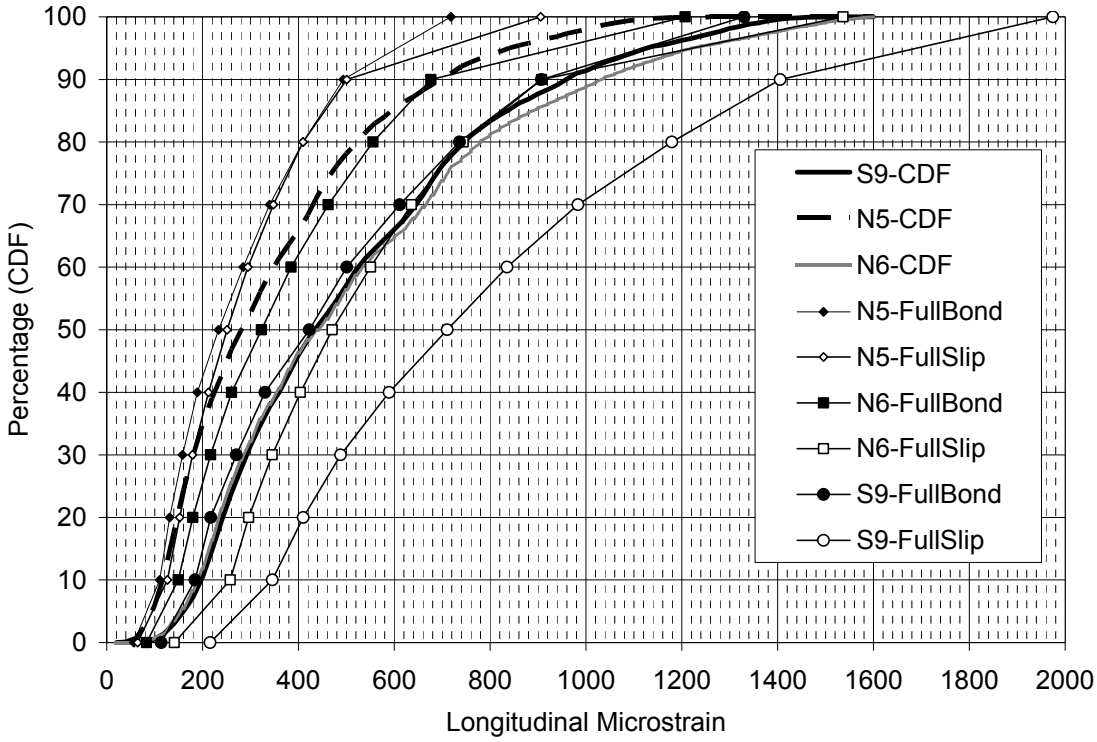

Figure 6.36 Measured and Predicted Strain–1Hz–Unconfined

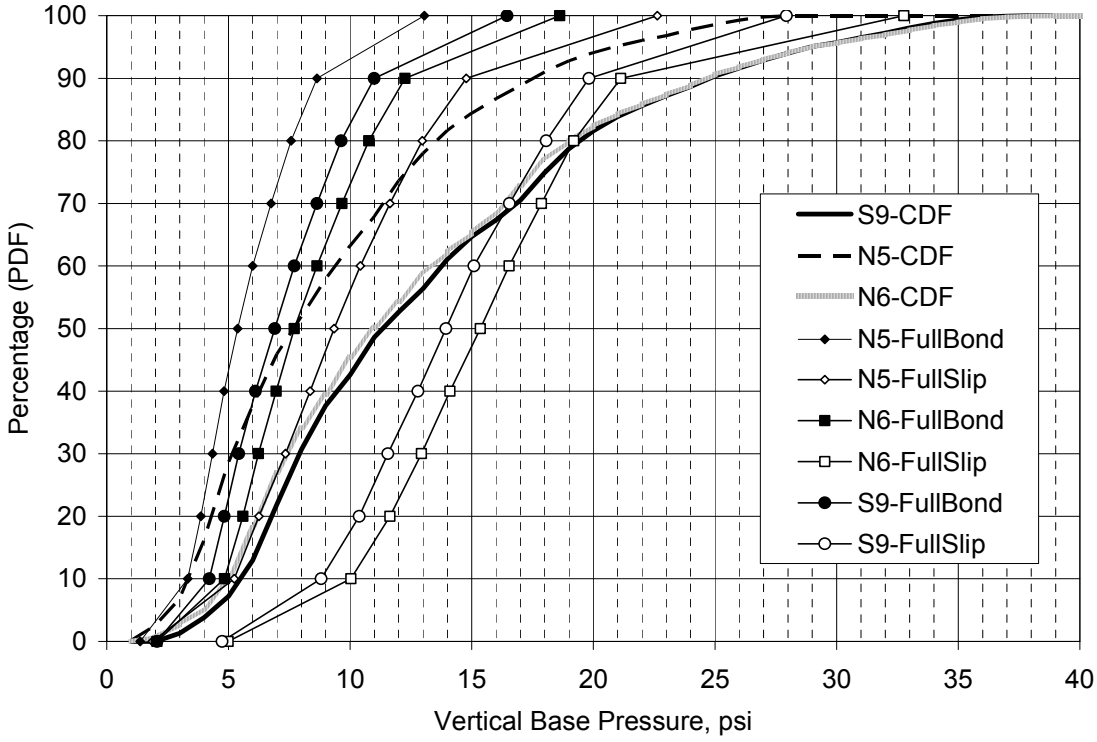

Figure 6.37 Measured and Predicted Base Pressure–1Hz–Unconfined

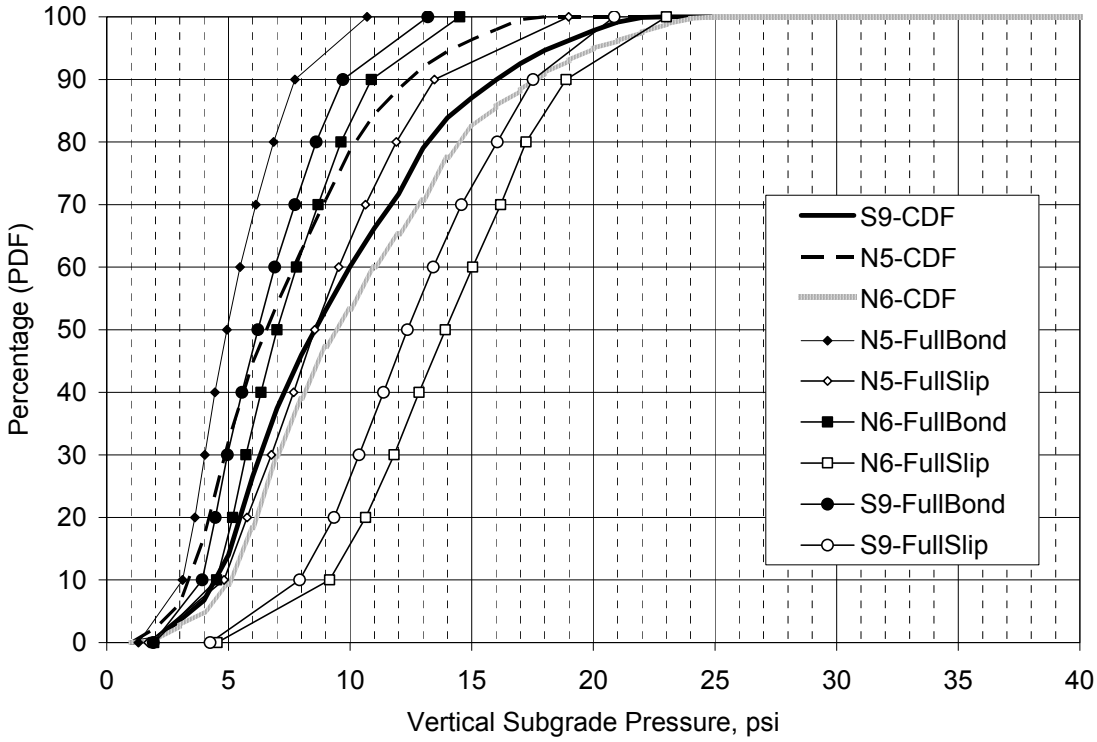

Figure 6.38 Measured and Predicted Subgrade Pressure–1Hz–Unconfined

6.5.1.6 Summary of Predicted versus Measured Pavement Responses

The data presented above did not provide a clear best-case set of conditions for simulating the structural responses of the test sections. In fact, there may be different sets of conditions needed to best represent each section. Furthermore, it may be that other approaches and models may need to be developed to better represent measured pavement responses. Though this effort is outside the scope of this report, it does highlight the need to have embedded pavement instrumentation to provide the "true" measure of pavement response since models may be flawed. For example, current practice in flexible pavement mechanistic analysis is to ignore the non-linear stress-dependent behavior of unbound materials. The relatively poor matches in base and subgrade pressure responses in all cases presented above may provide the motivation for developing methods of incorporating this behavior in analysis and design. Furthermore, PerRoad and other mechanics-base programs consider layers as fully-bonded or fully-slipped. In some cases noted above, these two conditions bracketed the measured pavement responses. A partial slip condition may need to be incorporated in these models. There are a host of other issues related to characterizing the in situ moduli of the AC with respect to temperature and loading frequency. As noted in the subsections above, higher responses could be achieved simply by dropping the load frequency or using unconfined E* test data. Better approaches should be developed for determining the appropriate laboratory characterization of E* to utilize for modeling purposes.

7. PAVEMENT PERFORMANCE

As of August 28, 2010, approximately 4.7 million ESALs had been applied to the test sections. At that time, there was no cracking evident on any of the sections. Weekly measurements of rut depths and roughness using the International Roughness Index (IRI) indicated comparable performance between all the sections. Figure 7.1 shows the rut progression with N5 having the highest magnitude and S9 the lowest. However, the difference between these sections was at most 2 mm, which is not practically significant. Figure 7.2 indicates that roughness has not increased appreciably since the start of testing. N5 appeared to be more rough directly after initial construction and is still slightly rougher than the other two sections, but 5 to 10 in./mile may not be practically significant. It can be stated at this time that both Thiopave sections are performing as well as the control section with very little difference between any of the test sections. Monitoring will continue through the end of trafficking in 2011.

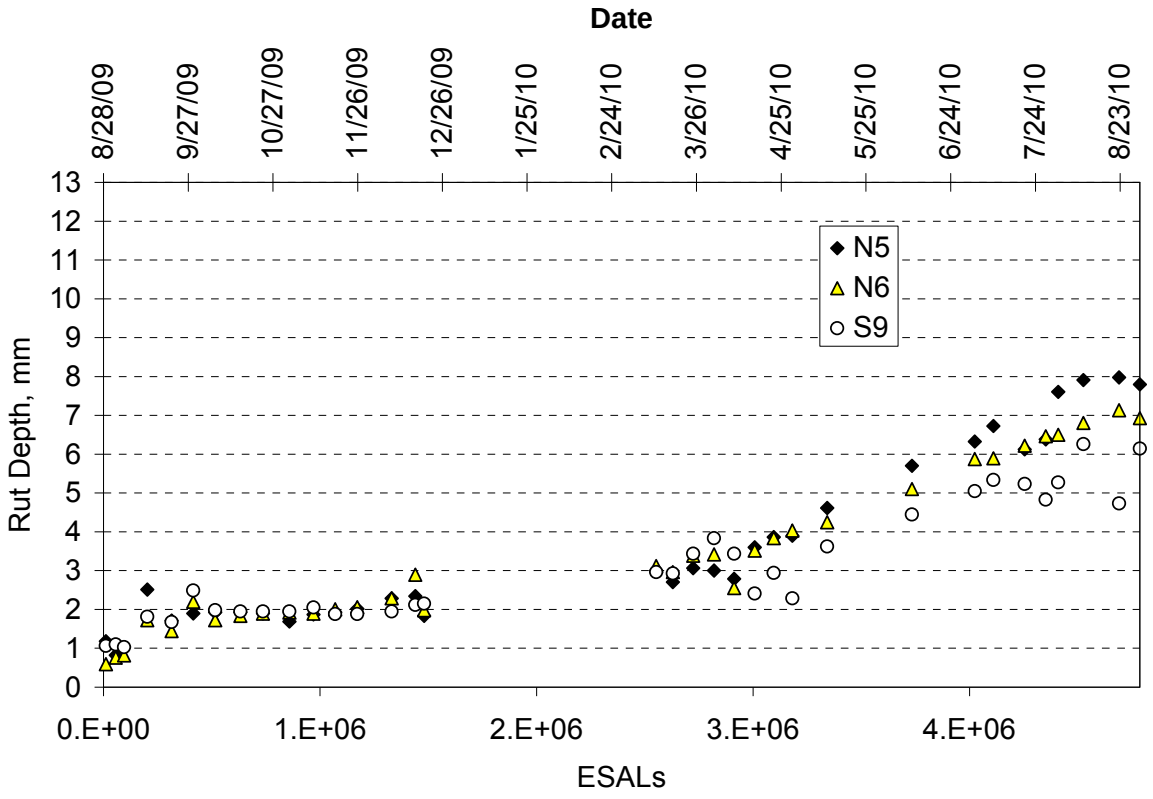

Figure 7.1 Measured Rut Depths

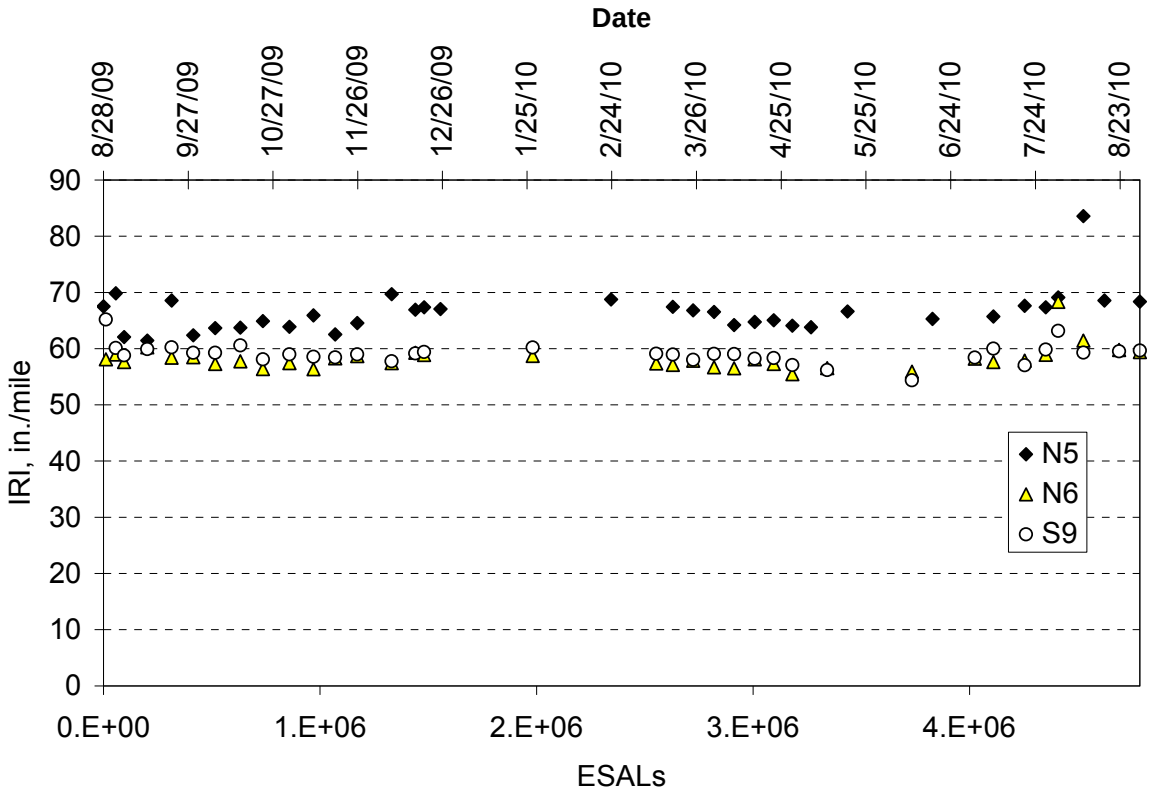

Figure 7.2 Measured IRI

8. KEY FINDINGS, CONCLUSIONS AND RECOMMENDATIONS

This report was intended to document the construction and testing conducted on the Thiopave and control test sections during the first year of testing (August 2009 – August 2010) at the NCAT Test Track. Based on the data presented herein the following key findings, conclusions and recommendations can be made:

1. The cooling of the AC layers during construction of the Thiopave sections, in addition to the control, was well-modeled by the MultiCool program. This finding will allow contractors to use MultiCool as a compaction planning/monitoring tool when using Thiopave materials in the future.
2. Dynamic modulus testing of plant-produced laboratory-compacted specimens ranked the mixtures according to decreasing stiffness as follows: Thiopave-intermediate, control-intermediate, Thiopave-base, control-base, control-surface. The Thiopave-base and control-base mixtures were the most similar mixtures among the five tested.
3. Significant increases in AC dynamic modulus were achieved when switching from unconfined to confined test conditions. This was the case for the control and Thiopave mixtures. This raises some question as to which mode of testing should be used for further structural modeling studies.
4. Beam fatigue testing of the base layers demonstrated significantly higher cycles to failure for the Thiopave base mix relative to the control base mix. This was especially apparent at the lowest strain level tested (200 με) where the average number of cycles to failure was 767% percent greater for the Thiopave mixture. This increased performance prediction should be viewed with caution, however, since the strain data were extrapolated at 200 με.
5. Fatigue transfer functions developed from laboratory beam fatigue testing were combined with measured AC strain data from each test section to compare estimated fatigue performance between sections. An estimated 3.9 times improvement in fatigue performance was found when comparing N6 (Thiopave 7") against S9 (control 7"). This improvement was attributed to each section having approximately the same strain level while the Thiopave base mixture had much improved fatigue performance over the control base mixture.
6. The predicted endurance limit for the Thiopave base mixture was 76% higher than the control base mixture.
7. The results of APA testing on the control surface, control base, Thiopave intermediate and Thiopave base mixtures were all less than 5.5 mm of rutting after 8,000 cycles. It is expected that all mixtures will withstand the 10 million ESALs to be applied over the two year traffic cycle without developing 12.5 mm of rutting.
8. FWD testing conducted prior to opening to traffic did not indicate appreciable increases from curing (sulfur crystallization) in backcalculated AC modulus in the Thiopave sections. The increases were approximately an order of magnitude less than those determined from laboratory testing during the initial phase of this project. The slight increases over time were comparable to the control section, but were not strongly correlated to the days of aging. These observations may be due to differences in how the testing was conducted (i.e., E* on lab-produced specimens for each individual lift vs. backcalculated composite modulus on plant-produced in-situ material) and that less Thiopave replacement was achieved in the plant produced materials relative to that incorporated during the mix design phase of the project.

9. Strong correlations between backcalculated composite AC moduli and mid-depth pavement temperature were determined for each test section. It was found that the Thiopave sections were influenced more by temperature than the control section. At colder temperatures (50F), the thickest Thiopave section (N5) had the statistically highest AC modulus, followed by the thinner Thiopave section (N6) and the control section (S9). At intermediate temperatures (68F), the backcalculated AC moduli amongst the sections were not statistically distinguishable. At warmer temperatures (110F), N5 was the softest followed by N6 and S9.
10. An examination of backcalculated composite AC modulus data versus test date through August, 2010 did not indicate the initial stages of bottom-up fatigue cracking in any of the test sections.
11. Strong correlations between mid-depth pavement temperature and pavement response (AC strain, base pressure and subgrade pressure) were found for each test section under each axle type (steer, tandem and singles). Despite statistically different AC moduli noted above, there were no statistical differences in the AC strain at the three reference temperatures (50, 68 and 110F) found between N6 (7" Thiopave) and S9 (7" control). N5 (9" Thiopave) was statistically lower in all cases, due primarily to the increased thickness. Statistical differences were noted between sections in terms of aggregate base and subgrade pressures. N5 was statistically lower due to its increased AC thickness, while differences in the other two sections, though statistically different, were not judged practically significant (differences less than 2 psi), especially since the thickness of the aggregate base in the N6 Thiopave section was less than the S9 control section.
12. An examination of pavement response over time, corrected to 68F, did not show any signs of fatigue crack initiation. This conclusion was consistent with the findings from the backcalculated composite AC moduli over time regarding crack initiation.
13. The cumulative pavement response distributions generated for each section had similar characteristics between sections though the magnitudes of pavement response were greater-than-expected based on prior analyses. Further PerRoad simulation, using a range of input data, demonstrates the complexity of matching measured and predicted pavement responses. Further investigation into the veracity of the results from strain instrumentation placed in hand compacted mixture prior to paving and rolling the surrounding mixture as well as model refinement is recommended.
14. As of August, 2010, all sections were exhibiting similar performance. There was no cracking evident in any section. The sections had similar rutting performance and virtually no change in pavement roughness. Monitoring will continue through the end of traffic in 2011.

REFERENCES

1. Allen, D.L. and R.C. Graves. Variability in Measurement of In-Situ Material Properties. *Proceedings, Fourth International Conference on the Bearing Capacity of Roads and Airfields*, Vol. 2, 1994, pp. 989-1005.
2. Chadbourn, B. A., D. E. Newcomb, V. R. Voller, R. A. De Sombre, J. A. Luoma and D. H. Timm. *An Asphalt Paving Tool for Adverse Conditions*. Report MN/RC-1998-18, Minnesota Department of Transportation, 1998.
3. Noureldin, A.S. Influence of Stress Levels and Seasonal Variations on In Situ Pavement Layer Properties. *Transportation Research Record No. 1448*, Washington, D.C., 1994, pp. 16-24.
4. Priest, A.L. and D.H. Timm. *Methodology and Calibration of Fatigue Transfer Functions for Mechanistic-Empirical Flexible Pavement Design*. Report No. 06-03, National Center for Asphalt Technology, Auburn University, 2006.
5. Prowell, B.D., E.R. Brown, R.M. Anderson, J. Sias-Daniel, H. Von Quintus, S. Shen, S.H. Carpenter, S. Bhattacharjee and S. Maghsoodloo. *Validating the Fatigue Endurance Limit for Hot Mix Asphalt*. NCHRP Report 646, Transportation Research Board, Washington, D.C., 2010.
6. Strickland, D., J. Colange, P. Shaw and N. Pugh. A Study of the Low-Temperature Properties of Sulphur Extended Asphalt Mixtures. *Canadian Technical Asphalt Association*, 2008.
7. Taylor, A.J. and D.H. Timm. *Mechanistic Characterization of Resilient Moduli for Unbound Pavement Layer Materials*. Report No. 09-06, National Center for Asphalt Technology, Auburn University, 2009.
8. Timm, D.H. *Design, Construction, and Instrumentation of the 2006 Test Track Structural Study*. Report No. 09-01, National Center for Asphalt Technology, Auburn University, 2009.
9. Timm, D.H., D.E. Newcomb and B. Birgisson. *Mechanistic-Empirical Flexible Pavement Thickness Design: The Minnesota Method*. Staff Paper, MN/RC-P99-10, Minnesota Department of Transportation, St. Paul, MN, 1999.
10. Timm, D.H. and A.L. Priest, "Wheel Wander at the NCAT Test Track," Report No. 05-02, National Center for Asphalt Technology, Auburn University, 2005.
11. Timm, D.H. and A.L. Priest, "Material Properties of the 2003 NCAT Test Track Structural Study," Report No. 06-01, National Center for Asphalt Technology, Auburn University, 2006.
12. Timm, D.H. and A.L. Priest. Flexible Pavement Fatigue Cracking and Measured Strain Response at the NCAT Test Track. *Proceedings of the 87th Annual Transportation Research Board*, Washington, D.C., 2008.
13. Timm, D.H., A.L. Priest and T.V. McEwen. *Design and Instrumentation of the Structural Pavement Experiment at the NCAT Test Track*. Report No. 04-01, National Center for Asphalt Technology, Auburn University, 2004.
14. Timm, D.H., N. Tran, A.J. Taylor, M.M. Robbins and R. Powell. *Evaluation of Mixture Performance and Structural Capacity of Pavements Using Shell Thiopave®*. Report No. 09-05, National Center for Asphalt Technology, Auburn University, 2009.
15. Timm, D. H., V. R. Voller, E. Lee and J. Harvey. Calcool: A multi-layer Asphalt Pavement Cooling Tool for Temperature Prediction During Construction. *The International Journal of Pavement Engineering*, Vol. 2, 2001, pp. 169-185.

16. Vargas-Nordcbeck, A. and D.H. Timm. Validation of Cooling Curves Prediction Model for Non-Conventional Asphalt Concrete Mixtures. *Transportation Research Record*, Journal of the Transportation Research Board, Washington, D.C., accepted for publication, 2011.
17. Willis, J.R. and D.H. Timm. *Forensic Investigation of a Rich Bottom Pavement*. Report No. 06-04, National Center for Asphalt Technology, Auburn University, 2006.
18. Willis, J.R. and D.H. Timm. A Forensic Investigation of Debonding in a Rich-Bottom Pavement. *Transportation Research Record No. 2040*, Transportation Research Board, 2007, pp. 107-114.
19. Willis, J.R. and D.H. Timm. *Field-Based Strain Thresholds for Flexible Perpetual Pavement Design*. Report No. 09-09, National Center for Asphalt Technology, Auburn University, 2009.

APPENDIX A – MIX DESIGN AND AS BUILT AC PROPERTIES

10/5/2009

Quadrant: N
Section: 5 *Mix Type = Surface - Control*
Sublot: 1

Laboratory Diary

General Desccription of Mix and Materials

Design Method:	Super
Compactive Effort:	80 gyrations
Binder Performance Grade:	76-22
Modifier Type:	SBS
Aggregate Type:	Grn/Sand/Lms
Design Gradation Type:	Fine

Avg. Lab Properties of Plant Produced Mix

Sieve Size	Design	QC
25 mm (1"):	100	100
19 mm (3/4"):	100	100
12.5 mm (1/2"):	100	100
9.5 mm (3/8"):	100	100
4.75 mm (#4):	78	83
2.36 mm (#8):	60	62
1.18 mm (#16):	46	47
0.60 mm (#30):	31	33
0.30 mm (#50):	16	16
0.15 mm (#100):	10	10
0.075 mm (#200):	5.8	6.4
Binder Content (Pb):	5.8	6.1
Eff. Binder Content (Pbe):	5.1	5.4
Dust-to-Binder Ratio:	1.1	1.2
Rice Gravity (Gmm):	2.483	2.472
Avg. Bulk Gravity (Gmb):	2.384	2.380
Avg Air Voids (Va):	4.0	3.7
Agg. Bulk Gravity (Gsb):	2.667	2.671
Avg VMA:	15.8	16.3
Avg. VFA:	75	77

Construction Diary

Relevant Conditions for Construction

Completion Date:	August 3, 2009
24 Hour High Temperature (F):	91
24 Hour Low Temperature (F):	72
24 Hour Rainfall (in):	0.00
Planned Subot Lift Thickness (in):	1.3
Paving Machine:	Roadtec

Plant Configuration and Placement Details

Component	% Setting
Asphalt Content (Plant Setting)	6.2
89 Columbus Granite	36.0
8910 Opelika Limestone Screenings	23.0
M10 Columbus Granite	13.0
Shorter Coarse Sand	28.0
As-Built Sublot Lift Thickness (in):	1.3
Total Thickness of All 2009 Sublots (in):	9.0
Approx. Underlying HMA Thickness (in):	0.0
Type of Tack Coat Utilized:	PG67-22
Target Tack Application Rate (gal/sy):	0.05
Approx. Avg. Temperature at Plant (F):	340
Avg. Measured Mat Compaction:	94.1%

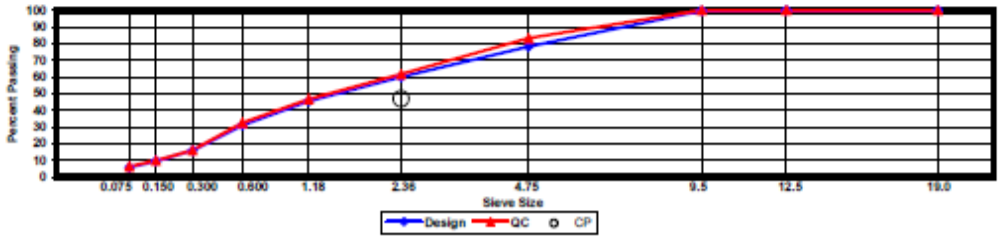

General Notes:

1) Mixes are referenced by quadrant (E=East, N=North, W=West, and S=South), section # (sequential) and sublot (top=1);
3) The total HMA thickness of all structural study sections (N1-N11 and S8-S12) ranges from 5-3/4 to 14 inches by design;
3) All non-structural sections are supprted by a uniform perpetual foundation in order to study surface mix performance;
4) SMA and OGFC refer to stone matrix asphalt and open-graded friction course, respectively; and
5) All liquid asphalt purchased for use in Track reconstruction contained LOF 6500 antistrip additive at a rate of 0.5 percent

10/5/2009

Quadrant: N
Section: 5
Sublot: 2

Mix Type = Intermediate - Thiopave

Laboratory Diary

General Description of Mix and Materials

Design Method:	WMA-T
Compactive Effort:	60 gyrations
Binder Performance Grade:	67-22
Modifier Type:	Thiopave
Aggregate Type:	Lms/Sand/Grn
Design Gradation Type:	Fine

Avg. Lab Properties of Plant Produced Mix

Sieve Size	Design	QC
25 mm (1"):	100	100
19 mm (3/4"):	93	90
12.5 mm (1/2"):	82	81
9.5 mm (3/8"):	71	73
4.75 mm (#4):	52	58
2.36 mm (#8):	45	46
1.18 mm (#16):	35	36
0.60 mm (#30):	24	24
0.30 mm (#50):	12	12
0.15 mm (#100):	7	8
0.075 mm (#200):	3.9	4.7
Binder Content (Pb):	6.2	5.7
Eff. Binder Content (Pbe):	5.6	5.3
Dust-to-Binder Ratio:	0.7	0.9
Rice Gravity (Gmm):	2.581	2.554
Avg. Bulk Gravity (Gmb):	2.491	2.439
Avg Air Voids (Va):	3.5	4.5
Agg. Bulk Gravity (Gsb):	2.737	2.772
Avg VMA:	14.6	17.1
Avg. VFA:	76	74

Construction Diary

Relevant Conditions for Construction

Completion Date:	July 24, 2009
24 Hour High Temperature (F):	90
24 Hour Low Temperature (F):	68
24 Hour Rainfall (in):	0.00
Planned Subot Lift Thickness (in):	2.8
Paving Machine:	Roadtec

Plant Configuration and Placement Details

Component	% Setting
Asphalt Content (Plant Setting)	4.0
78 Opelika Limestone	30.0
57 Opelika Limestone	18.0
M10 Columbus Granite	25.0
Shorter Coarse Sand	27.0
Thiopave	40.0
Compaction Agent	1.0

Actual Thiopave Content = 39%

As-Built Sublot Lift Thickness (in):	2.8
Total Thickness of All 2009 Sublots (in):	9.0
Approx. Underlying HMA Thickness (in):	0.0
Type of Tack Coat Utilized:	NTSS-1HM
Target Tack Application Rate (gal/sy):	0.05
Approx. Avg. Temperature at Plant (F):	275
Avg. Measured Mat Compaction:	93.0%

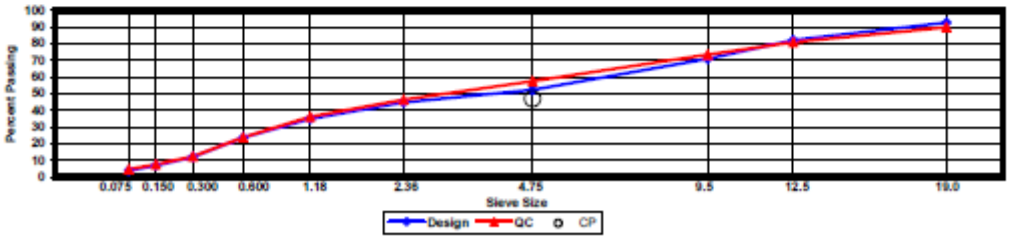

General Notes:

1) Mixes are referenced by quadrant (E=East, N=North, W=West, and S=South), section # (sequential) and sublot (top=1);
3) The total HMA thickness of all structural study sections (N1-N11 and S8-S12) ranges from 5-3/4 to 14 inches by design;
3) All non-structural sections are supprted by a uniform perpetual foundation in order to study surface mix performance;
4) SMA and OGFC refer to stone matrix asphalt and open-graded friction course, respectively; and
5) All liquid asphalt purchased for use in Track reconstruction contained LOF 6500 antistrip additive at a rate of 0.5 percent

10/5/2009

Quadrant: N
Section: 5 *Mix Type = Intermediate - Thiopave*
Sublot: 3

Laboratory Diary

General Desccription of Mix and Materials

Design Method:	WMA-T
Compactive Effort:	60 gyrations
Binder Performance Grade:	67-22
Modifier Type:	Thiopave
Aggregate Type:	Lms/Sand/Grn
Design Gradation Type:	Fine

Avg. Lab Properties of Plant Produced Mix

Sieve Size	Design	QC
25 mm (1"):	100	98
19 mm (3/4"):	93	92
12.5 mm (1/2"):	82	82
9.5 mm (3/8"):	71	72
4.75 mm (#4):	52	54
2.36 mm (#8):	45	44
1.18 mm (#16):	35	34
0.60 mm (#30):	24	23
0.30 mm (#50):	12	12
0.15 mm (#100):	7	8
0.075 mm (#200):	3.9	4.9
Binder Content (Pb):	6.2	5.6
Eff. Binder Content (Pbe):	5.6	5.1
Dust-to-Binder Ratio:	0.7	1.0
Rice Gravity (Gmm):	2.581	2.553
Avg. Bulk Gravity (Gmb):	2.491	2.440
Avg Air Voids (Va):	3.5	4.4
Agg. Bulk Gravity (Gsb):	2.737	2.762
Avg VMA:	14.6	16.6
Avg. VFA:	76	73

Construction Diary

Relevant Conditions for Construction

Completion Date:	July 23, 2009
24 Hour High Temperature (F):	89
24 Hour Low Temperature (F):	74
24 Hour Rainfall (in):	0.00
Planned Subot Lift Thickness (in):	2.3
Paving Machine:	Roadtec

Plant Configuration and Placement Details

Component	% Setting
Asphalt Content (Plant Setting)	4.0
78 Opelika Limestone	30.0
57 Opelika Limestone	18.0
M10 Columbus Granite	25.0
Shorter Coarse Sand	27.0
Thiopave	40.0
Compaction Agent	1.0

Actual Thiopave Content = 33%

As-Built Sublot Lift Thickness (in):	2.0
Total Thickness of All 2009 Sublots (in):	9.0
Approx. Underlying HMA Thickness (in):	0.0
Type of Tack Coat Utilized:	NTSS-1HM
Target Tack Application Rate (gal/sy):	0.07
Approx. Avg. Temperature at Plant (F):	275
Avg. Measured Mat Compaction:	92.9%

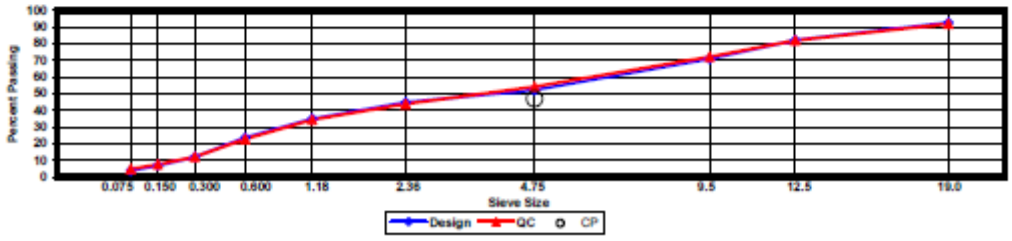

General Notes:

1) Mixes are referenced by quadrant (E=East, N=North, W=West, and S=South), section # (sequential) and sublot (top=1);
3) The total HMA thickness of all structural study sections (N1-N11 and S8-S12) ranges from 5-3/4 to 14 inches by design;
3) All non-structural sections are supprted by a uniform perpetual foundation in order to study surface mix performance;
4) SMA and OGFC refer to stone matrix asphalt and open-graded friction course, respectively; and
5) All liquid asphalt purchased for use in Track reconstruction contained LOF 6500 antistrip additive at a rate of 0.5 percent

10/5/2009

Quadrant: N
Section: 5
Sublot: 4

Mix Type = Base - Thiopave

Laboratory Diary

General Descciption of Mix and Materials

Design Method:	WMA-T
Compactive Effort:	60 gyrations
Binder Performance Grade:	67-22
Modifier Type:	Thiopave
Aggregate Type:	Lms/Sand/Grn
Design Gradation Type:	Fine

Avg. Lab Properties of Plant Produced Mix

Sieve Size	Design	QC
25 mm (1"):	100	100
19 mm (3/4"):	93	93
12.5 mm (1/2"):	82	82
9.5 mm (3/8"):	71	73
4.75 mm (#4):	52	55
2.36 mm (#8):	45	44
1.18 mm (#16):	35	35
0.60 mm (#30):	24	24
0.30 mm (#50):	12	12
0.15 mm (#100):	7	8
0.075 mm (#200):	3.9	4.8
Binder Content (Pb):	6.3	6.2
Eff. Binder Content (Pbe):	5.8	5.8
Dust-to-Binder Ratio:	0.7	0.8
Rice Gravity (Gmm):	2.558	2.518
Avg. Bulk Gravity (Gmb):	2.507	2.459
Avg Air Voids (Va):	2.0	2.3
Agg. Bulk Gravity (Gsb):	2.737	2.749
Avg VMA:	14.1	16.1
Avg. VFA:	86	85

Construction Diary

Relevant Conditions for Construction

Completion Date:	July 23, 2009
24 Hour High Temperature (F):	89
24 Hour Low Temperature (F):	74
24 Hour Rainfall (in):	0.00
Planned Subot Lift Thickness (in):	2.8
Paving Machine:	Roadtec

Plant Configuration and Placement Details

Component	% Setting
Asphalt Content (Plant Setting)	5.1
78 Opelika Limestone	30.0
57 Opelika Limestone	18.0
M10 Columbus Granite	25.0
Shorter Coarse Sand	27.0
Thiopave	30.0
Compaction Agent	1.0

Actual Thiopave Content = 22%

As-Built Sublot Lift Thickness (in):	2.9
Total Thickness of All 2009 Sublots (in):	9.0
Approx. Underlying HMA Thickness (in):	0.0
Type of Tack Coat Utilized:	NA
Target Tack Application Rate (gal/sy):	NA
Approx. Avg. Temperature at Plant (F):	275
Avg. Measured Mat Compaction:	93.6%

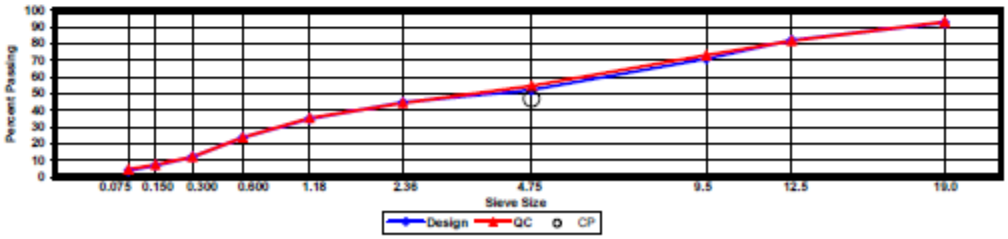

General Notes:

1) Mixes are referenced by quadrant (E=East, N=North, W=West, and S=South), section # (sequential) and sublot (top=1);
3) The total HMA thickness of all structural study sections (N1-N11 and S8-S12) ranges from 5-3/4 to 14 inches by design;
3) All non-structural sections are supprted by a uniform perpetual foundation in order to study surface mix performance;
4) SMA and OGFC refer to stone matrix asphalt and open-graded friction course, respectively; and
5) All liquid asphalt purchased for use in Track reconstruction contained LOF 6500 antistrip additive at a rate of 0.5 percent

10/5/2009

Quadrant: N
Section: 6 *Mix Type = Surface - Control*
Sublot: 1

Laboratory Diary

General Descciption of Mix and Materials

Design Method:	Super
Compactive Effort:	80 gyrations
Binder Performance Grade:	76-22
Modifier Type:	SBS
Aggregate Type:	Grn/Sand/Lms
Design Gradation Type:	Fine

Avg. Lab Properties of Plant Produced Mix

Sieve Size	Design	QC
25 mm (1"):	100	100
19 mm (3/4"):	100	100
12.5 mm (1/2"):	100	100
9.5 mm (3/8"):	100	100
4.75 mm (#4):	78	82
2.36 mm (#8):	60	55
1.18 mm (#16):	46	45
0.60 mm (#30):	31	30
0.30 mm (#50):	16	16
0.15 mm (#100):	10	10
0.075 mm (#200):	5.8	6.4
Binder Content (Pb):	5.8	6.1
Eff. Binder Content (Pbe):	5.1	5.4
Dust-to-Binder Ratio:	1.1	1.2
Rice Gravity (Gmm):	2.483	2.466
Avg. Bulk Gravity (Gmb):	2.384	2.370
Avg Air Voids (Va):	4.0	3.9
Agg. Bulk Gravity (Gsb):	2.667	2.662
Avg VMA:	15.8	16.4
Avg. VFA:	75	76

Construction Diary

Relevant Conditions for Construction

Completion Date:	August 3, 2009
24 Hour High Temperature (F):	91
24 Hour Low Temperature (F):	72
24 Hour Rainfall (in):	0.00
Planned Subot Lift Thickness (in):	1.3
Paving Machine:	Roadtec

Plant Configuration and Placement Details

Component	% Setting
Asphalt Content (Plant Setting)	6.2
89 Columbus Granite	36.0
8910 Opelika Limestone Screenings	23.0
M10 Columbus Granite	13.0
Shorter Coarse Sand	28.0

As-Built Sublot Lift Thickness (in):	1.1
Total Thickness of All 2009 Sublots (in):	6.9
Approx. Underlying HMA Thickness (in):	0.0
Type of Tack Coat Utilized:	PG67-22
Target Tack Application Rate (gal/sy):	0.05
Approx. Avg. Temperature at Plant (F):	340
Avg. Measured Mat Compaction:	93.8%

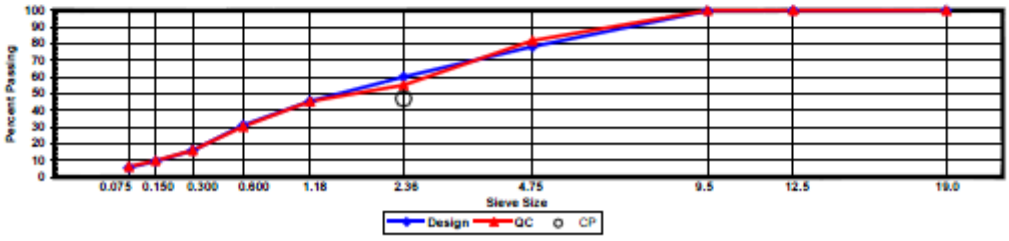

General Notes:
1) Mixes are referenced by quadrant (E=East, N=North, W=West, and S=South), section # (sequential) and sublot (top=1);
3) The total HMA thickness of all structural study sections (N1-N11 and S8-S12) ranges from 5-3/4 to 14 inches by design;
3) All non-structural sections are supprted by a uniform perpetual foundation in order to study surface mix performance;
4) SMA and OGFC refer to stone matrix asphalt and open-graded friction course, respectively; and
5) All liquid asphalt purchased for use in Track reconstruction contained LOF 6500 antistrip additive at a rate of 0.5 percent

10/5/2009

Quadrant: N
Section: 6
Sublot: 2

Mix Type = Intermediate - Thiopave

Laboratory Diary

General Descciption of Mix and Materials

Design Method:	WMA-T
Compactive Effort:	60 gyrations
Binder Performance Grade:	67-22
Modifier Type:	Thiopave
Aggregate Type:	Lms/Sand/Grn
Design Gradation Type:	Fine

Avg. Lab Properties of Plant Produced Mix

Sieve Size	Design	QC
25 mm (1"):	100	100
19 mm (3/4"):	93	89
12.5 mm (1/2"):	82	82
9.5 mm (3/8"):	71	75
4.75 mm (#4):	52	57
2.36 mm (#8):	45	46
1.18 mm (#16):	35	36
0.60 mm (#30):	24	24
0.30 mm (#50):	12	12
0.15 mm (#100):	7	8
0.075 mm (#200):	3.9	4.9
Binder Content (Pb):	6.2	5.7
Eff. Binder Content (Pbe):	5.6	5.2
Dust-to-Binder Ratio:	0.7	0.9
Rice Gravity (Gmm):	2.581	2.554
Avg. Bulk Gravity (Gmb):	2.491	2.440
Avg Air Voids (Va):	3.5	4.5
Agg. Bulk Gravity (Gsb):	2.737	2.768
Avg VMA:	14.6	16.9
Avg. VFA:	76	74

Construction Diary

Relevant Conditions for Construction

Completion Date:	July 24, 2009
24 Hour High Temperature (F):	90
24 Hour Low Temperature (F):	68
24 Hour Rainfall (in):	0.00
Planned Subot Lift Thickness (in):	2.8
Paving Machine:	Roadtec

Plant Configuration and Placement Details

Component	% Setting
Asphalt Content (Plant Setting)	4.0
78 Opelika Limestone	30.0
57 Opelika Limestone	18.0
M10 Columbus Granite	25.0
Shorter Coarse Sand	27.0
Thiopave	40.0
Compaction Agent	1.0

Actual Thiopave Content = 35%

As-Built Sublot Lift Thickness (in):	2.8
Total Thickness of All 2009 Sublots (in):	6.9
Approx. Underlying HMA Thickness (in):	0.0
Type of Tack Coat Utilized:	NTSS-1HM
Target Tack Application Rate (gal/sy):	0.05
Approx. Avg. Temperature at Plant (F):	275
Avg. Measured Mat Compaction:	92.9%

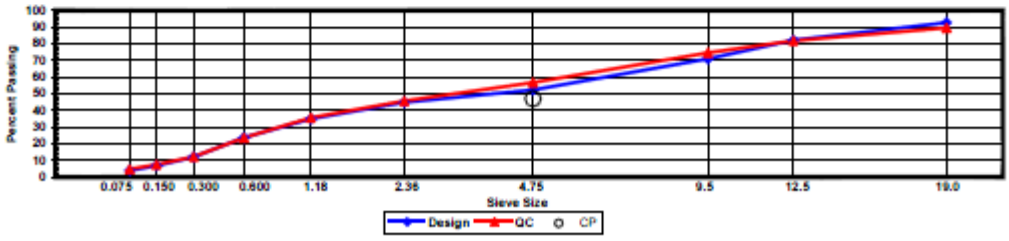

General Notes:

1) Mixes are referenced by quadrant (E=East, N=North, W=West, and S=South), section # (sequential) and sublot (top=1);
3) The total HMA thickness of all structural study sections (N1-N11 and S8-S12) ranges from 5-3/4 to 14 inches by design;
3) All non-structural sections are supprted by a uniform perpetual foundation in order to study surface mix performance;
4) SMA and OGFC refer to stone matrix asphalt and open-graded friction course, respectively; and
5) All liquid asphalt purchased for use in Track reconstruction contained LOF 6500 antistrip additive at a rate of 0.5 percent

10/5/2009

Quadrant: N
Section: 6 *Mix Type = Base - Thiopave*
Sublot: 3

Laboratory Diary

General Descciption of Mix and Materials

Design Method:	WMA-T
Compactive Effort:	60 gyrations
Binder Performance Grade:	67-22
Modifier Type:	Thiopave
Aggregate Type:	Lms/Sand/Grn
Design Gradation Type:	Fine

Avg. Lab Properties of Plant Produced Mix

Sieve Size	Design	QC
25 mm (1"):	100	100
19 mm (3/4"):	93	93
12.5 mm (1/2"):	82	82
9.5 mm (3/8"):	71	74
4.75 mm (#4):	52	55
2.36 mm (#8):	45	45
1.18 mm (#16):	35	35
0.60 mm (#30):	24	24
0.30 mm (#50):	12	12
0.15 mm (#100):	7	8
0.075 mm (#200):	3.9	4.8
Binder Content (Pb):	6.3	6.1
Eff. Binder Content (Pbe):	5.8	5.6
Dust-to-Binder Ratio:	0.7	0.8
Rice Gravity (Gmm):	2.568	2.521
Avg. Bulk Gravity (Gmb):	2.507	2.448
Avg Air Voids (Va):	2.0	2.9
Agg. Bulk Gravity (Gsb):	2.737	2.747
Avg VMA:	14.1	16.3
Avg. VFA:	86	82

Construction Diary

Relevant Conditions for Construction

Completion Date:	July 23, 2009
24 Hour High Temperature (F):	89
24 Hour Low Temperature (F):	74
24 Hour Rainfall (in):	0.00
Planned Subot Lift Thickness (in):	3.0
Paving Machine:	Roadtec

Plant Configuration and Placement Details

Component	% Setting
Asphalt Content (Plant Setting)	5.1
78 Opelika Limestone	30.0
57 Opelika Limestone	18.0
M10 Columbus Granite	25.0
Shorter Coarse Sand	27.0
Thiopave	30.0
Compaction Agent	1.0

Actual Thiopave Content = 22%

As-Built Sublot Lift Thickness (in):	3.1
Total Thickness of All 2009 Sublots (in):	6.9
Approx. Underlying HMA Thickness (in):	0.0
Type of Tack Coat Utilized:	NA
Target Tack Application Rate (gal/sy):	NA
Approx. Avg. Temperature at Plant (F):	275
Avg. Measured Mat Compaction:	93.7%

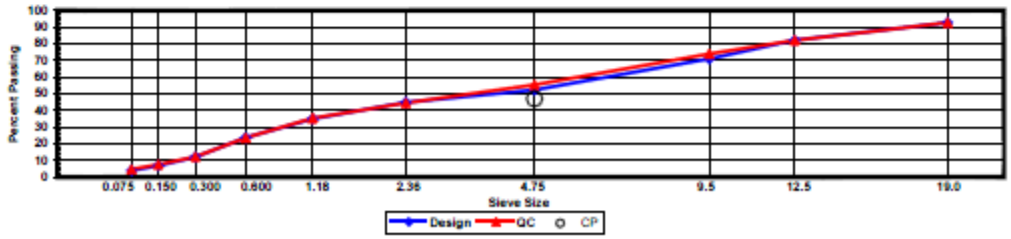

General Notes:
1) Mixes are referenced by quadrant (E=East, N=North, W=West, and S=South), section # (sequential) and sublot (top=1);
3) The total HMA thickness of all structural study sections (N1-N11 and S8-S12) ranges from 5-3/4 to 14 inches by design;
3) All non-structural sections are supprted by a uniform perpetual foundation in order to study surface mix performance;
4) SMA and OGFC refer to stone matrix asphalt and open-graded friction course, respectively; and
5) All liquid asphalt purchased for use in Track reconstruction contained LOF 6500 antistrip additive at a rate of 0.5 percent

10/5/2009

Quadrant: S
Section: 9 *Mix Type = Surface - Control*
Sublot: 1

Laboratory Diary

General Description of Mix and Materials

Design Method:	Super
Compactive Effort:	80 gyrations
Binder Performance Grade:	76-22
Modifier Type:	SBS
Aggregate Type:	Grn/Sand/Lms
Design Gradation Type:	Fine

Avg. Lab Properties of Plant Produced Mix

Sieve Size	Design	QC
25 mm (1"):	100	100
19 mm (3/4"):	100	100
12.5 mm (1/2"):	100	100
9.5 mm (3/8"):	100	100
4.75 mm (#4):	78	81
2.36 mm (#8):	60	59
1.18 mm (#16):	46	46
0.60 mm (#30):	31	31
0.30 mm (#50):	16	16
0.15 mm (#100):	10	9
0.075 mm (#200):	5.8	6.0
Binder Content (Pb):	5.8	6.1
Eff. Binder Content (Pbe):	5.1	5.4
Dust-to-Binder Ratio:	1.1	1.1
Rice Gravity (Gmm):	2.483	2.472
Avg. Bulk Gravity (Gmb):	2.384	2.374
Avg Air Voids (Va):	4.0	4.0
Agg. Bulk Gravity (Gsb):	2.667	2.670
Avg VMA:	15.8	16.5
Avg. VFA:	75	76

Construction Diary

Relevant Conditions for Construction

Completion Date:	July 16, 2009
24 Hour High Temperature (F):	92
24 Hour Low Temperature (F):	74
24 Hour Rainfall (in):	0.00
Planned Subot Lift Thickness (in):	1.3
Paving Machine:	Roadtec

Plant Configuration and Placement Details

Component	% Setting
Asphalt Content (Plant Setting)	6.5
89 Columbus Granite	36.0
8910 Opelika Limestone Screenings	23.0
M10 Columbus Granite	13.0
Shorter Coarse Sand	28.0
As-Built Sublot Lift Thickness (in):	1.2
Total Thickness of All 2009 Sublots (in):	7.0
Approx. Underlying HMA Thickness (in):	0.0
Type of Tack Coat Utilized:	NTSS-1HM
Target Tack Application Rate (gal/sy):	0.04
Approx. Avg. Temperature at Plant (F):	335
Avg. Measured Mat Compaction:	93.1%

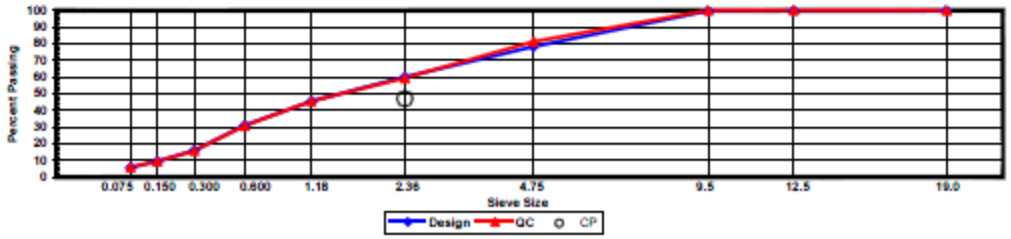

General Notes:
1) Mixes are referenced by quadrant (E=East, N=North, W=West, and S=South), section # (sequential) and sublot (top=1);
3) The total HMA thickness of all structural study sections (N1-N11 and S8-S12) ranges from 5-3/4 to 14 inches by design;
3) All non-structural sections are supprted by a uniform perpetual foundation in order to study surface mix performance;
4) SMA and OGFC refer to stone matrix asphalt and open-graded friction course, respectively; and
5) All liquid asphalt purchased for use in Track reconstruction contained LOF 6500 antistrip additive at a rate of 0.5 percent

10/5/2009

Quadrant: S
Section: 9 *Mix Type = Intermediate - Control*
Sublot: 2

Laboratory Diary

General Desccription of Mix and Materials

Design Method:	Super
Compactive Effort:	80 gyrations
Binder Performance Grade:	76-22
Modifier Type:	SBS
Aggregate Type:	Lms/Sand/Grn
Design Gradation Type:	Fine

Avg. Lab Properties of Plant Produced Mix

Sieve Size	Design	QC
25 mm (1"):	100	99
19 mm (3/4"):	93	92
12.5 mm (1/2"):	82	84
9.5 mm (3/8"):	71	76
4.75 mm (#4):	52	57
2.36 mm (#8):	45	47
1.18 mm (#16):	35	38
0.60 mm (#30):	24	26
0.30 mm (#50):	12	15
0.15 mm (#100):	7	9
0.075 mm (#200):	3.9	5.3
Binder Content (Pb):	4.7	4.4
Eff. Binder Content (Pbe):	4.1	3.9
Dust-to-Binder Ratio:	0.9	1.4
Rice Gravity (Gmm):	2.575	2.551
Avg. Bulk Gravity (Gmb):	2.472	2.439
Avg Air Voids (Va):	4.0	4.4
Agg. Bulk Gravity (Gsb):	2.737	2.695
Avg VMA:	13.9	13.5
Avg. VFA:	71	68

Construction Diary

Relevant Conditions for Construction

Completion Date:	July 14, 2009
24 Hour High Temperature (F):	93
24 Hour Low Temperature (F):	72
24 Hour Rainfall (in):	0.00
Planned Subot Lift Thickness (in):	2.8
Paving Machine:	Roadtec

Plant Configuration and Placement Details

Component	% Setting
Asphalt Content (Plant Setting)	4.7
78 Opelika Limestone	30.0
57 Opelika Limestone	18.0
M10 Columbus Granite	25.0
Shorter Coarse Sand	27.0

As-Built Sublot Lift Thickness (in):	2.8
Total Thickness of All 2009 Sublots (in):	7.0
Approx. Underlying HMA Thickness (in):	0.0
Type of Tack Coat Utilized:	NTSS-1HM
Target Tack Application Rate (gal/sy):	0.07
Approx. Avg. Temperature at Plant (F):	335
Avg. Measured Mat Compaction:	92.8%

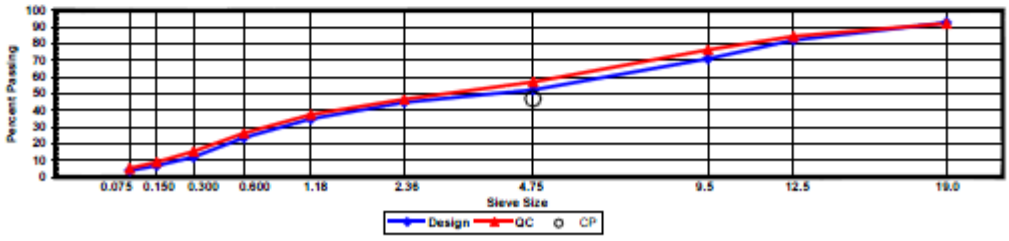

General Notes:
1) Mixes are referenced by quadrant (E=East, N=North, W=West, and S=South), section # (sequential) and sublot (top=1);
3) The total HMA thickness of all structural study sections (N1-N11 and S8-S12) ranges from 5-3/4 to 14 inches by design;
3) All non-structural sections are supprted by a uniform perpetual foundation in order to study surface mix performance;
4) SMA and OGFC refer to stone matrix asphalt and open-graded friction course, respectively; and
5) All liquid asphalt purchased for use in Track reconstruction contained LOF 6500 antistrip additive at a rate of 0.5 percent

10/5/2009

Quadrant: S
Section: 9
Sublot: 3

Mix Type = Base - Control

Laboratory Diary

General Descoription of Mix and Materials

Design Method:	Super
Compactive Effort:	80 gyrations
Binder Performance Grade:	67-22
Modifier Type:	NA
Aggregate Type:	Lms/Sand/Grn
Design Gradation Type:	Fine

Avg. Lab Properties of Plant Produced Mix

Sieve Size	Design	QC
25 mm (1"):	100	99
19 mm (3/4"):	93	95
12.5 mm (1/2"):	84	87
9.5 mm (3/8"):	73	77
4.75 mm (#4):	55	56
2.36 mm (#8):	47	46
1.18 mm (#16):	36	37
0.60 mm (#30):	25	26
0.30 mm (#50):	14	15
0.15 mm (#100):	8	9
0.075 mm (#200):	4.6	5.1
Binder Content (Pb):	4.6	4.7
Eff. Binder Content (Pbe):	4.1	4.2
Dust-to-Binder Ratio:	1.1	1.2
Rice Gravity (Gmm):	2.574	2.540
Avg. Bulk Gravity (Gmb):	2.471	2.439
Avg Air Voids (Va):	4.0	4.0
Agg. Bulk Gravity (Gsb):	2.738	2.699
Avg VMA:	13.9	13.9
Avg. VFA:	71	71

Construction Diary

Relevant Conditions for Construction

Completion Date:	July 3, 2009
24 Hour High Temperature (F):	92
24 Hour Low Temperature (F):	69
24 Hour Rainfall (in):	0.00
Planned Subot Lift Thickness (in):	3.0
Paving Machine:	Roadtec

Plant Configuration and Placement Details

Component	% Setting
Asphalt Content (Plant Setting)	4.9
78 Opelika Limestone	30.0
57 Opelika Limestone	18.0
M10 Columbus Granite	25.0
Shorter Coarse Sand	27.0

As-Built Sublot Lift Thickness (in):	3.0
Total Thickness of All 2009 Sublots (in):	7.0
Approx. Underlying HMA Thickness (in):	0.0
Type of Tack Coat Utilized:	NA
Target Tack Application Rate (gal/sy):	NA
Approx. Avg. Temperature at Plant (F):	325
Avg. Measured Mat Compaction:	92.6%

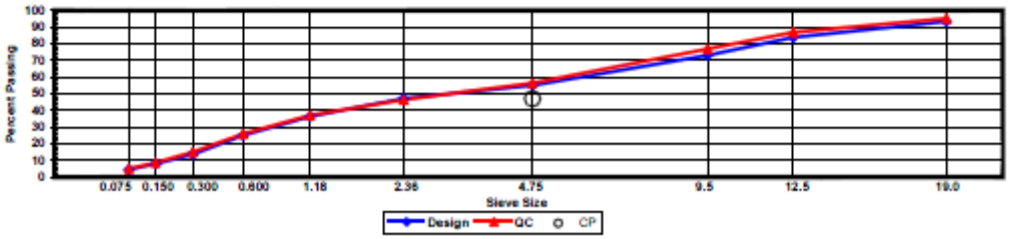

General Notes:

1) Mixes are referenced by quadrant (E=East, N=North, W=West, and S=South), section # (sequential) and sublot (top=1);
3) The total HMA thickness of all structural study sections (N1-N11 and S8-S12) ranges from 5-3/4 to 14 inches by design;
3) All non-structural sections are supprted by a uniform perpetual foundation in order to study surface mix performance;
4) SMA and OGFC refer to stone matrix asphalt and open-graded friction course, respectively; and
5) All liquid asphalt purchased for use in Track reconstruction contained LOF 6500 antistrip additive at a rate of 0.5 percent

APPENDIX B – SURVEYED PAVEMENT DEPTHS

TABLE B1. Surveyed Pavement Depths

			Layer Thickness, in.					
Section-Location	RL	Offset	Lift 1	Lift 2	Lift 3	Lift 4	Total AC	Aggregate Base
N5-1	1	I	1.236	3.012	1.908	3.012	9.168	5.892
N5-2	1	B	1.284	2.964	1.896	3.252	9.396	5.4
N5-3	1	O	1.320	2.736	1.920	3.432	9.408	5.292
N5-4	2	I	1.200	2.940	1.968	3.084	9.192	5.448
N5-5	2	B	1.356	2.832	1.848	2.712	8.748	5.904
N5-6	2	O	1.536	2.652	1.740	2.424	8.352	6.18
N5-7	3	I	0.996	2.820	2.136	3.168	9.120	5.148
N5-8	3	B	1.260	2.652	2.028	2.724	8.664	5.724
N5-9	3	O	1.284	2.676	2.064	2.448	8.472	6.036
N5-10	4	I	1.464	2.244	2.088	3.228	9.024	5.388
N5-11	4	B	1.536	2.196	2.112	2.952	8.796	5.808
N5-12	4	O	1.092	2.568	2.148	2.880	8.688	5.784
N6-1	1	I	1.344	2.688	3.360	0.000	7.392	3.828
N6-2	1	B	1.356	2.712	3.348	0.000	7.416	4.344
N6-3	1	O	1.260	2.784	3.084	0.000	7.128	5.112
N6-4	2	I	1.116	2.604	3.324	0.000	7.044	4.572
N6-5	2	B	1.032	2.772	3.312	0.000	7.116	4.824
N6-6	2	O	0.888	2.820	2.940	0.000	6.648	5.52
N6-7	3	I	0.864	2.868	3.048	0.000	6.780	4.368
N6-8	3	B	0.936	2.928	2.760	0.000	6.624	4.896
N6-9	3	O	0.900	2.916	2.832	0.000	6.648	5.268
N6-10	4	I	0.768	2.652	3.336	0.000	6.756	4.716
N6-11	4	B	0.840	2.976	2.784	0.000	6.600	5.064
N6-12	4	O	1.008	2.940	3.132	0.000	7.080	5.4
S9-1	1	I	1.524	2.784	2.952	0.000	7.260	5.868
S9-2	1	B	1.272	2.916	2.988	0.000	7.176	5.628
S9-3	1	O	1.224	2.772	3.048	0.000	7.044	5.808
S9-4	2	I	1.212	2.868	2.988	0.000	7.068	5.856
S9-5	2	B	1.188	2.892	2.856	0.000	6.936	6.036
S9-6	2	O	1.104	2.916	2.832	0.000	6.852	6.12
S9-7	3	I	1.140	2.796	2.880	0.000	6.816	5.208
S9-8	3	B	1.164	2.640	3.060	0.000	6.864	5.46
S9-9	3	O	1.164	2.712	3.072	0.000	6.948	5.832
S9-10	4	I	1.320	2.628	3.324	0.000	7.272	5.628
S9-11	4	B	1.152	2.700	3.132	0.000	6.984	5.88
S9-12	4	O	1.128	2.724	2.976	0.000	6.828	6.216

RL = Random Location
Offset: B = Between Wheelpath, I = Inside Wheelpath, O = Outside Wheelpath

APPENDIX C – BINDER GRADING

Table C.1 PG Grading of Virgin Binder Used in Base Lifts of Sections N5 and N6

Test Method			**Results**	**Specification**
Original Binder				
Rotational Viscosity @ 135°C, AASHTO T 316, PaS			0.49	≤ 3 PaS
Dynamic Shear Rheometer AASHTO T 315				
Test Temperature, °C	G*, kPa	Phase Angle δ, °	G* / sinδ, kPa	
64	1.85	84.7	1.86	≥ 1.00 kPa
70	0.89	86.2	0.89	
Rolling Thin Film (RTFO) Aged Binder, AASHTO T 240				
Mass Change, %			-0.872	≤ 1.00%
Dynamic Shear Rheometer AASHTO T 315				
Test Temperature, °C	G*, kPa	Phase Angle δ, °	G* / sinδ, kPa	
64	4.64	80.1	4.71	≥ 2.20 kPa
70	2.18	82.5	2.2	
Pressure Aging Vessel (PAV) Aged Binder, AASHTO R28				
Dynamic Shear Rheometer AASHTO T 315				
Test Temperature, °C	G*, kPa	Phase Angle δ, °	G* sinδ, kPa	
22	7548	41.0	4953	≤ 5,000 kPa
19	11200	38.4	6948	
Bending Beam Rheometer (BBR) AASHTO T313				
Test Temperature, °C				
-12	Stiffness, Mpa		151	≤ 300 Mpa
	m-value		0.327	≥ 0.300
-18	Stiffness, Mpa		304	
	m-value		0.269	
True Grade	69.1 -24.8			
PG Grade	64 -22			

1. DSR Original: T_{max}
   Temperature at which G*/sinδ = 1.00 kPa — 69.1
2. DSR RTFO: T_{max}
   Temperature at which G*/sinδ = 2.20 kPa — 70.0
3. DSR PAV: T_{int}
   Temperature at which G*sinδ = 5,000 kPa — 21.9
4. BBR PAV: T_{min}
   Temperature at which S(t) = 300 Mpa — -27.8
   Temperature at which m = 0.300 — -24.8

Table C.2 PG Grading of Virgin Binder Used in Intermediate Lifts of Sections N5 and N6

Test Method			**Results**	**Specification**
Original Binder				
Rotational Viscosity @ 135°C, AASHTO T 316, PaS			0.55	≤ 3 PaS
Dynamic Shear Rheometer AASHTO T 315				
Test Temperature, °C	G*, kPa	Phase Angle δ, °	G* / sinδ, kPa	
64	1.81	84.6	1.82	≥ 1.00 kPa
70	0.88	86.2	0.88	
Rolling Thin Film (RTFO) Aged Binder, AASHTO T 240				
Mass Change, %				≤ 1.00%
Dynamic Shear Rheometer AASHTO T 315				
Test Temperature, °C	G*, kPa	Phase Angle δ, °	G* / sinδ, kPa	
64	6.17	78.5	6.29	≥ 2.20 kPa
70	2.95	81.13	2.99	
Pressure Aging Vessel (PAV) Aged Binder, AASHTO R28				
Dynamic Shear Rheometer AASHTO T 315				
Test Temperature, °C	G*, kPa	Phase Angle δ, °	G* sinδ, kPa	
22	7158	41.9	4781	≤ 5,000 kPa
19	10580	39.3	6700	
Bending Beam Rheometer (BBR) AASHTO T313				
Test Temperature, °C				
-12	Stiffness, Mpa		147	≤ 300 Mpa
	m-value		0.327	≥ 0.300
-18	Stiffness, Mpa		295	
	m-value		0.288	
True Grade	68.9 -26.2			
PG Grade	64 -22			

1. DSR Original: T_{max}

   Temperature at which G*/sinδ = 1.00 kPa — 68.9

2. DSR RTFO: T_{max}

   Temperature at which G*/sinδ = 2.20 kPa — 72.5

3. DSR PAV: T_{int}

   Temperature at which G*sinδ = 5,000 kPa — 21.6

4. BBR PAV: T_{min}

   Temperature at which S(t) = 300 Mpa — -28.2

   Temperature at which m = 0.300 — -26.2

Table C.3 PG Grading of Virgin Binder Used in Base Lift of Section S9

Test Method			**Test Results**	**Specification**
Original Binder				
Rotational Viscosity @ 135°C, AASHTO T 316, PaS				≤ 3 PaS
Dynamic Shear Rheometer AASHTO T 315				
Test Temperature, °C	G*, kPa	Phase Angle δ, °	G* / sinδ, kPa	
64	1.91	84.9	1.91	≥ 1.00 kPa
70	0.94	86.3	0.94	
Rolling Thin Film (RTFO) Aged Binder, AASHTO T 240				
Mass Change, %				≤ 1.00%
Dynamic Shear Rheometer AASHTO T 315				
Test Temperature, °C	G*, kPa	Phase Angle δ, °	G* / sinδ, kPa	
70	2.40	82.4	2.42	≥ 2.20 kPa
76	1.186	84.5	1.19	
Pressure Aging Vessel (PAV) Aged Binder, AASHTO R28				
Dynamic Shear Rheometer AASHTO T 315				
Test Temperature, °C	G*, kPa	Phase Angle δ, °	G* sinδ, kPa	
22	6245	41.9	4169	≤ 5,000 kPa
19	9212	39.3	5837	
Bending Beam Rheometer (BBR) AASHTO T313				
Test Temperature, °C				
-12	Stiffness, Mpa		141	≤ 300 Mpa
	m-value		0.333	≥ 0.300
-18	Stiffness, Mpa		313	
	m-value		0.283	
True Grade	69.5 -26.0			
PG Grade	64 - 22			

1. DSR Original: T_{max}

   Temperature at which G*/sinδ = 1.00 kPa — 69.5

2. DSR RTFO: T_{max}

   Temperature at which G*/sinδ = 2.20 kPa — 70.8

3. DSR PAV: T_{int}

   Temperature at which G*sinδ = 5,000 kPa — 20.4

4. BBR PAV: T_{min}

   Temperature at which S(t) = 300 Mpa — -27.5

   Temperature at which m = 0.300 — -26.0

Table C.4 PG Grading of Virgin Binder Used in Intermediate Lift of Section S9

Test Method			**Test Results**	**Specification**
Original Binder				
Rotational Viscosity @ 135°C, AASHTO T 316, PaS			1.444	≤ 3 PaS
Dynamic Shear Rheometer AASHTO T 315				
Test Temperature, °C	G*, kPa	Phase Angle δ, °	G* / sinδ, kPa	
76	1.22	84.1	1.27	≥ 1.00 kPa
82	0.71	76.3	0.73	
Rolling Thin Film (RTFO) Aged Binder, AASHTO T 240				
Mass Change, %			-0.042	≤ 1.00%
Dynamic Shear Rheometer AASHTO T 315				
Test Temperature, °C	G*, kPa	Phase Angle δ, °	G* / sinδ, kPa	
76	2.83	67.9	3.06	≥ 2.20 kPa
82	1.66	70	1.77	
Pressure Aging Vessel (PAV) Aged Binder, AASHTO R28				
Dynamic Shear Rheometer AASHTO T 315				
Test Temperature, °C	G*, kPa	Phase Angle δ, °	G* sinδ, kPa	
22	6383	41.0	4185	≤ 5,000 kPa
19	9350	38.6	5834	
Bending Beam Rheometer (BBR) AASHTO T313				
Test Temperature, °C				
-12	Stiffness, Mpa		135	≤ 300 Mpa
	m-value		0.326	≥ 0.300
-18	Stiffness, Mpa		285	
	m-value		0.282	
True Grade	78.6 -25.5			
PG Grade	76 - 22			

1. DSR Original: T_{max}

   Temperature at which G*/sinδ = 1.00 kPa — 78.6

2. DSR RTFO: T_{max}

   Temperature at which G*/sinδ = 2.20 kPa — 79.6

3. DSR PAV: T_{int}

   Temperature at which G*sinδ = 5,000 kPa — 20.4

4. BBR PAV: T_{min}

   Temperature at which S(t) = 300 Mpa — -28.6

   Temperature at which m = 0.300 — -25.5

Table C.5 PG Grading of Binder Extracted from Mixtures Used in Surface Lifts of Sections S9, N5, N6

Test, Method			**Test Results**	**Specification**
Rolling Thin Film (RTFO) Aged Binder, AASHTO T 240				
Rotational Viscosity @ 135°C, AASHTO T 316, PaS			2.287	≤ 3 PaS
Dynamic Shear Rheometer AASHTO T 315				
Test Temperature, °C	G*, kPa	Phase Angle δ, °	G* / sinδ, kPa	
76	3.45	67.3	3.74	≥ 2.20 kPa
82	2.00	69.5	2.14	
Pressure Aging Vessel (PAV) Aged Binder, AASHTO R28				
Dynamic Shear Rheometer AASHTO T 315				
Test Temperature, °C	G*, kPa	Phase Angle δ, °	G* sinδ, kPa	
22	7607	40.7	4964	≤ 5,000 kPa
19	11060	38.5	6880	
Bending Beam Rheometer (BBR) AASHTO T313				
Test Temperature, °C				
-12	Stiffness, Mpa		124	≤ 300 Mpa
	m-value		0.317	≥ 0.300
-18	Stiffness, Mpa		277	
	m-value		0.279	
True Grade	81.7 -24.7			
PG Grade	76 - 22			

1. DSR RTFO: T_{max}

   Temperature at which G*/sinδ = 2.20 kPa — 81.7

2. DSR PAV: T_{int}

   Temperature at which G*sinδ = 5,000 kPa — 21.9

3. BBR PAV: T_{min}

   Temperature at which S(t) = 300 Mpa — -28.9

   Temperature at which m = 0.300 — -24.7

APPENDIX D - MASTER CURVE DATA

TABLE D1. MEPDG Input values for Dynamic Modulus Testing (Unconfined)

Section-Lift ID	Temp (deg C)	Temp (deg F)	Frequency (Hz)	Shift Factor	Reduced Frequency	E*, (ksi)	E*, (Mpa)
CONTROL-SURFACE	-10.0	14	25	4.035	2.71E+05	2516.5	17356.1
CONTROL-SURFACE	-10.0	14	10	4.035	1.09E+05	2418.3	16679.0
CONTROL-SURFACE	-10.0	14	5	4.035	5.43E+04	2334.7	16102.4
CONTROL-SURFACE	-10.0	14	1	4.035	1.09E+04	2108.1	14539.8
CONTROL-SURFACE	-10.0	14	0.5	4.035	5.43E+03	1996.7	13771.1
CONTROL-SURFACE	-10.0	14	0.1	4.035	1.09E+03	1709.2	11788.0
CONTROL-SURFACE	4.4	40	25	1.984	2.41E+03	1856.1	12801.8
CONTROL-SURFACE	4.4	40	10	1.984	9.63E+02	1686.5	11631.5
CONTROL-SURFACE	4.4	40	5	1.984	4.81E+02	1551.9	10703.6
CONTROL-SURFACE	4.4	40	1	1.984	9.63E+01	1229.4	8479.3
CONTROL-SURFACE	4.4	40	0.5	1.984	4.81E+01	1091.3	7526.5
CONTROL-SURFACE	4.4	40	0.1	1.984	9.63E+00	789.0	5442.0
CONTROL-SURFACE	21.1	70	25	-0.134	1.84E+01	906.1	6249.6
CONTROL-SURFACE	21.1	70	10	-0.134	7.35E+00	742.3	5119.7
CONTROL-SURFACE	21.1	70	5	-0.134	3.68E+00	629.1	4338.8
CONTROL-SURFACE	21.1	70	1	-0.134	7.35E-01	409.1	2821.8
CONTROL-SURFACE	21.1	70	0.5	-0.134	3.68E-01	334.0	2303.5
CONTROL-SURFACE	21.1	70	0.1	-0.134	7.35E-02	202.3	1395.4
CONTROL-SURFACE	37.8	100	25	-2.024	2.37E-01	292.2	2015.5
CONTROL-SURFACE	37.8	100	10	-2.024	9.46E-02	219.3	1512.8
CONTROL-SURFACE	37.8	100	5	-2.024	4.73E-02	175.5	1210.5
CONTROL-SURFACE	37.8	100	1	-2.024	9.46E-03	104.0	717.2
CONTROL-SURFACE	37.8	100	0.5	-2.024	4.73E-03	83.3	574.3
CONTROL-SURFACE	37.8	100	0.1	-2.024	9.46E-04	50.9	350.9
CONTROL-SURFACE	54.4	130	25	-3.722	4.74E-03	83.3	574.7
CONTROL-SURFACE	54.4	130	10	-3.722	1.90E-03	62.6	431.9
CONTROL-SURFACE	54.4	130	5	-3.722	9.48E-04	50.9	351.1
CONTROL-SURFACE	54.4	130	1	-3.722	1.90E-04	32.7	225.6
CONTROL-SURFACE	54.4	130	0.5	-3.722	9.48E-05	27.6	190.1
CONTROL-SURFACE	54.4	130	0.1	-3.722	1.90E-05	19.4	134.0
THIOPAVE-INTERMEDIATE	-10.0	14	25	3.924	2.10E+05	2898.8	19993.3
THIOPAVE-INTERMEDIATE	-10.0	14	10	3.924	8.39E+04	2851.1	19663.7
THIOPAVE-INTERMEDIATE	-10.0	14	5	3.924	4.19E+04	2808.2	19368.0
THIOPAVE-INTERMEDIATE	-10.0	14	1	3.924	8.39E+03	2681.7	18495.5
THIOPAVE-INTERMEDIATE	-10.0	14	0.5	3.924	4.19E+03	2613.7	18026.6

Section-Lift ID	Temp (deg C)	Temp (deg F)	Frequency (Hz)	Shift Factor	Reduced Frequency	E*, (ksi)	E*, (Mpa)
THIOPAVE-INTERMEDIATE	-10.0	14	0.1	3.924	8.39E+02	2419.0	16683.8
THIOPAVE-INTERMEDIATE	4.4	40	25	1.929	2.12E+03	2537.8	17503.3
THIOPAVE-INTERMEDIATE	4.4	40	10	1.929	8.48E+02	2420.6	16694.8
THIOPAVE-INTERMEDIATE	4.4	40	5	1.929	4.24E+02	2319.7	15999.1
THIOPAVE-INTERMEDIATE	4.4	40	1	1.929	8.48E+01	2044.3	14099.2
THIOPAVE-INTERMEDIATE	4.4	40	0.5	1.929	4.24E+01	1908.9	13165.8
THIOPAVE-INTERMEDIATE	4.4	40	0.1	1.929	8.48E+00	1565.2	10794.9
THIOPAVE-INTERMEDIATE	21.1	70	25	-0.130	1.85E+01	1736.3	11975.1
THIOPAVE-INTERMEDIATE	21.1	70	10	-0.130	7.41E+00	1535.1	10587.4
THIOPAVE-INTERMEDIATE	21.1	70	5	-0.130	3.71E+00	1379.2	9512.5
THIOPAVE-INTERMEDIATE	21.1	70	1	-0.130	7.41E-01	1023.6	7059.4
THIOPAVE-INTERMEDIATE	21.1	70	0.5	-0.130	3.71E-01	880.7	6073.9
THIOPAVE-INTERMEDIATE	21.1	70	0.1	-0.130	7.41E-02	592.1	4083.4
THIOPAVE-INTERMEDIATE	37.8	100	25	-1.968	2.69E-01	818.0	5641.9
THIOPAVE-INTERMEDIATE	37.8	100	10	-1.968	1.08E-01	652.8	4502.1
THIOPAVE-INTERMEDIATE	37.8	100	5	-1.968	5.38E-02	543.3	3746.8
THIOPAVE-INTERMEDIATE	37.8	100	1	-1.968	1.08E-02	343.5	2369.2
THIOPAVE-INTERMEDIATE	37.8	100	0.5	-1.968	5.38E-03	279.7	1929.1
THIOPAVE-INTERMEDIATE	37.8	100	0.1	-1.968	1.08E-03	173.8	1198.8
THIOPAVE-INTERMEDIATE	54.4	130	25	-3.619	6.01E-03	289.1	1993.7
THIOPAVE-INTERMEDIATE	54.4	130	10	-3.619	2.41E-03	220.1	1517.8
THIOPAVE-INTERMEDIATE	54.4	130	5	-3.619	1.20E-03	179.5	1237.9

Section-Lift ID	Temp (deg C)	Temp (deg F)	Frequency (Hz)	Shift Factor	Reduced Frequency	E*, (ksi)	E*, (Mpa)
THIOPAVE-INTERMEDIATE	54.4	130	1	-3.619	2.41E-04	114.5	789.8
THIOPAVE-INTERMEDIATE	54.4	130	0.5	-3.619	1.20E-04	95.8	661.0
THIOPAVE-INTERMEDIATE	54.4	130	0.1	-3.619	2.41E-05	66.4	458.0
THIOPAVE-BASE	-10.0	14	25	3.955	2.25E+05	2714.8	18723.8
THIOPAVE-BASE	-10.0	14	10	3.955	9.01E+04	2643.3	18231.0
THIOPAVE-BASE	-10.0	14	5	3.955	4.50E+04	2580.8	17799.6
THIOPAVE-BASE	-10.0	14	1	3.955	9.01E+03	2403.5	16577.1
THIOPAVE-BASE	-10.0	14	0.5	3.955	4.50E+03	2312.2	15947.0
THIOPAVE-BASE	-10.0	14	0.1	3.955	9.01E+02	2063.4	14231.3
THIOPAVE-BASE	4.4	40	25	1.944	2.20E+03	2207.5	15225.3
THIOPAVE-BASE	4.4	40	10	1.944	8.79E+02	2059.2	14202.1
THIOPAVE-BASE	4.4	40	5	1.944	4.39E+02	1936.4	13355.1
THIOPAVE-BASE	4.4	40	1	1.944	8.79E+01	1621.6	11184.2
THIOPAVE-BASE	4.4	40	0.5	1.944	4.39E+01	1477.0	10186.5
THIOPAVE-BASE	4.4	40	0.1	1.944	8.79E+00	1136.1	7836.0
THIOPAVE-BASE	21.1	70	25	-0.131	1.85E+01	1293.2	8919.4
THIOPAVE-BASE	21.1	70	10	-0.131	7.40E+00	1100.3	7588.4
THIOPAVE-BASE	21.1	70	5	-0.131	3.70E+00	959.1	6615.2
THIOPAVE-BASE	21.1	70	1	-0.131	7.40E-01	663.0	4572.6
THIOPAVE-BASE	21.1	70	0.5	-0.131	3.70E-01	553.8	3819.4
THIOPAVE-BASE	21.1	70	0.1	-0.131	7.40E-02	349.9	2413.0
THIOPAVE-BASE	37.8	100	25	-1.983	2.60E-01	503.0	3469.0
THIOPAVE-BASE	37.8	100	10	-1.983	1.04E-01	387.1	2669.7
THIOPAVE-BASE	37.8	100	5	-1.983	5.19E-02	314.3	2168.1
THIOPAVE-BASE	37.8	100	1	-1.983	1.04E-02	190.0	1310.6
THIOPAVE-BASE	37.8	100	0.5	-1.983	5.19E-03	152.6	1052.5
THIOPAVE-BASE	37.8	100	0.1	-1.983	1.04E-03	92.9	640.7
THIOPAVE-BASE	54.4	130	25	-3.647	5.63E-03	156.5	1079.6
THIOPAVE-BASE	54.4	130	10	-3.647	2.25E-03	117.5	810.5
THIOPAVE-BASE	54.4	130	5	-3.647	1.13E-03	95.2	656.3
THIOPAVE-BASE	54.4	130	1	-3.647	2.25E-04	60.2	415.4
THIOPAVE-BASE	54.4	130	0.5	-3.647	1.13E-04	50.3	347.3
THIOPAVE-BASE	54.4	130	0.1	-3.647	2.25E-05	34.9	240.6
CONTROL-INTERMEDIATE	-10.0	14	25	4.037	2.72E+05	2808.7	19371.7
CONTROL-INTERMEDIATE	-10.0	14	10	4.037	1.09E+05	2737.7	18881.9
CONTROL-INTERMEDIATE	-10.0	14	5	4.037	5.44E+04	2676.4	18459.2
CONTROL-INTERMEDIATE	-10.0	14	1	4.037	1.09E+04	2506.0	17283.7

Section-Lift ID	Temp (deg C)	Temp (deg F)	Frequency (Hz)	Shift Factor	Reduced Frequency	E*, (ksi)	E*, (Mpa)
CONTROL-INTERMEDIATE	-10.0	14	0.5	4.037	5.44E+03	2419.5	16687.1
CONTROL-INTERMEDIATE	-10.0	14	0.1	4.037	1.09E+03	2186.7	15081.6
CONTROL-INTERMEDIATE	4.4	40	25	1.984	2.41E+03	2307.3	15913.5
CONTROL-INTERMEDIATE	4.4	40	10	1.984	9.64E+02	2167.4	14948.4
CONTROL-INTERMEDIATE	4.4	40	5	1.984	4.82E+02	2052.2	14154.0
CONTROL-INTERMEDIATE	4.4	40	1	1.984	9.64E+01	1757.5	12121.2
CONTROL-INTERMEDIATE	4.4	40	0.5	1.984	4.82E+01	1621.4	11182.5
CONTROL-INTERMEDIATE	4.4	40	0.1	1.984	9.64E+00	1295.7	8936.7
CONTROL-INTERMEDIATE	21.1	70	25	-0.134	1.84E+01	1426.8	9840.4
CONTROL-INTERMEDIATE	21.1	70	10	-0.134	7.35E+00	1240.8	8557.6
CONTROL-INTERMEDIATE	21.1	70	5	-0.134	3.68E+00	1102.4	7603.4
CONTROL-INTERMEDIATE	21.1	70	1	-0.134	7.35E-01	802.0	5531.5
CONTROL-INTERMEDIATE	21.1	70	0.5	-0.134	3.68E-01	686.2	4733.1
CONTROL-INTERMEDIATE	21.1	70	0.1	-0.134	7.35E-02	458.6	3163.1
CONTROL-INTERMEDIATE	37.8	100	25	-2.025	2.36E-01	617.7	4260.5
CONTROL-INTERMEDIATE	37.8	100	10	-2.025	9.45E-02	490.1	3380.2
CONTROL-INTERMEDIATE	37.8	100	5	-2.025	4.72E-02	406.9	2806.2
CONTROL-INTERMEDIATE	37.8	100	1	-2.025	9.45E-03	256.7	1770.3
CONTROL-INTERMEDIATE	37.8	100	0.5	-2.025	4.72E-03	208.7	1439.7
CONTROL-INTERMEDIATE	37.8	100	0.1	-2.025	9.45E-04	128.6	886.7
CONTROL-INTERMEDIATE	54.4	130	25	-3.723	4.73E-03	208.8	1440.1
CONTROL-INTERMEDIATE	54.4	130	10	-3.723	1.89E-03	158.4	1092.5

Section-Lift ID	Temp (deg C)	Temp (deg F)	Frequency (Hz)	Shift Factor	Reduced Frequency	E*, (ksi)	E*, (Mpa)
CONTROL-INTERMEDIATE	54.4	130	5	-3.723	9.46E-04	128.6	886.9
CONTROL-INTERMEDIATE	54.4	130	1	-3.723	1.89E-04	80.3	554.0
CONTROL-INTERMEDIATE	54.4	130	0.5	-3.723	9.46E-05	66.3	457.1
CONTROL-INTERMEDIATE	54.4	130	0.1	-3.723	1.89E-05	43.9	302.7
CONTROL-BASE	-10.0	14	25	3.618	1.04E+05	2739.1	18891.4
CONTROL-BASE	-10.0	14	10	3.618	4.15E+04	2649.4	18272.8
CONTROL-BASE	-10.0	14	5	3.618	2.08E+04	2571.4	17734.8
CONTROL-BASE	-10.0	14	1	3.618	4.15E+03	2353.1	16229.2
CONTROL-BASE	-10.0	14	0.5	3.618	2.08E+03	2242.2	15464.7
CONTROL-BASE	-10.0	14	0.1	3.618	4.15E+02	1946.5	13425.2
CONTROL-BASE	4.4	40	25	1.779	1.50E+03	2186.9	15083.1
CONTROL-BASE	4.4	40	10	1.779	6.01E+02	2018.8	13923.8
CONTROL-BASE	4.4	40	5	1.779	3.00E+02	1881.1	12973.7
CONTROL-BASE	4.4	40	1	1.779	6.01E+01	1534.3	10581.9
CONTROL-BASE	4.4	40	0.5	1.779	3.00E+01	1378.3	9506.1
CONTROL-BASE	4.4	40	0.1	1.779	6.01E+00	1020.6	7039.3
CONTROL-BASE	21.1	70	25	-0.120	1.90E+01	1274.7	8791.6
CONTROL-BASE	21.1	70	10	-0.120	7.59E+00	1071.2	7388.3
CONTROL-BASE	21.1	70	5	-0.120	3.79E+00	923.7	6371.0
CONTROL-BASE	21.1	70	1	-0.120	7.59E-01	619.0	4269.0
CONTROL-BASE	21.1	70	0.5	-0.120	3.79E-01	508.8	3509.0
CONTROL-BASE	21.1	70	0.1	-0.120	7.59E-02	307.8	2122.9
CONTROL-BASE	37.8	100	25	-1.815	3.83E-01	510.2	3518.7
CONTROL-BASE	37.8	100	10	-1.815	1.53E-01	386.1	2663.1
CONTROL-BASE	37.8	100	5	-1.815	7.66E-02	308.8	2129.5
CONTROL-BASE	37.8	100	1	-1.815	1.53E-02	178.3	1229.8
CONTROL-BASE	37.8	100	0.5	-1.815	7.66E-03	139.9	964.7
CONTROL-BASE	37.8	100	0.1	-1.815	1.53E-03	80.1	552.4
CONTROL-BASE	54.4	130	25	-3.337	1.15E-02	161.3	1112.5
CONTROL-BASE	54.4	130	10	-3.337	4.60E-03	117.0	806.9
CONTROL-BASE	54.4	130	5	-3.337	2.30E-03	92.0	634.5
CONTROL-BASE	54.4	130	1	-3.337	4.60E-04	54.0	372.4
CONTROL-BASE	54.4	130	0.5	-3.337	2.30E-04	43.6	301.0
CONTROL-BASE	54.4	130	0.1	-3.337	4.60E-05	28.0	193.0

TABLE D2 Confined Master Curve Data

Section-Lift ID	Temp (deg C)	Temp (deg F)	Frequency (Hz)	Shift Factor	Reduced Frequency	E*, (ksi)	E*, (Mpa)
CONTROL-SURFACE	-10.0	14	25	3.882	1.90E+05	2574.6	17756.8
CONTROL-SURFACE	-10.0	14	10	3.882	7.62E+04	2472.4	17051.9
CONTROL-SURFACE	-10.0	14	5	3.882	3.81E+04	2383.8	16441.4
CONTROL-SURFACE	-10.0	14	1	3.882	7.62E+03	2139.5	14756.2
CONTROL-SURFACE	-10.0	14	0.5	3.882	3.81E+03	2018.0	13918.0
CONTROL-SURFACE	-10.0	14	0.1	3.882	7.62E+02	1704.3	11754.8
CONTROL-SURFACE	4.4	40	25	1.908	2.02E+03	1899.4	13099.9
CONTROL-SURFACE	4.4	40	10	1.908	8.09E+02	1716.8	11840.5
CONTROL-SURFACE	4.4	40	5	1.908	4.05E+02	1572.5	10845.8
CONTROL-SURFACE	4.4	40	1	1.908	8.09E+01	1232.3	8499.4
CONTROL-SURFACE	4.4	40	0.5	1.908	4.05E+01	1090.3	7519.9
CONTROL-SURFACE	4.4	40	0.1	1.908	8.09E+00	790.4	5451.7
CONTROL-SURFACE	21.1	70	25	-0.129	1.86E+01	939.1	6477.2
CONTROL-SURFACE	21.1	70	10	-0.129	7.44E+00	776.2	5353.8
CONTROL-SURFACE	21.1	70	5	-0.129	3.72E+00	666.2	4595.0
CONTROL-SURFACE	21.1	70	1	-0.129	7.44E-01	458.8	3164.1
CONTROL-SURFACE	21.1	70	0.5	-0.129	3.72E-01	389.6	2687.1
CONTROL-SURFACE	21.1	70	0.1	-0.129	7.44E-02	269.3	1857.5
CONTROL-SURFACE	37.8	100	25	-1.947	2.83E-01	365.3	2519.4
CONTROL-SURFACE	37.8	100	10	-1.947	1.13E-01	295.7	2039.8
CONTROL-SURFACE	37.8	100	5	-1.947	5.65E-02	253.6	1748.9
CONTROL-SURFACE	37.8	100	1	-1.947	1.13E-02	182.8	1260.8
CONTROL-SURFACE	37.8	100	0.5	-1.947	5.65E-03	161.3	1112.3
CONTROL-SURFACE	37.8	100	0.1	-1.947	1.13E-03	125.5	865.8
CONTROL-SURFACE	54.4	130	25	-3.580	6.57E-03	165.6	1142.1
CONTROL-SURFACE	54.4	130	10	-3.580	2.63E-03	142.2	980.5
CONTROL-SURFACE	54.4	130	5	-3.580	1.31E-03	128.2	884.3
CONTROL-SURFACE	54.4	130	1	-3.580	2.63E-04	105.0	724.0
CONTROL-SURFACE	54.4	130	0.5	-3.580	1.31E-04	97.8	674.8
CONTROL-SURFACE	54.4	130	0.1	-3.580	2.63E-05	85.8	591.7
THIOPAVE-INTERMEDIATE	-10.0	14	25	3.914	2.05E+05	2934.3	20237.7
THIOPAVE-INTERMEDIATE	-10.0	14	10	3.914	8.20E+04	2889.8	19931.0
THIOPAVE-INTERMEDIATE	-10.0	14	5	3.914	4.10E+04	2849.1	19650.6
THIOPAVE-INTERMEDIATE	-10.0	14	1	3.914	8.20E+03	2725.9	18800.5
THIOPAVE-INTERMEDIATE	-10.0	14	0.5	3.914	4.10E+03	2658.1	18332.9
THIOPAVE-INTERMEDIATE	-10.0	14	0.1	3.914	8.20E+02	2460.0	16966.8
THIOPAVE-	4.4	40	25	1.924	2.10E+03	2582.8	17813.9

Section-Lift ID	Temp (deg C)	Temp (deg F)	Frequency (Hz)	Shift Factor	Reduced Frequency	E*, (ksi)	E*, (Mpa)
INTERMEDIATE							
THIOPAVE-INTERMEDIATE	4.4	40	10	1.924	8.39E+02	2463.3	16989.2
THIOPAVE-INTERMEDIATE	4.4	40	5	1.924	4.20E+02	2359.3	16272.1
THIOPAVE-INTERMEDIATE	4.4	40	1	1.924	8.39E+01	2073.1	14298.1
THIOPAVE-INTERMEDIATE	4.4	40	0.5	1.924	4.20E+01	1932.3	13327.3
THIOPAVE-INTERMEDIATE	4.4	40	0.1	1.924	8.39E+00	1578.3	10885.3
THIOPAVE-INTERMEDIATE	21.1	70	25	-0.130	1.85E+01	1756.2	12112.7
THIOPAVE-INTERMEDIATE	21.1	70	10	-0.130	7.42E+00	1550.3	10692.6
THIOPAVE-INTERMEDIATE	21.1	70	5	-0.130	3.71E+00	1393.1	9608.3
THIOPAVE-INTERMEDIATE	21.1	70	1	-0.130	7.42E-01	1044.2	7202.1
THIOPAVE-INTERMEDIATE	21.1	70	0.5	-0.130	3.71E-01	908.6	6266.9
THIOPAVE-INTERMEDIATE	21.1	70	0.1	-0.130	7.42E-02	643.4	4437.6
THIOPAVE-INTERMEDIATE	37.8	100	25	-1.963	2.72E-01	852.0	5876.1
THIOPAVE-INTERMEDIATE	37.8	100	10	-1.963	1.09E-01	699.8	4826.8
THIOPAVE-INTERMEDIATE	37.8	100	5	-1.963	5.44E-02	601.0	4145.2
THIOPAVE-INTERMEDIATE	37.8	100	1	-1.963	1.09E-02	423.7	2922.0
THIOPAVE-INTERMEDIATE	37.8	100	0.5	-1.963	5.44E-03	367.2	2532.5
THIOPAVE-INTERMEDIATE	37.8	100	0.1	-1.963	1.09E-03	271.9	1875.1
THIOPAVE-INTERMEDIATE	54.4	130	25	-3.610	6.14E-03	376.2	2594.7
THIOPAVE-INTERMEDIATE	54.4	130	10	-3.610	2.46E-03	314.5	2169.0
THIOPAVE-INTERMEDIATE	54.4	130	5	-3.610	1.23E-03	277.5	1914.2
THIOPAVE-INTERMEDIATE	54.4	130	1	-3.610	2.46E-04	216.2	1491.0
THIOPAVE-INTERMEDIATE	54.4	130	0.5	-3.610	1.23E-04	197.6	1363.1

Section-Lift ID	Temp (deg C)	Temp (deg F)	Frequency (Hz)	Shift Factor	Reduced Frequency	E*, (ksi)	E*, (Mpa)
THIOPAVE-INTERMEDIATE	54.4	130	0.1	-3.610	2.46E-05	166.9	1151.1
THIOPAVE-BASE	-10.0	14	25	4.203	3.99E+05	2758.7	19027.0
THIOPAVE-BASE	-10.0	14	10	4.203	1.60E+05	2691.5	18563.6
THIOPAVE-BASE	-10.0	14	5	4.203	7.98E+04	2632.1	18153.8
THIOPAVE-BASE	-10.0	14	1	4.203	1.60E+04	2461.5	16977.0
THIOPAVE-BASE	-10.0	14	0.5	4.203	7.98E+03	2372.6	16364.1
THIOPAVE-BASE	-10.0	14	0.1	4.203	1.60E+03	2128.8	14682.7
THIOPAVE-BASE	4.4	40	25	2.066	2.91E+03	2225.9	15352.0
THIOPAVE-BASE	4.4	40	10	2.066	1.16E+03	2075.0	14311.6
THIOPAVE-BASE	4.4	40	5	2.066	5.82E+02	1950.7	13453.7
THIOPAVE-BASE	4.4	40	1	2.066	1.16E+02	1635.3	11278.9
THIOPAVE-BASE	4.4	40	0.5	2.066	5.82E+01	1492.7	10295.3
THIOPAVE-BASE	4.4	40	0.1	2.066	1.16E+01	1163.8	8026.7
THIOPAVE-BASE	21.1	70	25	-0.139	1.81E+01	1252.9	8641.0
THIOPAVE-BASE	21.1	70	10	-0.139	7.26E+00	1071.5	7390.0
THIOPAVE-BASE	21.1	70	5	-0.139	3.63E+00	942.4	6499.6
THIOPAVE-BASE	21.1	70	1	-0.139	7.26E-01	680.9	4696.0
THIOPAVE-BASE	21.1	70	0.5	-0.139	3.63E-01	587.3	4050.6
THIOPAVE-BASE	21.1	70	0.1	-0.139	7.26E-02	414.9	2861.6
THIOPAVE-BASE	37.8	100	25	-2.108	1.95E-01	513.5	3541.5
THIOPAVE-BASE	37.8	100	10	-2.108	7.80E-02	421.3	2905.8
THIOPAVE-BASE	37.8	100	5	-2.108	3.90E-02	363.8	2508.8
THIOPAVE-BASE	37.8	100	1	-2.108	7.80E-03	263.9	1820.0
THIOPAVE-BASE	37.8	100	0.5	-2.108	3.90E-03	232.6	1604.5
THIOPAVE-BASE	37.8	100	0.1	-2.108	7.80E-04	179.8	1240.0
THIOPAVE-BASE	54.4	130	25	-3.877	3.32E-03	226.2	1560.3
THIOPAVE-BASE	54.4	130	10	-3.877	1.33E-03	194.7	1342.8
THIOPAVE-BASE	54.4	130	5	-3.877	6.64E-04	175.7	1212.0
THIOPAVE-BASE	54.4	130	1	-3.877	1.33E-04	143.7	991.2
THIOPAVE-BASE	54.4	130	0.5	-3.877	6.64E-05	133.8	922.8
THIOPAVE-BASE	54.4	130	0.1	-3.877	1.33E-05	116.9	806.3
CONTROL-INTERMEDIATE	-10.0	14	25	4.116	3.27E+05	2878.7	19854.1
CONTROL-INTERMEDIATE	-10.0	14	10	4.116	1.31E+05	2810.0	19380.7
CONTROL-INTERMEDIATE	-10.0	14	5	4.116	6.54E+04	2749.4	18962.7
CONTROL-INTERMEDIATE	-10.0	14	1	4.116	1.31E+04	2575.7	17764.9
CONTROL-INTERMEDIATE	-10.0	14	0.5	4.116	6.54E+03	2485.4	17141.9
CONTROL-INTERMEDIATE	-10.0	14	0.1	4.116	1.31E+03	2237.7	15433.4

Section-Lift ID	Temp (deg C)	Temp (deg F)	Frequency (Hz)	Shift Factor	Reduced Frequency	E*, (ksi)	E*, (Mpa)
CONTROL-INTERMEDIATE	4.4	40	25	2.023	2.64E+03	2352.3	16223.6
CONTROL-INTERMEDIATE	4.4	40	10	2.023	1.06E+03	2200.8	15178.9
CONTROL-INTERMEDIATE	4.4	40	5	2.023	5.28E+02	2075.5	14315.0
CONTROL-INTERMEDIATE	4.4	40	1	2.023	1.06E+02	1756.0	12111.3
CONTROL-INTERMEDIATE	4.4	40	0.5	2.023	5.28E+01	1610.3	11106.5
CONTROL-INTERMEDIATE	4.4	40	0.1	2.023	1.06E+01	1270.7	8764.1
CONTROL-INTERMEDIATE	21.1	70	25	-0.136	1.83E+01	1385.3	9554.3
CONTROL-INTERMEDIATE	21.1	70	10	-0.136	7.31E+00	1195.4	8245.0
CONTROL-INTERMEDIATE	21.1	70	5	-0.136	3.65E+00	1058.5	7300.8
CONTROL-INTERMEDIATE	21.1	70	1	-0.136	7.31E-01	775.8	5350.8
CONTROL-INTERMEDIATE	21.1	70	0.5	-0.136	3.65E-01	672.5	4638.6
CONTROL-INTERMEDIATE	21.1	70	0.1	-0.136	7.31E-02	478.8	3302.2
CONTROL-INTERMEDIATE	37.8	100	25	-2.065	2.15E-01	602.0	4151.7
CONTROL-INTERMEDIATE	37.8	100	10	-2.065	8.62E-02	495.8	3419.5
CONTROL-INTERMEDIATE	37.8	100	5	-2.065	4.31E-02	428.6	2955.9
CONTROL-INTERMEDIATE	37.8	100	1	-2.065	8.62E-03	310.1	2138.7
CONTROL-INTERMEDIATE	37.8	100	0.5	-2.065	4.31E-03	272.5	1879.5
CONTROL-INTERMEDIATE	37.8	100	0.1	-2.065	8.62E-04	208.4	1437.5
CONTROL-INTERMEDIATE	54.4	130	25	-3.797	3.99E-03	268.8	1853.9
CONTROL-INTERMEDIATE	54.4	130	10	-3.797	1.60E-03	229.7	1584.1
CONTROL-INTERMEDIATE	54.4	130	5	-3.797	7.99E-04	206.0	1421.0
CONTROL-INTERMEDIATE	54.4	130	1	-3.797	1.60E-04	165.9	1144.4
CONTROL-	54.4	130	0.5	-3.797	7.99E-05	153.5	1058.4

Section-Lift ID	Temp (deg C)	Temp (deg F)	Frequency (Hz)	Shift Factor	Reduced Frequency	E*, (ksi)	E*, (Mpa)
INTERMEDIATE							
CONTROL-INTERMEDIATE	54.4	130	0.1	-3.797	1.60E-05	132.2	911.7
CONTROL-BASE	-10.0	14	25	3.651	1.12E+05	2805.8	19351.5
CONTROL-BASE	-10.0	14	10	3.651	4.47E+04	2716.7	18736.9
CONTROL-BASE	-10.0	14	5	3.651	2.24E+04	2637.5	18190.7
CONTROL-BASE	-10.0	14	1	3.651	4.47E+03	2409.9	16620.9
CONTROL-BASE	-10.0	14	0.5	3.651	2.24E+03	2292.0	15808.2
CONTROL-BASE	-10.0	14	0.1	3.651	4.47E+02	1974.6	13618.7
CONTROL-BASE	4.4	40	25	1.794	1.56E+03	2225.8	15351.3
CONTROL-BASE	4.4	40	10	1.794	6.23E+02	2044.5	14100.8
CONTROL-BASE	4.4	40	5	1.794	3.11E+02	1895.9	13075.9
CONTROL-BASE	4.4	40	1	1.794	6.23E+01	1526.2	10525.9
CONTROL-BASE	4.4	40	0.5	1.794	3.11E+01	1363.7	9405.3
CONTROL-BASE	4.4	40	0.1	1.794	6.23E+00	1004.7	6929.6
CONTROL-BASE	21.1	70	25	-0.121	1.89E+01	1248.7	8612.0
CONTROL-BASE	21.1	70	10	-0.121	7.57E+00	1045.8	7213.2
CONTROL-BASE	21.1	70	5	-0.121	3.78E+00	903.7	6232.7
CONTROL-BASE	21.1	70	1	-0.121	7.57E-01	624.4	4306.3
CONTROL-BASE	21.1	70	0.5	-0.121	3.78E-01	528.3	3643.5
CONTROL-BASE	21.1	70	0.1	-0.121	7.57E-02	358.6	2473.4
CONTROL-BASE	37.8	100	25	-1.831	3.69E-01	525.0	3621.1
CONTROL-BASE	37.8	100	10	-1.831	1.48E-01	420.5	2900.2
CONTROL-BASE	37.8	100	5	-1.831	7.38E-02	356.5	2458.7
CONTROL-BASE	37.8	100	1	-1.831	1.48E-02	248.8	1716.2
CONTROL-BASE	37.8	100	0.5	-1.831	7.38E-03	216.3	1492.2
CONTROL-BASE	37.8	100	0.1	-1.831	1.48E-03	163.2	1125.7
CONTROL-BASE	54.4	130	25	-3.367	1.07E-02	233.1	1607.4
CONTROL-BASE	54.4	130	10	-3.367	4.30E-03	195.4	1347.9
CONTROL-BASE	54.4	130	5	-3.367	2.15E-03	173.3	1195.4
CONTROL-BASE	54.4	130	1	-3.367	4.30E-04	137.2	946.1
CONTROL-BASE	54.4	130	0.5	-3.367	2.15E-04	126.4	871.6
CONTROL-BASE	54.4	130	0.1	-3.367	4.30E-05	108.5	748.2